

**Development of chemical and chemogenetic tools  
for elucidating glutamate receptor function**

**Kento Ojima**

**2022**



## **Preface and Acknowledgements**

The studies presented in this dissertation have been carried out under the direction of Professor Itaru Hamachi at the Department of Synthetic Chemistry and Biological Chemistry, Graduate School of Engineering, Kyoto University from April 2016 to September 2021 and Professor Shigeki Kiyonaka at Department of Biomolecular Chemistry, Graduate School of Engineering, Nagoya University from April 2019. This study is focused on the development of rapid and selective labeling method for analyzing glutamate receptor trafficking in neurons and direct activation method of glutamate receptor.

My heartfelt appreciation goes to Prof. Itaru Hamachi and Prof. Shigeki Kiyonaka whose comment, suggestions, and encouragement were of inestimable value for my study. I extend my sincere gratitude to Assistant Prof. Hiroshi Nonaka, Junior Assoc. Prof. Tomonori Tamura, Junior Assoc. Prof. Ryou Kubota, Assist. Prof. Seiji Sakamoto, their suggestions.

I wish to acknowledge Prof. Michisuke Yuzaki, Assoc. Prof. Wataru Kakegawa, Assist. Prof. Tokiwa Yamasaki, Dr. Eriko Miura for histological and electrophysiological experiments and for giving me great comments in chapter 3.

I thank the past and present members of Hamachi laboratory and Kiyonaka laboratory for their suggestions and cooperation, and with whom I shared an enjoyable time. In particular, I express my appreciation to Mr. Kazuki Shiraiwa, Mr. Kyohei Soga, Ms. Mikiko Takato, Dr. Tomohiro Doura, Ms. Yukiko Michibata and Mr. Yuta Miura in this thesis. I also acknowledge Prof. Kenichi Nishijima, Assistant Prof. Hiroshi Nonaka, Assistant Prof. Hideki Nakamura, Junior Assoc. Prof. Tomonori Tamura, Junior Assoc. Prof. Ryou Kubota, Assist. Prof. Seiji Sakamoto, Assist. Prof. Hidenori Kaneoka, Assist.

Prof. Hajime Shigemitsu, Assist. Prof. Kazuma Amaike, Assist. Prof. Takayuki Miki, Assist. Prof. Hao Zhu, Assist. Prof. Masaki Tsuchiya, Dr. Muneo Tsujikawa, Dr. Yuki Yasueda, Dr. Kyohei Kanomata, Dr. Zhining Song, Dr. Kei Yamaura, Dr. Marie Masuda, Dr. Sho Wakayama, Dr. Alma Fujisawa, Dr. Tsuyoshi Ueda, Dr. Yuki Nishikawa, Mr. Yuma Morikawa, Mr. Kyohei Okuno, Mr. Ryosuke Ikeda, Mr. Wataru Nomura, Mr. Sin Li, Assist. Prof. Wataru Tanaka, Mr. Shinichiro Hagi, Dr. Taku Tsukidate, Dr. Takahiro Fujisaku, Dr. Akinobu Senoo, Mr. Ryotaro Matsumura , Mr. Keisuke Nakamura, Mr. Takuma Iwasaka, Mr. Taiki Goto, Mr. Sadatoshi Yamagami, Mr. Tomonobu Matsuzaki, Mr. Vikram Thimaradka, Mr. Shogo Trigoe, Mr. Fumio Harada, Ms. Rong Cheng, Mr. Yuying Shen, Mr. Daiki Ogawa, Mr. Kazuma Matsubayashi, Mr. Takeharu Mino, Mr. Keiya Shiono, Mr. Kazutoshi Nagao, Mr. Yutaro Yamada, Mr. Kanta Hasegawa, Mr. Kota Sugimoto, Mr. Yoshitaka Makita, Mr. Ziyang Li, Mr. Yuta Ikeda, Mr. Yu Watanabe, Mr. Kei Sada, Mr. Taku Kanaya, Ms. Mizuki Sano, Ms. Risako Fukata, Mr. Takumitsu Shakuno, Ms. Yukina Kuno, Mr. Taro Sugihara, Mr. Ryo Kamiya, Mr. Shunraro Kashiwa, Mr. Takuto Matsuoka, Mr. Yuki Tsuruhata, Mr. Yuma Matsuoka, Mr. Akihiro Shibata, Ms. Airi Watanabe, Ms. Suzuka Kurakake and Ms. Midori Makino.

I also wish to express my gratitude to Ms. Ikuyo Miyamae, Ms. Asami Ozaki, and Kyoko Kusakabe for their help with official business, and I would like to thank JSPS (Japan Society for the Promotion of Science) Young Scientist Fellowship for the financial support that made it possible to complete this study.

Finally, I wish to express my deepest gratitude to my parents, Shinya and Yoko Ojima, to my brother Ichirota Ojima who have supported my education and encouraged me affectionately.

November 2021

小島 憲人

## **Table of Contents**

<i>General Introduction</i>	1
<i>Chapter 1</i>	18
Development of ligand-directed two-step labeling for rapid labeling of cell-surface AMPA receptors	
<i>Chapter 2</i>	45
Quantification of AMPA receptor trafficking by ligand-directed two-step labeling	
<i>Chapter 3</i>	86
Coordination chemogenetics for activation of GPCR-type glutamate receptors in brain tissue	
<i>List of Publications and Presentations</i>	143



# **General introduction**

## **Introduction**

Glutamate is a major excitatory neurotransmitter, which mediates excitatory neurotransmission via ionotropic glutamate receptors (iGluRs) and metabotropic glutamate receptors (mGluRs)<sup>1</sup>. iGluRs form tetrameric ligand-gated ion-channels that induce depolarization of neurons by opening the cation channels<sup>2</sup>. On the other hand, mGluRs are G protein-coupled receptors (GPCRs) that control cellular functions via G-protein coupled signaling<sup>3</sup>. Change of the expression levels on the synaptic surface and the activities are essential for the molecular basis of memory and learning<sup>4,5</sup>. As a result, impaired membrane trafficking and abnormal function of the receptors cause cognitive impairment and psychiatric disturbance such as anxiety and depression. Therefore, analyzing the trafficking of the receptors and regulation of the receptor function is indispensable for elucidating the molecular mechanism of memory, learning, and neurological diseases.

Genetic incorporation of a fluorescent protein to a target receptor and pharmacological activation of the receptor have been widely used to analyze the receptor trafficking and control the receptor function, respectively. However, given the high molecular weight of fluorescent proteins (about 25 kDa), the fusion of fluorescent proteins may disturb original receptor function. With respect to the pharmacological approach, glutamate receptors have many subtypes with high structural similarity of orthosteric ligand-binding site. Thus, it is difficult to develop selective ligands for each subtype.

In recent years, chemical biology and chemogenetics methods have been developed to overcome these problems. In this chapter, I focus on the current methods of analyzing the protein function using chemical labeling and control of the receptor function using chemogenetics.



## **Protein labeling method by chemical probes**

### **Genetic code expansion combined with bioorthogonal reaction**

Genetic incorporation of fluorescent proteins to the receptors is problematic due to the size of the fluorescent proteins. Ideally, the receptors should be labeled with chemical probes. To incorporate chemical probes to the target receptors, genetic code expansion, which enables the site-specific incorporations of various kinds of unnatural amino acids (UAAs), has been developed<sup>6</sup>. Schultz's group firstly reported that various kinds of UAAs could be incorporated into proteins by genetic code expansion, using mutant tRNA/aminoacyl-tRNA synthetase pairs, in living cells<sup>7</sup>. Chin's group reported a genetic code expansion combined with a bioorthogonal labeling method<sup>8,9</sup>. In this method, UAA bearing a *trans*-cyclooctene (TCO) was incorporated into protein and successfully labeled the protein by inverse electron demand Diels-Alder (IEDDA) reaction between TCO and tetrazine-conjugated probe. IEDDA reaction is one of the fastest bioorthogonal reactions and some tetrazine conjugated-fluorophores have a fluorogenic response upon the IEDDA reaction, which contributes to a high signal-to-noise (S/N) ratio in fluorescence imaging. Doose's group recently reported super-resolution imaging of NMDA receptors, one of the iGluRs, by genetic code expansion for site-specific incorporation of TCO-bearing UAAs<sup>10</sup> (Fig.1). Although genetic code expansion combined with bioorthogonal reaction is an undoubtedly powerful tool, it also has some limitations. For example, considering the heterotetrameric formation of iGluRs, overexpression of the single iGluR subunits may perturb the original function.

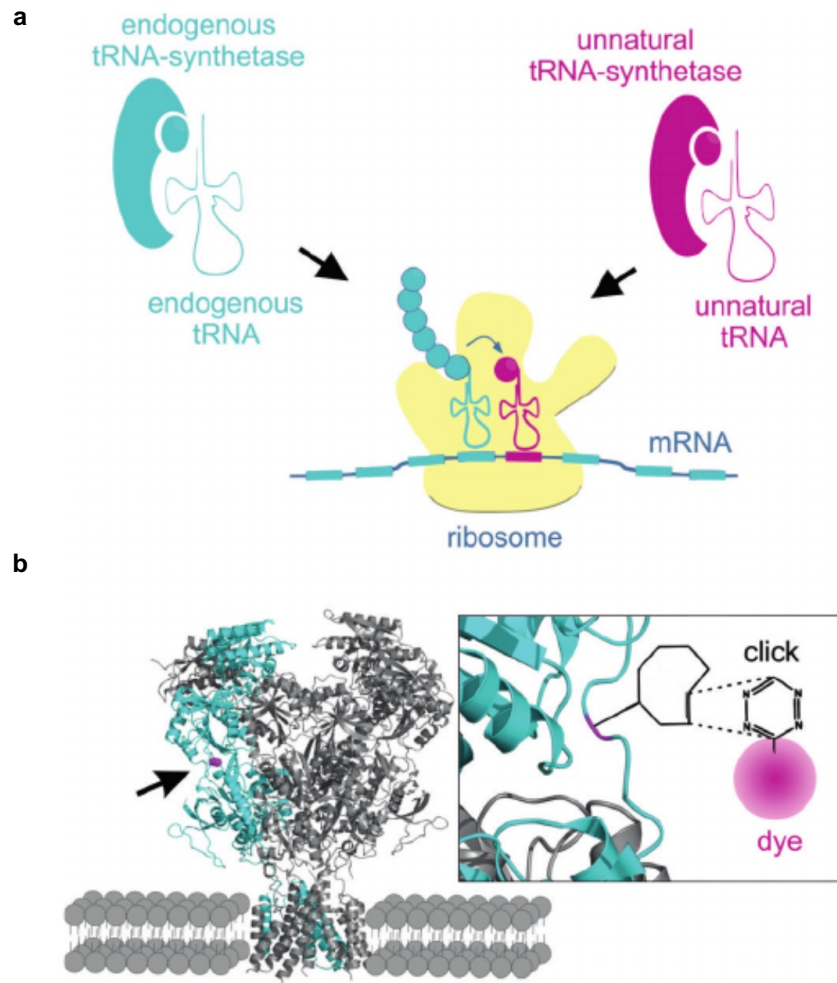


**Fig 1. | Protein labeling with genetic code expansion combined with IEDDA reaction.** (a) Schematic illustration of genetic code expansion for site-directed incorporation of the UAAs bearing a TCO for IEDDA reaction. (b) Fluorescent labeling to NMDA receptor by IEDDA reaction. The figure is adapted from Neubert *et al.* (2018).

### Affinity-based protein labeling

Protein labeling by genetic code expansion requires genetic manipulation, which causes functional perturbation and overexpression of the target protein. Thus, the development of endogenous protein labeling methods by chemical probes without any genetic manipulation is required for analyzing native protein function in living cells. Affinity-based protein labeling with synthetic probes bearing a ligand for the target protein and a reactive site is a powerful technique for the selective modification of target proteins. Sames's group developed an epoxide probe to successfully label human carbonic anhydrase II (CAII) in cell lysates<sup>11</sup>. Cravatt's group developed an activity-based protein profiling (ABPP) that utilized active site-directed probes to analyze the functional state of enzymes in complex proteomes<sup>12-14</sup> (Fig. 2). These affinity-based methods realized selective chemical protein labeling without genetic manipulation. Although these methods are powerful, the covalently attached ligands remain even after labeling, and inhibition of the protein activity is problematic for analyzing the protein function in living cells.

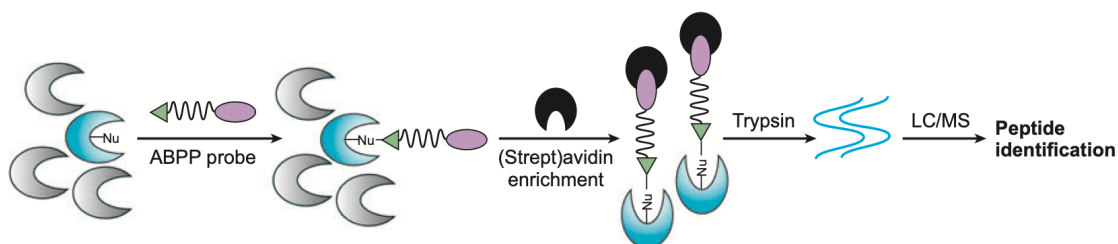


**Fig. 2 | Schematic illustration of activity-based protein profiling.** The figure is adapted from Cravatt *et al.* (2008).

### **Ligand-directed chemistry**

To overcome the limitation of affinity-based protein labeling, a traceless affinity-based labeling method for endogenous proteins was developed. Hamachi's group has been developed a labeling strategy "ligand-directed chemistry". This strategy uses a labeling reagent bearing a ligand for the target protein, a cleavable reactive site, and a chemical probe<sup>15</sup> (Fig. 3). Selective protein recognition of the ligand promotes substitution reaction between reactive site and nucleophilic amino acids on protein surface by the proximity effect. Importantly, the residual ligand that inhibits protein activity is not covalently linked to the protein and removed by washing. Several reactive moieties such as tosylate<sup>16</sup>, acyl imidazole<sup>17,18</sup>, and *N*-acyl-*N*-alkyl sulfonamide<sup>19,20</sup> for ligand-directed chemistry have been developed, in which the reaction kinetics and the selectivity to amino acid are different. The variety allowed the expansion of the range of the target proteins and the applications of ligand-directed chemistry. Hamachi's group recently reported chemical labeling of endogenous iGluRs in neurons by ligand-directed acyl imidazole (LDAI) chemistry<sup>21</sup>.

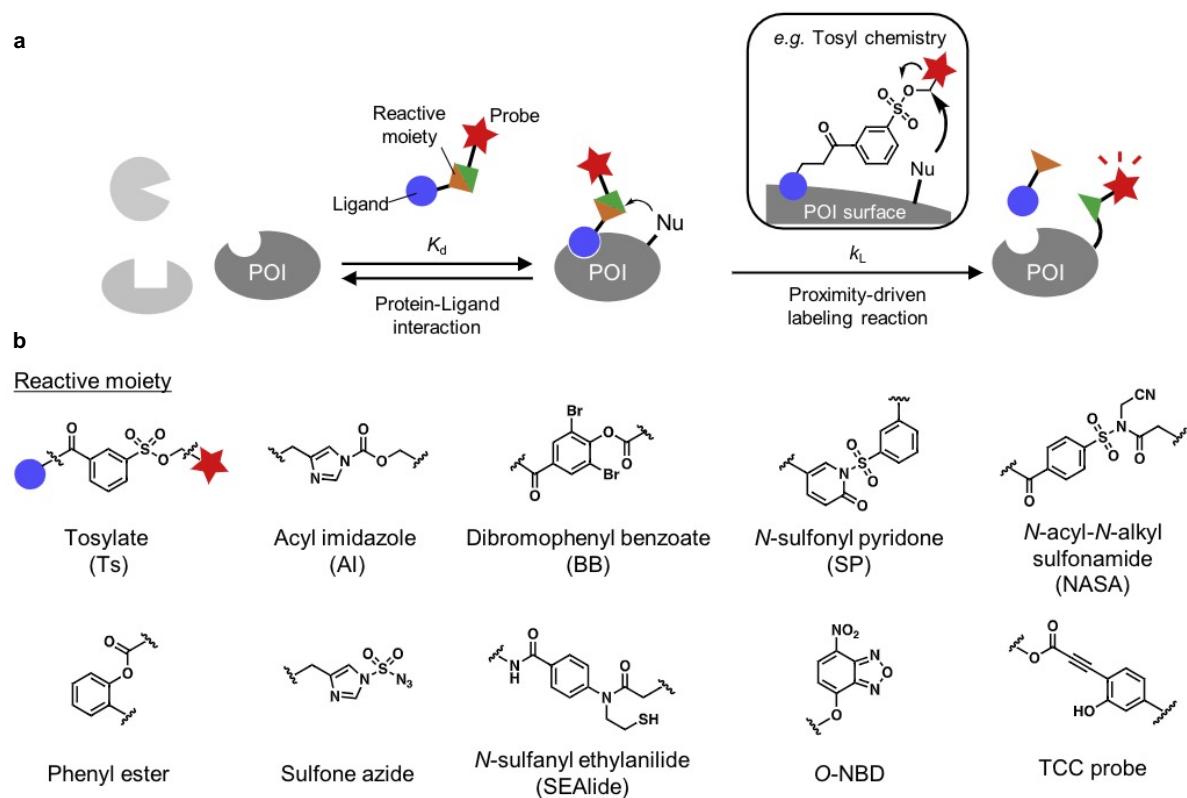


**Fig. 3 | Ligand-directed chemistry for protein labeling. (a)** Schematic illustration of ligand-directed chemistry. **(b)** Reactive moieties for ligand-directed chemistry. The figure is adapted from Siraiwa *et al.* (2020).

**Control the protein function by chemogenetic approaches.**

**Manipulation of neuronal activities by chemogenetics.**

Glutamate receptors have high structural homology of the orthosteric ligand-binding site between each subtype. Thus, it is difficult to develop a subtype-selective ligand. A potential method for subtype-selective activation of target receptors is chemogenetics<sup>22,23</sup>, in which proteins are genetically engineered to interact with the designed ligand selectively. As early attempts, Conklin's group developed a family of engineered receptors termed RASSLs (receptor activated solely by synthetic ligand)<sup>24</sup>. In this method,  $\kappa$ -opioid receptor mutant, which abrogated affinity to the natural peptide ligands yet preserved stimulation by an artificial ligand, was utilized to control cardiac activity<sup>25</sup>. However, their utility in the central nervous system has been hampered due to the high constitutive activity. To overcome the disadvantage, Roth's group developed DREADDs (designer receptors exclusively activated by designer drugs), which have low constitutive activity and high selectivity to an artificial ligand, clozapine-*N*-oxide (CNO), by directed molecular evolution of M3-muscarinic acetylcholine receptors<sup>26,27</sup>. The resulting M3-muscarinic receptor mutant selectively activated G $\alpha$ q-mediated signaling pathways in the targeted neuronal cells in living animals by oral administration of CNO. Furthermore, they developed other DREADD-based muscarinic receptor subtypes. M1-, and M5-DREADDs activate G $\alpha$ q pathway, whereas M2- and M4-DREADDs activate G $\alpha$ i pathway. Subsequently, Wess's group generated a chimeric muscarinic-adrenergic DREADD that selectively activates G $\alpha$ s pathway<sup>28</sup>. Various DREADDs allow for chemogenetic activation of various signaling pathways using CNO and lead to burst firing, silencing of firing, and modulation of neuronal activity in living animals (Fig. 4a). With respect to ligand-gated ion channels based chemogenetics, Sternson's group reported engineered receptors (PSAMs) and designed

agonists (PSEMs) pairs that have been reported using the bump-and-hole strategy<sup>29,30</sup> (Fig. 4b,c).

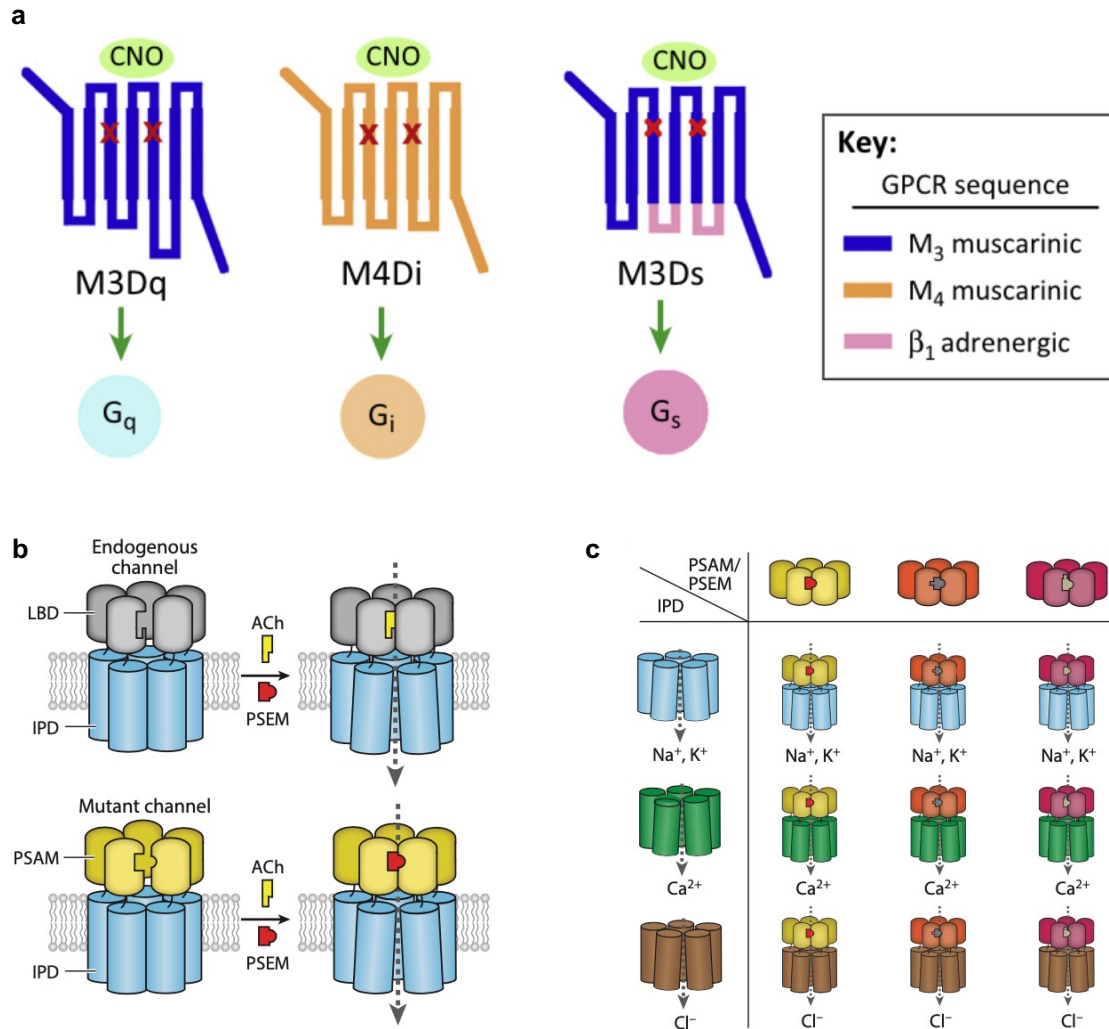


**Fig. 4 | Chemogenetic activation of mutant receptors by synthetic ligands. (a)** Schematic illustration of chemogenetic activation of G-protein pathways by DREADD. **(b)** Schematic illustration of chemogenetic activation of ligand-gated ion-channels by PSAM/PSEM. The figures are adapted from Wess (2016) and Sternson & Roth (2014).

**Chemogenetic activation of receptors by chemical probes.**

In addition to well-used chemogenetic methods such as DREADD and PSAM/PSEM, functional regulation of cell-surface proteins has been achieved by chemical biology manipulations. Trauner's group reported light-activatable receptors by tethering a native ligand with a photoisomerizable azobenzene moiety to the target protein via cysteine modification or a protein tag<sup>31-33</sup>. In a dark state of azobenzene, the ligand can not bind to the receptor. Only after photoisomerization of azobenzene, the ligand can bind to the receptor. These methods are used successfully for photo-switching of iGluR in neurons by covalent attachment of the glutamate photoswitch to a cysteine mutant of the receptor<sup>31</sup>. In another direction, Schwartz's group also reported functional switching of cell-surface receptors, in which amino acids were mutated in the ligand-binding region of GPCRs for metal-induced activation<sup>34,35</sup>.



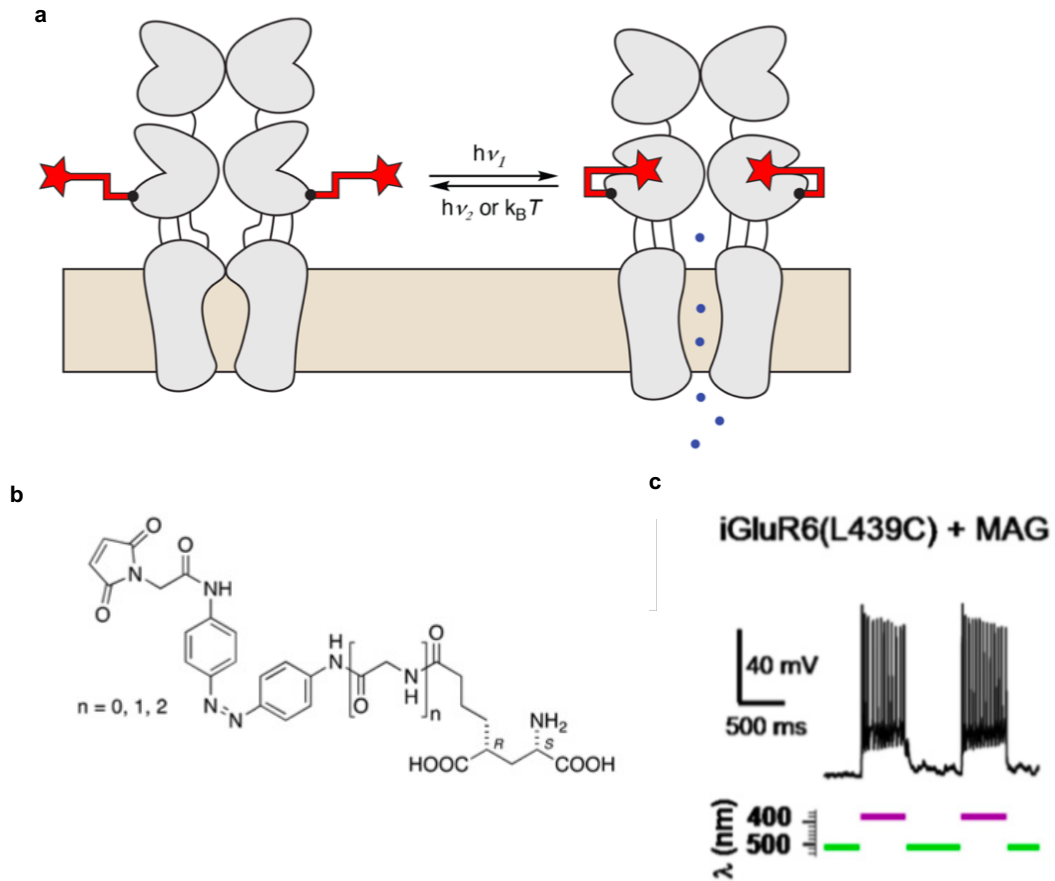


**Fig. 5 | Chemogenetic activation of photoactivatable ligand-tethered receptors (a)** Schematic illustration of photoactivation of mutant iGluR by photoisomerizable ligand (L-MAG). **(b)** Chemical structure of L-MAG. **(c)** Mutant iGluRs are activated by photoirradiation. The figure is adapted from Hüll *et al.* (2018).

**Chemogenetic activation of receptors without affecting the original receptor function.**

Although most of current chemogenetic methods are powerful for the functional regulation of target receptors, the original receptor function is often affected. Consequently, chemogenetic control of endogenous receptors is quite challenging, and only a few successful examples have been reported. As a potential approach, Hamachi's group recently reported new chemogenetic methods for allosteric activation of glutamate receptor subtypes using coordination chemistry without affecting the original receptor function<sup>36,37</sup>. In this method, site-specific incorporation of coordinating amino acid residues in allosteric site based on structural information. It allowed metal-complex-associated activation of glutamate receptors without affecting the original receptor function.

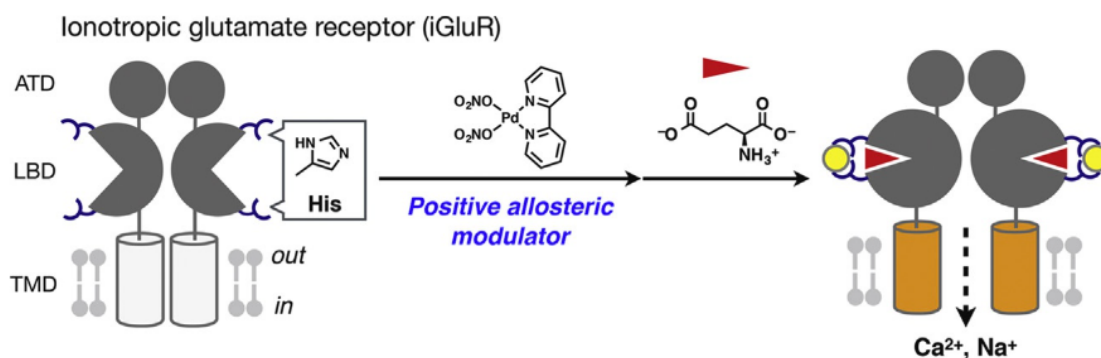


**Fig. 6 | Schematic illustration of chemogenetic activation of coordinating amino acid incorporated receptor by metal coordination.** Figure is adapted from Kubota *et al.* (2019).

### **Summary of this thesis**

As described above, various chemistry-based methods for protein labeling and chemogenetic methods for controlling protein function have been developed. Although these methods are useful in a model system, there are some limitations on their application to the central nervous system such as vulnerability of the neuronal cells.

In this thesis, I developed a rapid and selective labeling method for analyzing glutamate receptor dynamics in neurons and direct activation method of glutamate receptor.

In chapter 1, I develop a novel method for the rapid and selective labeling of an iGluR under physiological conditions by ligand-directed two-step labeling combining LDAI chemistry and inverse-electron demand Diels-Alder (IEEDA) reaction. In chapter 2, I analyzed the localization and trafficking of endogenous iGluRs with a cell-friendly condition by ligand-directed two-step labeling. This method allowed for investigating the quantitative analysis of iGluR trafficking in neurons.

In chapter 3, I developed a direct activation method of mGluR by chemogenetics, termed dA-CBC (direct-activation via coordination-based chemogenetics). In the engineered receptor, palladium complex directly activated the mGluR mutant without potentiating the affinity of glutamate. I also designed a novel palladium complex with low toxicity to neurons. dA-CBC method allowed the chemogenetic regulation of endogenous mGluRs in the brain tissue prepared from mouse. Thus, the dA-CBC method would be a notable chemogenetic strategy for controlling endogenous receptor function.

## Reference

1. Reiner, A. & Levitz, J. Glutamatergic Signaling in the Central Nervous System: Ionotropic and Metabotropic Receptors in Concert. *Neuron* **98**, 1080–1098 (2018).
2. Traynelis, S. F. *et al.* Glutamate receptor ion channels: Structure, regulation, and function. *Pharmacol. Rev.* **62**, 405–496 (2010).
3. Niswender, C. M. & Conn, P. J. Metabotropic glutamate receptors: Physiology, pharmacology, and disease. *Annu. Rev. Pharmacol. Toxicol.* **50**, 295–322 (2010).
4. Breddt, D. S. & Nicoll, R. A. AMPA receptor trafficking at excitatory synapses. *Neuron* **40**, 361–379 (2003).
5. Diering, G. H. & Huganir, R. L. The AMPA Receptor Code of Synaptic Plasticity. *Neuron* **100**, 314–329 (2018).
6. Nödling, A. R., Spear, L. A., Williams, T. L., Luk, L. Y. P. & Tsai, Y. H. Using genetically incorporated unnatural amino acids to control protein functions in mammalian cells. *Essays Biochem.* **63**, 237–266 (2019).
7. Xiao, H. *et al.* Genetic incorporation of multiple unnatural amino acids into proteins in mammalian cells. *Angew. Chemie - Int. Ed.* **52**, 14080–14083 (2013).
8. Lang, K. *et al.* Genetically encoded norbornene directs site-specific cellular protein labelling via a rapid bioorthogonal reaction. *Nat. Chem.* **4**, 298–304 (2012).
9. Lang, K. *et al.* Genetic encoding of bicyclononynes and trans-cyclooctenes for site-specific protein labeling in vitro and in live mammalian cells via rapid fluorogenic Diels-Alder reactions. *J. Am. Chem. Soc.* **134**, 10317–10320 (2012).
10. Neubert, F. *et al.* Bioorthogonal Click Chemistry Enables Site-specific Fluorescence Labeling of Functional NMDA Receptors for Super-Resolution Imaging. *Angew. Chemie - Int. Ed.* **57**, 16364–16369 (2018).
11. Chen, G. *et al.* Reactivity of functional groups on the protein surface: Development of epoxide probes for protein labeling. *J. Am. Chem. Soc.* **125**, 8130–8133 (2003).
12. Adam, G. C., Cravatt, B. F. & Sorensen, E. J. Profiling the specific reactivity of the

- proteome with non-directed activity-based probes. *Chem. Biol.* **8**, 81–95 (2001).
13. Adam, G. C., Sorensen, E. J. & Cravatt, B. F. Proteomic profiling of mechanistically distinct enzyme classes using a common chemotype. *Nat. Biotechnol.* **20**, 805–809 (2002).
  14. Cravatt, B. F., Wright, A. T. & Kozarich, J. W. Activity-based protein profiling: From enzyme chemistry to proteomic chemistry. *Annu. Rev. Biochem.* **77**, 383–414 (2008).
  15. Shiraiwa, K., Cheng, R., Nonaka, H., Tamura, T. & Hamachi, I. Chemical Tools for Endogenous Protein Labeling and Profiling. *Cell Chem. Biol.* **27**, 970–985 (2020).
  16. Tsukiji, S., Miyagawa, M., Takaoka, Y., Tamura, T. & Hamachi, I. Ligand-directed tosyl chemistry for protein labeling in vivo. *Nat. Chem. Biol.* **5**, 341–343 (2009).
  17. Fujishima, S. H., Yasui, R., Miki, T., Ojida, A. & Hamachi, I. Ligand-directed acyl imidazole chemistry for labeling of membrane-bound proteins on live cells. *J. Am. Chem. Soc.* **134**, 3961–3964 (2012)
  18. Miki, T. *et al.* LDAI-based chemical labeling of intact membrane proteins and its pulse-chase analysis under live cell conditions. *Chem. Biol.* **21**, 1013–1022 (2014)
  19. Tamura, T. *et al.* Rapid labelling and covalent inhibition of intracellular native proteins using ligand-directed *N*-Acyl-*N*-Alkyl sulfonamide. *Nat. Commun.* **9**, 1–12 (2018).
  20. Ueda, T., Tamura, T. & Hamachi, I. Development of a Cell-Based Ligand-Screening System for Identifying Hsp90 Inhibitors. *Biochemistry* **59**, 179–182 (2020)
  21. Wakayama, S. *et al.* Chemical labelling for visualizing native AMPA receptors in live neurons. *Nat. Commun.* **8**, (2017).
  22. Wess, J. Use of Designer G Protein-Coupled Receptors to Dissect Metabolic Pathways. *Trends Endocrinol. Metab.* **27**, 600–603 (2016)
  23. Sternson, S. M. & Roth, B. L. Chemogenetic tools to interrogate brain functions.

## *General Introduction*

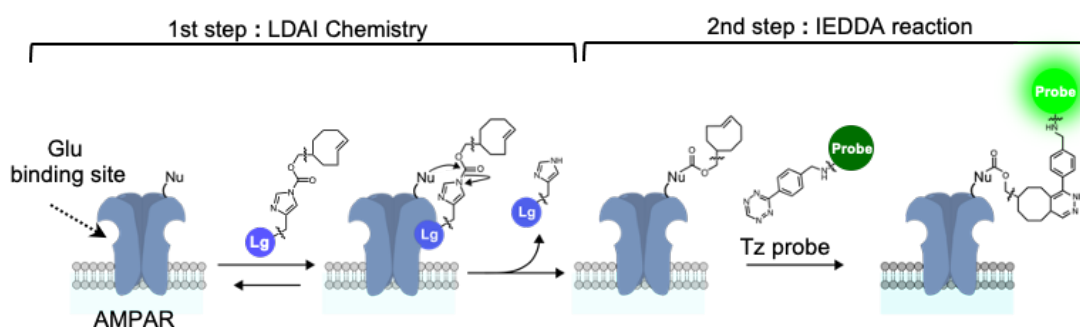
- Annu. Rev. Neurosci.* **37**, 387–407 (2014).
24. Coward, P. *et al.* Controlling signaling with a specifically designed Gi-coupled receptor. *Proc. Natl. Acad. Sci. U. S. A.* **95**, 352–357 (1998).
  25. Redfern, C. H. *et al.* Conditional expression and signaling of a specifically designed G(i)- coupled receptor in transgenic mice. *Nat. Biotechnol.* **17**, 165–169 (1999).
  26. Armbruster, B. N., Li, X., Pausch, M. H., Herlitze, S. & Roth, B. L. Evolving the lock to fit the key to create a family of G protein-coupled receptors potently activated by an inert ligand. *Proc. Natl. Acad. Sci. U. S. A.* **104**, 5163–5168 (2007).
  27. Alexander, G. M. *et al.* Remote control of neuronal activity in transgenic mice expressing evolved G protein-coupled receptors. *Neuron* **63**, 27–39 (2009).
  28. Guettier, J. M. *et al.* A chemical-genetic approach to study G protein regulation of  $\beta$  cell function in vivo. *Proc. Natl. Acad. Sci. U. S. A.* **106**, 19197–19202 (2009).
  29. Magnus, C. J. *et al.* Chemical and genetic engineering of selective ion channel-ligand interactions. *Science* **333**, 1292–1296 (2011).
  30. Magnus, C. J. *et al.* Ultrapotent chemogenetics for research and potential clinical applications. *Science* **364**, (2019).
  31. Volgraf, M. *et al.* Allosteric control of an ionotropic glutamate receptor with an optical switch. *Nat. Chem. Biol.* **2**, 47–52 (2006).
  32. Broichhagen, J. *et al.* Orthogonal optical control of a G protein-coupled receptor with a SNAP-tethered photochromic ligand. *ACS Cent. Sci.* **1**, 383–393 (2015).
  33. Hüll, K., Morstein, J. & Trauner, D. In Vivo Photopharmacology. *Chem. Rev.* **118**, 10710–10747 (2018).
  34. Elling, C. E., Thirstrup, K., Holst, B. & Schwartz, T. W. Conversion of agonist site to metal-ion chelator site in the  $\beta$ 2-adrenergic receptor. *Proc. Natl. Acad. Sci. U. S. A.* **96**, 12322–12327 (1999).
  35. Holst, B., Elling, C. E. & Schwartz, T. W. Partial agonism through a zinc-ion

- switch constructed between transmembrane domains III and VII in the tachykinin NK1 receptor. *Mol. Pharmacol.* **58**, 263–270 (2000).
36. Kiyonaka, S. *et al.* Allosteric activation of membrane-bound glutamate receptors using coordination chemistry within living cells. *Nat. Chem.* **8**, 958–967 (2016).
37. Kubota, R., Kiyonaka, S., & Hamachi, I. On-cell coordination chemistry: Chemogenetic activation of membrane-bound glutamate receptors in living cells. *Meth. enzymol.* **622**, 411-430 (2019).

## Chapter 1

**Development of ligand-directed two-step labeling for rapid labeling of cell-surface AMPA receptors****Abstract**

AMPA receptor (AMPA) is a subtype of the ionotropic glutamate receptors, which mediates fast excitatory neurotransmission in the central nervous system. The number of AMPARs on the postsynaptic surface changes dramatically during synaptic plasticity, a cellular mechanism of memory and learning. Conventional biochemical and molecular biological approaches have been widely used to analyze trafficking of AMPARs. However, conflicting findings have been reported because of a lack of useful tools for analyzing endogenous AMPARs. Here, I develop a method for the rapid and selective labeling of endogenous AMPARs under physiological condition by ligand-directed two-step labeling combining LDAI chemistry and inverse-electron demand Diels-Alder (IEDDA) reaction. This method enabled to label various kind of chemical probes on AMPARs within five minutes under physiological condition.





**1-1, Introduction**

In the central nervous system, AMPA receptor (GluA1–4) mediate fast excitatory neurotransmission. Recent studies have revealed that AMPARs are constitutively cycled in and out of the postsynaptic membrane through endocytosis and exocytosis. The precise regulation of this process is critical for synaptic plasticity, which is the basis of learning and memory<sup>1,2</sup>. Thus, to understand the molecular mechanisms of learning and memory, it is critical to analyze the membrane localization and trafficking of AMPARs. Conventional biochemical and molecular biological approaches have been widely used to analyze localization and trafficking of AMPARs. However, it is difficult for these methods to analyze endogenous AMPAR dynamics without affecting cellular functions. Ideally, endogenously expressed AMPARs should be tagged with small chemical probes.

In situ chemical protein labeling is ideal for analyzing native proteins in live cells. Affinity-based protein labeling is a powerful technique for the selective modification of target proteins<sup>3-9</sup>. As a traceless affinity-based labeling method for cell-surface proteins, our group has reported ligand-directed acyl imidazole (LDAI) chemistry<sup>7,8</sup>. With this technique, small chemical probes including fluorophores are covalently attached to nucleophilic amino acid residues located near the ligand-binding site. Recently, our group have developed an AMPAR-selective LDAI reagent, termed “chemical AMPAR modification 2” (CAM2) reagents which allows us to label chemical probes to AMPARs endogenously expressed in cultured neurons or acutely prepared brain slices<sup>9</sup>. Although this technique is powerful for the selective modification of chemical probes to AMPARs, there are some restrictions for visualizing or analyzing cell-surface AMPARs. First, live cells need to be kept at low temperatures (e.g., 17 °C during CAM2 labeling (1–4 h) to suppress the internalization of labeled AMPARs<sup>10</sup>. Second, the neuronal culture medium needs to be exchanged for serum-free medium or buffered saline during labeling to decrease non-specific labeling of serum proteins such as albumin. The

relatively long-term exposure (1–4 h) to these non-physiological conditions may interfere with neuronal activity or survival<sup>11-13</sup>. Ideally, neurons should be kept under physiological conditions during chemical labeling.

In this chapter, I develop a method for the rapid and selective labeling of AMPARs under physiological temperature in culture medium by ligand-directed two-step labeling combining LDAI chemistry and inverse-electron demand Diels-Alder (IEDDA) reaction<sup>14-16</sup>.

## **1-2, Results and discussion**

### **1-2-1, Rapid labeling of surface AMPARs by ligand-directed two-step labeling.**

I propose a ligand-directed two-step labeling technique, which combines LDAI-based protein labeling with the bioorthogonal IEDDA reaction for the rapid and selective modification of chemical probes to cell-surface AMPARs. For the first step, a strained alkene is covalently attached to AMPARs using LDAI chemistry, where the acyl substitution reaction to nucleophilic amino acid residues is facilitated by selective ligand–protein recognition (first step in Fig. 1a).

Next, the labeled alkene group is rapidly modified with tetrazine-conjugated probes (Tz-probes) on the cell-surface, as a result of the high selectivity and high reaction rate of the IEDDA reaction (second step in Fig. 1a). For the selective labeling of a strained alkene to AMPARs in the first step, I designed a CAM2 reagent bearing *trans*-cyclooctene (TCO), which I termed CAM2(TCO) (Fig. 1b). TCO was selected as the strained alkene because of its extremely fast cycloaddition kinetics in the IEDDA reaction. Compared with the original CAM2 reagents (e.g., CAM2(Ax488)) that bear aromatic fluorophores (see Fig. 2a, b), an ethylene glycol linker is added between the reactive acyl imidazole unit and the TCO group in CAM2(TCO) to increase its hydrophilicity. Hydrophobic or aromatic groups have high affinity to albumin abundantly contained in serum<sup>17</sup>; therefore, this improvement decreases the undesired

labeling of albumin, which allows the chemical labeling of AMPARs to be conducted in cell culture medium containing serum or substitutes. In addition, the first labeling is conducted at a physiological temperature (37 °C). Although some of the labeled AMPARs are likely to be internalized in this condition, this is not problematic with the two-step labeling technique. This is because the chemical probes are selectively tethered to cell-surface AMPARs in the second step reaction (Fig. 1d).

Regarding the second step (the IEDDA reaction), the reaction rate is highly dependent on the chemical structure of the tetrazine group. I selected monoaryl tetrazine, which has both a fast reaction rate and high bioorthogonality, and prepared cell impermeable Tz-probes bearing hydrophilic and anionic fluorophores or biotin for cell-surface labeling (Fig. 1c and Fig. 3). Shortening the reaction time of the probe labeling not only contributes to cell-surface specific labeling, but also decreases the adsorption of the chemical probes to cells, culture dishes, or coverslips. Moreover, some tetrazine-fluorophore conjugates have a “turn-on” response upon the IEDDA cycloaddition, which contributes to a high signal-to-noise (S/N) ratio in fluorescence imaging<sup>18-20</sup>.

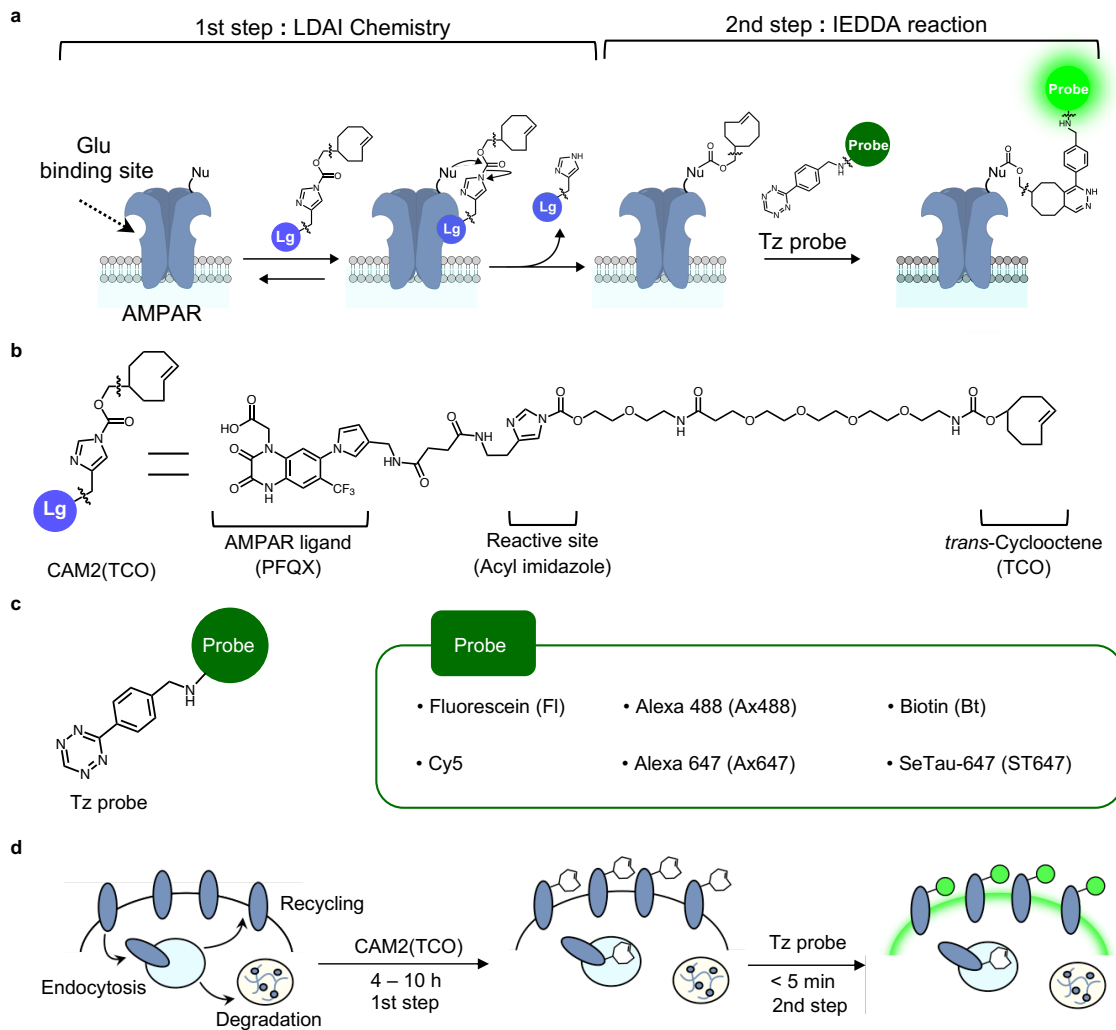


**Fig. 1 | Rapid labeling of cell-surface AMPARs by ligand-directed two-step labeling.** (a) Schematic illustration of the two-step labeling to AMPARs. In the 1st step, a strained alkene is covalently attached to AMPARs by LDAI chemistry. In the 2nd step, Tz probe is selectively tethered by IEDDA reaction. Lg, selective ligand for AMPARs; Nu, nucleophilic amino acid residue. Glu, glutamate. (b) Chemical structure of CAM2(TCO). (c) Chemical structure of Tz probes. The detailed chemical structures are shown in Fig. 3. (d) Schematic illustration of the two-step labeling in live cell.

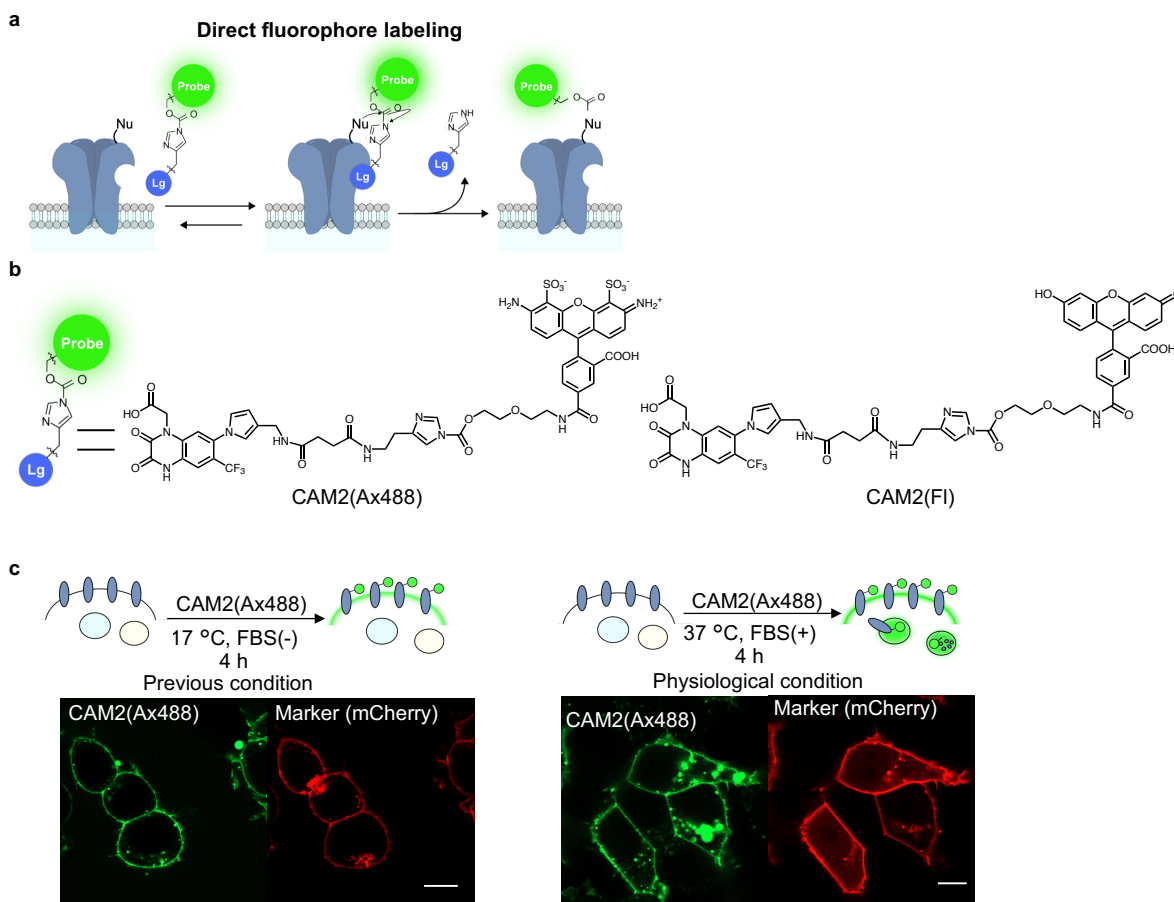


**Fig. 2 | Direct fluorophore labeling to AMPARs using CAM2(Ax488) or CAM2(FI) in HEK293T cells.** (a) Schematic illustration of direct fluorophore labeling to AMPARs using CAM2 reagent. Lg, selective ligand for AMPARs; Nu, nucleophilic amino acid residue. (b) Chemical structure of CAM2(Ax488) or CAM2(FI). (c) Confocal live imaging of the HEK293T cells labeled with 2  $\mu\text{M}$  CAM2(Ax488) under previous condition (in left) or under physiological cell culture condition (in right). In left, chemical labeling was conducted in serum-free medium at 17  $^{\circ}\text{C}$ . In right, chemical labeling was conducted in growth medium containing 10% FBS at 37  $^{\circ}\text{C}$ . mCherry-F was utilized as a transfection marker. Scale bars, 10  $\mu\text{m}$ .

## Chapter 1

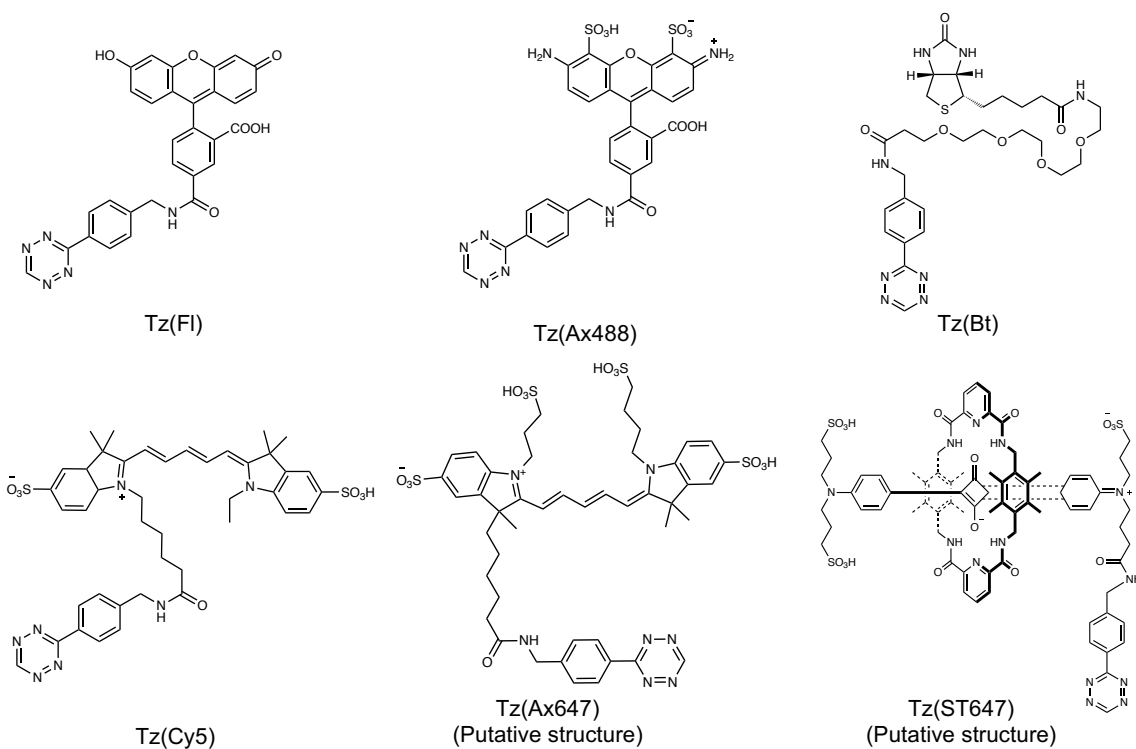


**Fig 3 | Detailed chemical structure of Tz probes.** Chemical structure of Tz(Fl), Tz(Ax488), Tz(Bt), Tz(Cy5), Tz(Ax647) and Tz(ST647) are shown.

### **1-2-2, Chemical labeling of surface AMPARs ectopically expressed in HEK293T cells.**

The designed two-step labeling method was initially examined in HEK293T cells transiently expressing GluA2, a main subunit of AMPARs. For the first step reaction, CAM2(TCO) was added to the culture medium, which included 10% fetal bovine serum (FBS), and the culture dish was incubated at 37 °C for 4 h. The second step reaction was performed for 5 min by adding membrane-impermeable Tz(FI) for fluorescein labeling on the cell-surface. As shown in Fig. 4a, western blotting of the cell lysate using anti-fluorescein (anti-FI) antibodies showed a strong band around 110 kDa (lane 1). This band was not observed in the cells co-treated with a competitive ligand (NBQX) or in any other control conditions (lanes 2–5). Furthermore, in the case of direct fluorescein labeling using the original CAM2(FI) under the same conditions (see Fig. 2b for its structure), there was a strong band around 70 kDa as well as the 110 kDa band (lanes 6–7 in Fig. 4a and Fig. 4b). The 70 kDa band, whose intensity did not change even in the presence of NBQX, corresponds to albumin contained in serum (for details, see Fig. 4a legend). These results therefore indicate the high selectivity of the two-step labeling technique using CAM2(TCO) compared with the original CAM2 (FI) under cell culture conditions. With regard to the molecular weight of the labeled band, the anti-FI signal corresponded to the highest signal among multiple bands that were detected using anti-GluA2/3 antibodies (Fig. 4c). The multiple GluA2 bands converged into a single lower band after treatment with peptide-*N*-glycosidase F (PNGase F), which is consistent with previous reports showing that GluA2 is highly glycosylated with *N*-linked sugars<sup>21</sup>. Importantly, in the PNGase F-treated samples, the shifted anti-GluA2 band merged with the anti-FI signal (Fig. 4c). These findings indicate that highly glycosylated GluA2 is selectively labeled using our methods. With regard to labeling efficacy, quantification of the remaining unlabeled GluA2 fraction showed that  $35 \pm 3\%$  of surface AMPARs were visualized in the two-step labeling (Fig. 5).

## *Chapter 1*

Moreover, AMPAR function was not visibly affected by the two-step labeling (Fig. 6), which is consistent with our previous analyses that showed minimal disturbance of AMPAR ion channel properties by CAM2 labeling<sup>9</sup>.



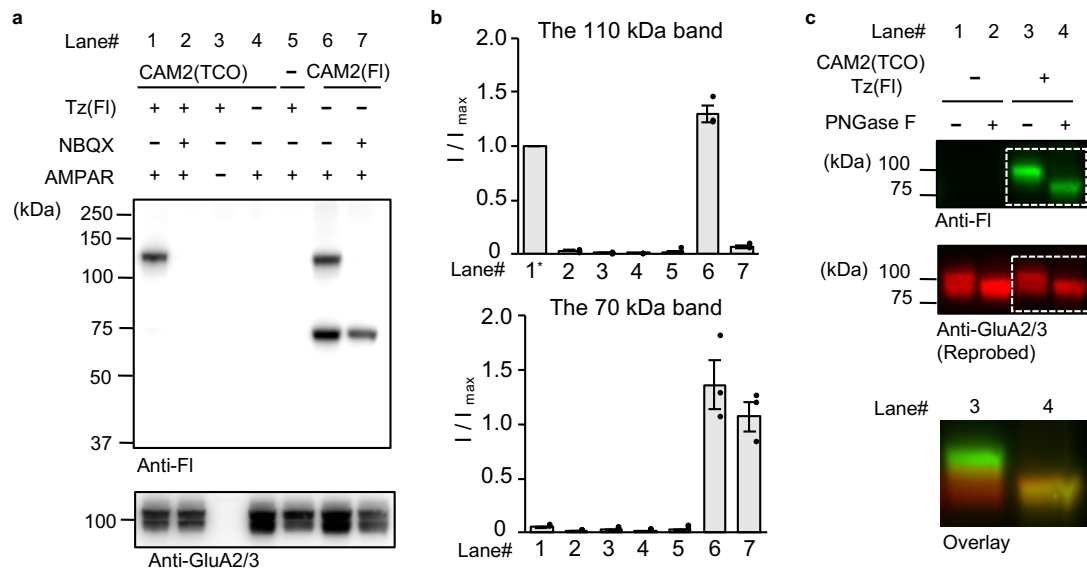


**Fig. 4 | The two-step labeling of cell-surface AMPARs ectopically expressed in HEK293T cells. (a)** Western blotting analyses of HEK293T cells after the two-step labeling. HEK293T cells transfected with GluA2<sup>flip(Q)</sup> (AMPA(+)) or vector control (AMPA(-)) were treated with 2  $\mu$ M CAM2(TCO) for 4 h followed by the addition of 1  $\mu$ M Tz(FI) for 5 min, or treated with 2  $\mu$ M CAM2(FI) for 4 h in the presence or absence of 50  $\mu$ M NBQX in culture medium at 37 °C. The cell lysates were analyzed by western blotting using anti-fluorescein or anti-GluA2/3 antibody. When CAM2(FI) is added in serum free medium, strong bands around 70 kDa in lane #6 and #7 disappear (for details see ref.9). **(b)** Quantification of band intensity of the 110 kDa band and the 70 kDa band ( $n = 3$  biological replicates). For details, see Fig. 2a legend. Each band intensity was normalized with the intensity of the 110 kDa band at lane#1. Data are represented as mean  $\pm$  s.e.m. **(c)** Effects of PNGase F treatment on the western blotting of labeled AMPAR in HEK293T cells expressing GluA2. Lower image shows the overlay of anti-FI image and anti-GluA2/3 image for lane #3 and #4. Two-step labeling was conducted as described in **(a)**. PNGase F (1000 units/100  $\mu$ L) was added to the cell lysate. For details, see Methods section.

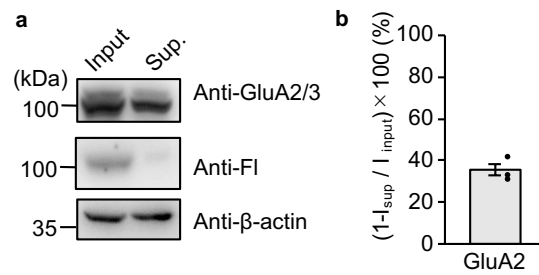


**Fig. 5 | Quantification of labeling efficiency of AMPARs on cell-surface by immunodepletion assay.** HEK293T cells expressing AMPARs were labeled with 2  $\mu$ M CAM2(TCO) for 4 h and 1  $\mu$ M Tz(FI) for 5 min at 37 °C. **(a)** Western blotting analyses of the cell lysate (Input) and supernatant (Sup.) after immunoprecipitation using anti-fluorescein antibody. Anti- $\beta$ -actin was utilized as a loading control. **(b)** Quantification of labeling efficiency from band intensity of Sup. and Input (n =3 biological replicates). Data are represented as mean  $\pm$  s.e.m.

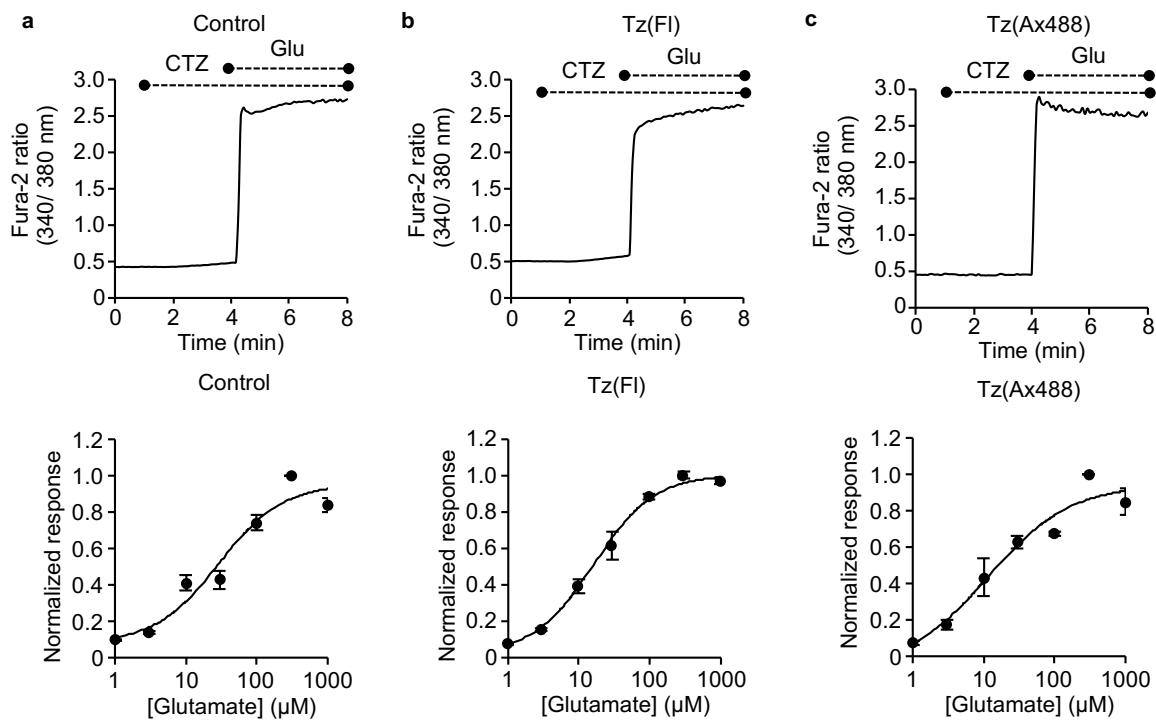


**Fig. 6 | Effects of the two-step labeling to AMPAR function.** HEK293T cells transfected with  $\text{Ca}^{2+}$ -permeable GluA2 ( $\text{GluA2}^{\text{Flip(Q)}}$ ) was labeled with  $2 \mu\text{M}$  of CAM2(TCO) for 4 h followed by the addition of  $1 \mu\text{M}$  Tz(Fl) in (b) or Tz(Ax488) in (c) for 5 min. The cells were subjected to intracellular  $\text{Ca}^{2+}$  concentration measurements by using a  $\text{Ca}^{2+}$  indicator, Fura-2. The cells not treated with CAM2(TCO) was utilized as the control in (a).  $100 \mu\text{M}$  cyclothiazide (CTZ) and each concentration of glutamate (Glu) were applied during periods indicated by bars, and  $[\text{Ca}^{2+}]_i$  changes (340/380 nm excitation fluorescence ratio; ratio(ex340/ex380)) evoked by Glu were measured. Left, representative trace of  $\text{Ca}^{2+}$  responses to  $1,000 \mu\text{M}$  Glu. Right, dose-response curves for Glu. ( $n = 3$  biological replicates). These results indicate that two-step labeling doesn't affect to AMPAR function. Data are represented as mean  $\pm$  s.e.m.

### **1-2-3, Visualization of surface AMPARs expressed in HEK293T cells.**

For visualizing fluorescently labeled AMPARs on the cell-surface, confocal microscopic live imaging was performed after the two-step labeling process under cell culture conditions. Here, Tz(Ax488) was used in the second step of labeling. Alexa 488 has bright fluorescence that is unaffected under endosomal acidic conditions; in contrast, fluorescein has weakened fluorescence under acidic conditions. Thus, Alexa 488 is more suitable to quantify the cellular distribution or trafficking of labeled AMPARs using fluorescent imaging. As shown in Fig. 7a, prominent fluorescence was observed exclusively from the cell-surface in cells co-transfected with mCherry-F, a membrane targeted transfection marker. In contrast, fluorescent signals were not observed in control conditions, such as in CAM2(TCO)-untreated or NBQX-co-treated cells (Fig. 8). In the case of direct Alexa 488 labeling using CAM2(Ax488) in the same cell culture conditions, labeled signals were observed not only from the cell-surface but also from the intracellular space (Fig. 2c). This suggests that the two-step labeling technique is superior for the fluorescent visualization of cell-surface AMPARs under cell culture conditions. I also determined the reaction kinetics of rapid fluorophore labeling of cell-surface AMPARs with the help of the turn-on fluorescent property of Tz(Ax488) upon the IEDDA reaction. Immediately after adding Tz(Ax488), prominent fluorescent signals were observed from the cells co-transfected with the transfection marker mCherry-F (Fig. 7b), and the fluorescent signals were saturated within 3 min. Thus, cell-surface AMPARs can be labeled by the fluorophore with fast kinetics. By taking advantage of the high bioorthogonality of the IEDDA reaction, cell-surface AMPARs were successfully labeled with various kinds of chemical probes, ranging from small molecules to middle-sized molecules such as SeTau-647, a squaraine rotaxane dye that has high photostability and a long fluorescence lifetime<sup>22,23</sup> (Fig. 3 and 9). This probe flexibility is another feature of the two-step labeling technique that is superior compared

with the direct labeling of probes using original CAM2 reagents, where each probe-tethered CAM2 needs to be synthesized (Fig. 2b).

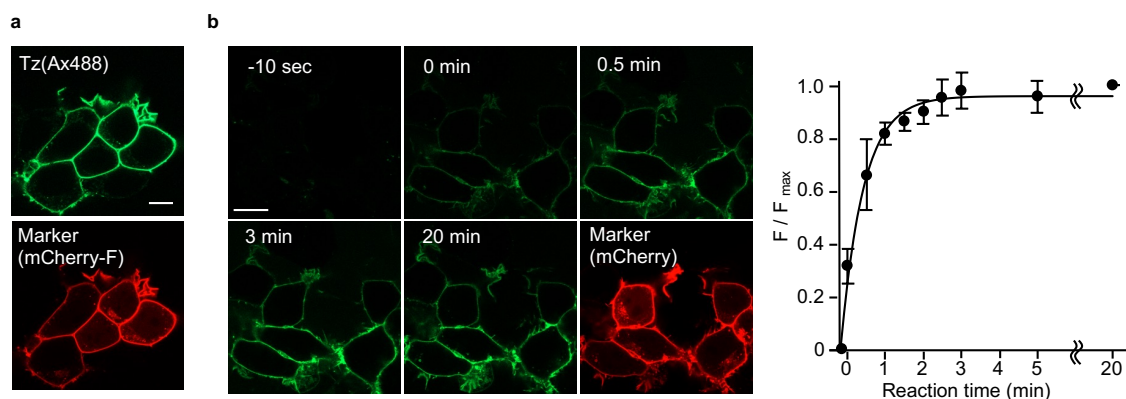


**Fig. 7 | Visualization of cell-surface AMPARs ectopically expressed in HEK293T cells. (a)** Confocal live imaging of the HEK293T cells labeled with 2  $\mu\text{M}$  CAM2(TCO) and 0.1  $\mu\text{M}$  Tz(Ax488). mCherry-F was utilized as a transfection marker. Scale bars, 10  $\mu\text{m}$ . **(b)** Reaction kinetics of tetrazine ligation on live cells by confocal live imaging of the HEK293T cells labeled with 2  $\mu\text{M}$  CAM2(TCO) after addition of 0.3  $\mu\text{M}$  Tz(Ax488) at 37  $^{\circ}\text{C}$ . In left, confocal images are shown. Scale bars, 20  $\mu\text{m}$ . In right, time-course of the fluorescent intensity of Alexa 488 is shown ( $n = 6$  cells). Data are represented as mean  $\pm$  s.e.m.

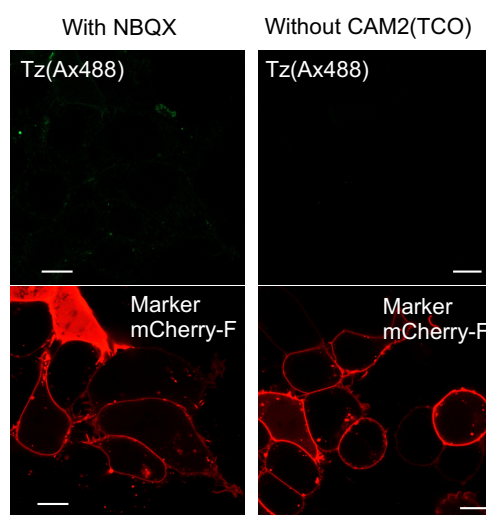


**Fig. 8 | Control experiment for the confocal live imaging of the HEK293T cells expressing AMPARs labeled with 2  $\mu\text{M}$  CAM2(TCO) and 0.1  $\mu\text{M}$  Tz(Ax488).** Copresence of 50  $\mu\text{M}$  NBQX or absence of CAM2(TCO) hampers fluorescent labeling to cell-surface AMPARs in the two-step labeling. See also Fig. 7a. mCherry-F was utilized as a transfection marker. [CAM2(TCO)] = 2  $\mu\text{M}$ , [Tz(Ax488)] = 0.1  $\mu\text{M}$ . Scale bars, 10  $\mu\text{m}$ .

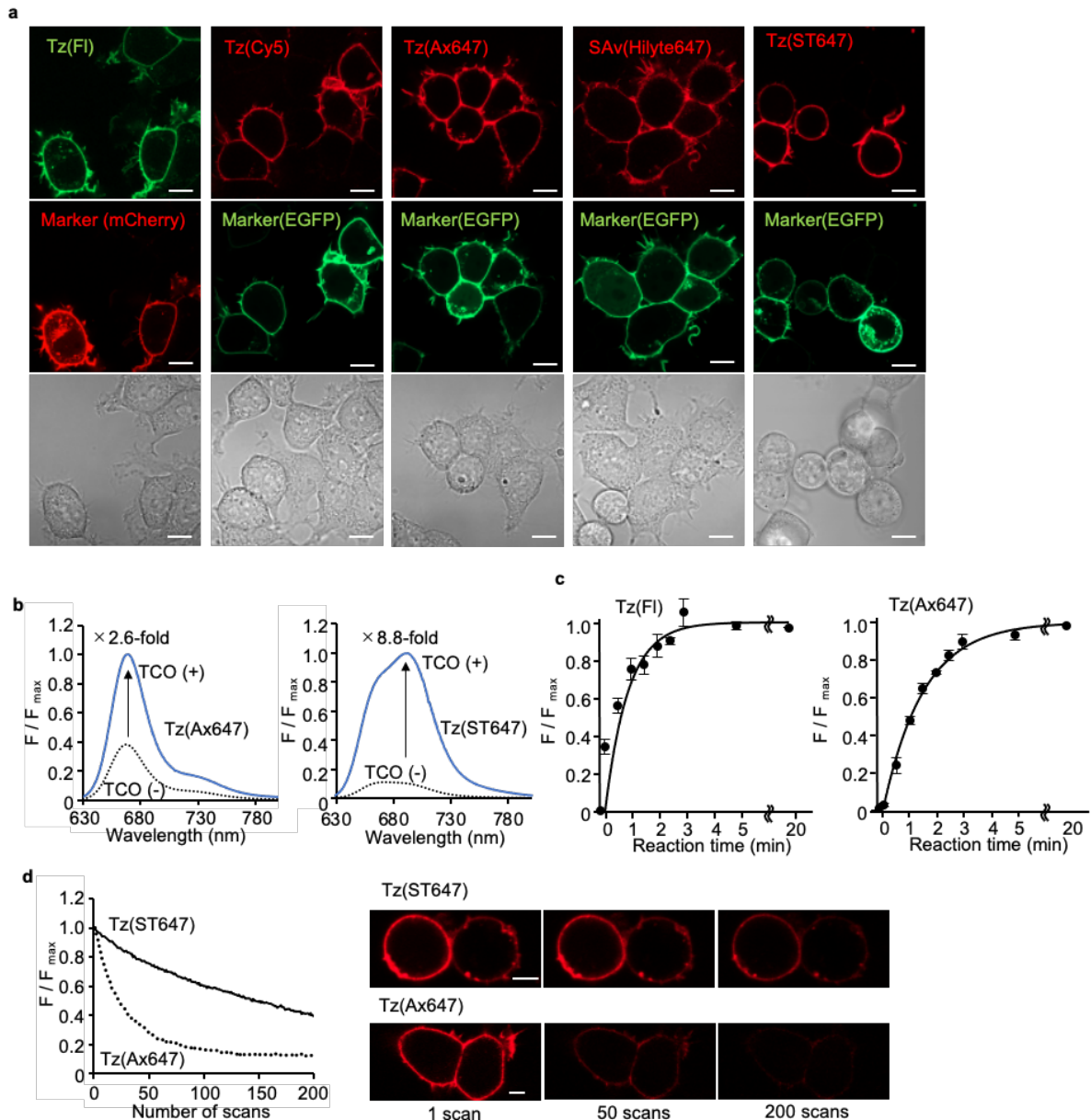


**Fig. 9 | Tethering various kinds of Tz-probes for visualization of cell-surface AMPARs in HEK293T cells. (a)** Confocal live imaging of the HEK293T cells labeled with 2  $\mu\text{M}$  CAM2(TCO) and 0.1  $\mu\text{M}$  of each Tz-probe. Labeling was conducted as described in Fig. 7a. In the case of the Tz(Bt) labeling, SAv(Hilyte647) was added for visualizing biotin labeled AMPARs. mCherry-F or EGFP-F was utilized as a transfection marker. Scale bars, 10  $\mu\text{m}$ . **(b)** Turn-on type fluorescent property of Tz(Ax647) or Tz(ST647) after addition of TCO-PEG4-COOH. Fluorescent spectra before and after addition of TCO-PEG4-COOH. [Tz(Ax647) or Tz(ST647)] = 0.1  $\mu\text{M}$ . [TCO-PEG4-COOH] = 1  $\mu\text{M}$ . e.x. = 610 nm. **(c)** Reaction kinetics of tetrazine ligation on live cells by confocal imaging of the HEK293T cells labeled with 2  $\mu\text{M}$  CAM2(TCO) after addition of 300 nM of Tz(Fl) or Tz(Ax647) at 37  $^{\circ}\text{C}$ . Time-course of the fluorescent intensity fluorescein and Alexa 647 are shown. (n = 3 biological replicates) **(d)** Photostability of SeTau-647 labeled to cell-surface AMPARs in

HEK293T cells. Photostability of SeTau-647 or Alexa 647 labeled to cell-surface AMPAR were evaluated by confocal live cell imaging. This result indicates that SeTau-647 has high photostability compared with Alexa 647. Scale bars, 5  $\mu\text{m}$ . Data are represented as mean  $\pm$  s.e.m.

### **1-3, Conclusion**

I developed ligand-directed two-step labeling method combining LDAI chemistry and IEEDA reaction. This method allowed to label various kind of chemical probes to surface AMPARs within 5 min. In the previous CAM2 labeling, fluorophores were directly labeled to cell-surface AMPARs using CAM2 reagents in serum-free medium at 17 °C. This non-physiological condition may affect the receptor function and induce cellular damage. In contrast, the present ligand-directed two-step labeling method enabled to label in the cell culture medium and physiological temperature. Thus, ligand-directed two-step labeling can be used to analyze trafficking of AMPARs even in vulnerable neurons for a long period.

## 1-4, Experimental Section

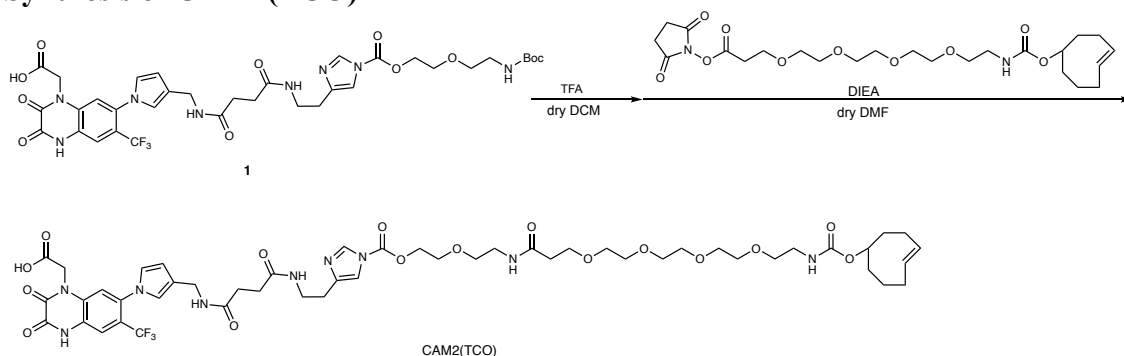
### Synthesis and Characterization

#### General materials and methods for organic synthesis

All chemical reagents and solvents were purchased from commercial sources (FUJIFILM Wako pure chemical, TCI chemical, Sigma-Aldrich, Sasaki Chemical) and were used without further purification. Thin layer chromatography (TLC) was performed on silica gel 60 F254 precoated aluminum sheets (Merck). Chromatographic purification was performed using flash column chromatography on silica gel 60 N (neutral, 40–50  $\mu\text{m}$ , Kanto Chemical).  $^1\text{H-NMR}$  spectra were recorded in deuterated solvents on a Varian Mercury 400 (400 MHz) or JEOL JNM-ECA (600 MHz). Chemical shifts were referenced to residual solvent peaks or tetramethylsilane ( $\delta = 0$  ppm). Multiplicities are abbreviated as follows: s = singlet, d = doublet, t = triplet, m = multiplet, brs = broad singlet. High resolution mass spectra were measured on an Exactive (Thermo Scientific) equipped with electron spray ionization (ESI). Reversed-phase HPLC (RP-HPLC) was carried out on a Hitachi Chromaster system equipped with a diode array, and an YMC Pack Triart C18 or ODS-A column.



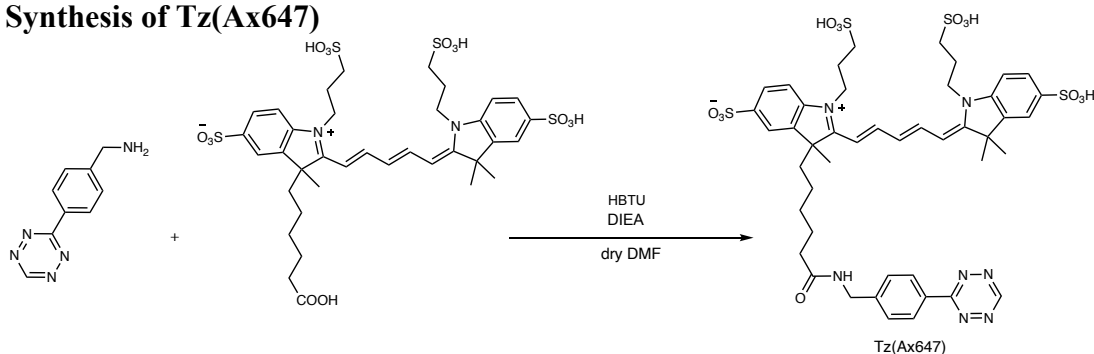
### Synthesis of CAM2(TCO)



A solution of **1**<sup>(ref.9)</sup> (6.0 mg, 7.4  $\mu\text{mol}$ ) and TFA (0.5 mL) in dry DCM (0.5 mL) was stirred at room temperature for 4 h under  $\text{N}_2$  atmosphere. After removal of the solvent by evaporation, the residual TFA was azeotropically removed with toluene ( $\times 3$ ). The crude was used for the next step without further purification. A solution of the crude, TCO-PEG4-NHS (5.0 mg, 9.7  $\mu\text{mol}$ ) and DIEA (10  $\mu\text{L}$ , 57  $\mu\text{mol}$ ) in dry DMF (0.5 mL) was stirred at room temperature for 13 h under  $\text{N}_2$  atmosphere. The reaction mixture was purified by RP-HPLC (ODS-A, 250 x 25 mm, mobile phase;  $\text{CH}_3\text{CN} : 10 \text{ mM AcONH}_4 \text{ aq.} = 10:90$  for 5 min to 50:50 until 60 min (linear gradient over 55 min), flow rate; 10 mL/min, detection; UV (220 nm)), giving CAM2(TCO) (2.4 mg, 3.9  $\mu\text{mol}$ , 53% yield in 2 steps) as a transparent oil.  $^1\text{H-NMR}$  (600 MHz,  $\text{CD}_3\text{OD}$ )  $\delta$  8.22 (s, 1H), 7.57 (s, 1H), 7.38 (s, 1H), 7.15 (s, 1H), 6.81 (s, 1H), 6.78 (s, 1H), 6.20 (m, 1H), 5.61-5.56 (m, 1H), 5.49-5.44 (m, 1H), 4.86 (s, 2H), 4.55 (m, 2H), 4.30 (m, 1H), 4.25 (s, 2H), 3.81 (m, 2H), 3.70 (t,  $J = 6.1 \text{ Hz}$ , 2H), 3.63-3.58 (m, 14H), 3.50 (t,  $J = 6.8 \text{ Hz}$ , 2H), 3.42 (t,  $J = 7.2 \text{ Hz}$ , 2H), 3.37 (t,  $J = 7.2 \text{ Hz}$ , 2H), 3.24 (m, 2H), 2.72 (t,  $J = 7.2 \text{ Hz}$ , 2H), 2.49-2.48 (m, 4H), 2.42 (t,  $J = 6.3 \text{ Hz}$ , 2H), 2.34 (m, 3H), 1.98-1.89 (m, 4H), 1.72-1.58 (m, 3H).  $^{13}\text{C-NMR}$  (150 MHz,  $\text{CD}_3\text{OD}$ )  $\delta$  174.67 (s, 1C), 174.09 (m, 2C), 158.66 (s, 1C), 157.36 (s, 1C), 149.80 (s, 1C), 138.51 (s, 1C), 136.07 (s, 1C), 135.96 (s, 1C), 133.75 (s, 1C), 131.63 (s, 1C), 130.74 (s, 1C), 127.47 (s, 1C), 126.52 (s, 1C), 126.49 (s, 1C), 125.12 (s, 1C), 125.02 (s, 1C), 123.36 (s, 1C), 122.91 (s, 1C), 117.76 (s, 1C), 115.44 (2C), 110.45 (s, 1C), 81.7 (s, 1C), 71.55 (2H), 71.51 (s, 1C), 71.43 (s, 1C),

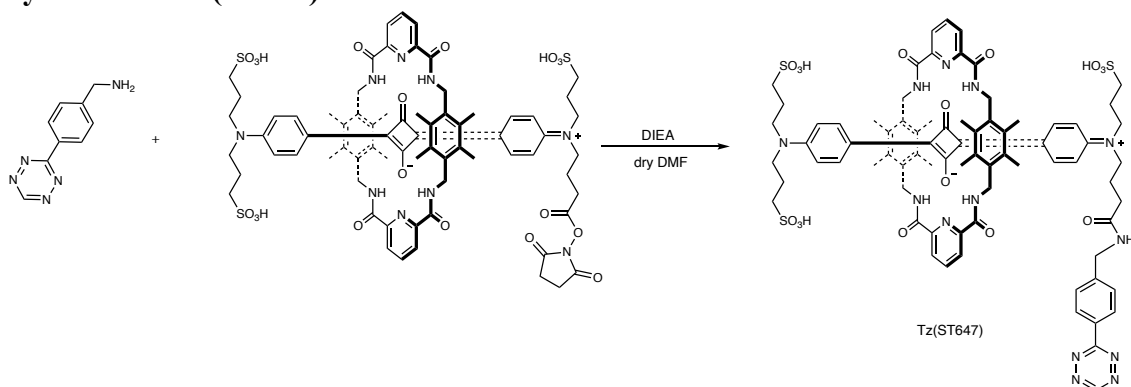
71.33 (s, 1C), 71.25 (s, 1C), 71.03 (s, 1C), 70.58 (s, 1C), 69.40 (s, 1C), 68.46 (s, 1C), 68.26 (s, 1C), 42.24 (s, 1C), 41.61 (s, 1C), 40.31 (s, 1C), 39.74 (s, 1C), 39.66 (s, 1C), 37.58 (s, 1C), 37.26 (s, 1C), 35.19 (s, 1C), 33.50 (s, 1C), 32.53 (s, 1C), 32.42 (s, 1C), 32.19 (s, 1C), 28.73 (s, 1C). HR-ESI MS  $m/z$  calcd for  $[M+H]^+$  1106.4652, found 1106.4627.

### Synthesis of Tz(Ax647)



A solution of Alexa647 Carboxylic Acid (2.0 mg, 1.8  $\mu\text{mol}$ ), tetrazine benzylamine (1.2 mg, 5.3  $\mu\text{mol}$ ), HBTU (1.2 mg, 3.1  $\mu\text{mol}$ ) and DIEA (2.4  $\mu\text{L}$ , 14  $\mu\text{mol}$ ) in dry DMF (0.4 mL) was stirred at room temperature for 10 h under  $\text{N}_2$  atmosphere. The reaction mixture was purified by RP-HPLC (ODS-A, 250 x 25 mm, mobile phase;  $\text{CH}_3\text{CN} : 10 \text{ mM AcONH}_4 \text{ aq.} = 5:95$  for 5 min to 50:50 until 60 min (linear gradient over 55 min) , flow rate; 10 mL/min, detection; UV (220 nm)), giving Tz(Ax647) (0.8 mg, 0.15  $\mu\text{mol}$ , 28%) as a blue solid. HR-ESI MS  $m/z$  calcd for  $[M]^+$  1028.2657, found 1028.2659.

### Synthesis of Tz(ST647)



A solution of SeTau-647-NHS (1.0 mg, 0.54  $\mu\text{mol}$ ), tetrazine benzylamine (0.36 mg, 1.62  $\mu\text{mol}$ ) and DIEA (10  $\mu\text{L}$ , 57  $\mu\text{mol}$ ) in dry DMF (1 mL) was stirred at room temperature for 3 h under  $\text{N}_2$  atmosphere. The reaction mixture was purified by RP-HPLC (ODS-A, 250 x 10 mm, mobile phase;  $\text{CH}_3\text{CN}$  : 10 mM  $\text{AcONH}_4$  aq. = 5:95 to 50:50 (linear gradient over 60 min) , flow rate; 3.0 mL/min, detection; UV (220 nm)), giving Tz(ST647) (0.3 mg, 0.15  $\mu\text{mol}$ , 28%) as a dark green solid HR-ESI MS  $m/z$  calcd for  $[\text{M}-3\text{H}]^{3-}$  509.5060, found 509.5061.

### **General methods for biochemical and biological experiments.**

SDS-PAGE and western blotting were carried out using a BIO-RAD Mini-Protean III electrophoresis apparatus. Samples were applied to SDS-PAGE and electrotransferred onto polyvinylidene fluoride membranes (BIO-RAD), followed by blocking with 5% nonfat dry milk in Tris-buffered saline containing 0.05% Tween 20. Primary antibody was indicated in each experimental procedure, and anti-rabbit IgG-HRP conjugate (CST, 7074S, 1:3,000) or anti-mouse IgG-HRP conjugate (CST, 7076S, 1:3,000) was utilized as the secondary antibody. Chemiluminescent signals generated with ECL Prime (GE Healthcare) were detected with a Fusion Solo S imaging system (Vilber Lourmat).

### **Expression of AMPARs in HEK293T cells.**

HEK293T cells (ATCC) were cultured in Dulbecco's modified Eagle's medium (DMEM)-GlutaMAX (Invitrogen) supplemented with 10% dialyzed FBS (Invitrogen), penicillin (100 units/ml), and streptomycin (100  $\mu\text{g}/\text{ml}$ ), and incubated in a 5%  $\text{CO}_2$  humidified chamber at 37  $^\circ\text{C}$ . Cells were transfected with a plasmid encoding rat GluA2 ( $\text{GluA2}^{\text{flip(Q)}}$ ) or the control vector pCAGGS (kindly provided by Dr. H. Niwa from RIKEN) using Lipofectamine 2000 (Invitrogen) according to the manufacturer's instructions, and subjected to labeling experiments after 36–48 h of the transfection.

**Confocal live cell imaging of AMPARs labeled by CAM2(Ax488).**

HEK293T cells were co-transfected with GluA2<sup>flip</sup>(Q) and mCherry-F as a transfection marker. GluA2-expressing HEK293T cells were treated with 2  $\mu$ M CAM2(Ax488) in serum free DMEM-GlutaMAX at 17 °C or DMEM-GlutaMAX supplemented with 10% dialyzed FBS at 37 °C for 4 h. The cells were washed 3 times with HBS. Confocal live imaging was performed with a confocal microscope (LSM900, Carl Zeiss) equipped with a 63 $\times$ , numerical aperture (NA) = 1.4 oil-immersion objective. Fluorescence images were acquired by excitation at 405, 488, 561, or 640 nm derived from diode lasers.

**Two-step labeling of AMPARs in HEK293T cells.**

For the first step labeling of AMPARs, HEK293T cells transfected with GluA2 were treated with 2  $\mu$ M CAM2(TCO) in the absence or presence of 50  $\mu$ M NBQX in the culture medium at 37 °C for 4 h. For the second step labeling, the culture medium was removed, and 1  $\mu$ M Tz(F1) in PBS was added for 5 min at room temperature. To quench excess Tz(F1), 1  $\mu$ M TCO-PEG4-COOH in PBS was added.

For western blot analyses of labeled AMPARs, labeled cells were washed three times with PBS, lysed with radio immunoprecipitation assay (RIPA) buffer containing 1% protease inhibitor cocktail (Nacalai tesque), and mixed with 5 $\times$  Laemmli sample buffer containing 250 mM DTT. Western blotting analyses were performed as described in “General methods for biochemical and biological experiments.” The F1-labeled GluA2 was detected using rabbit anti-fluorescein antibody (abcam, ab19491, 1:3,000). GluA2 was detected using a rabbit anti-GluA2/3 antibody (Millipore, 07-598, 1:3,000).

CAM2(TCO) and Tz-probes were stored in DMSO solution. The stock solutions were kept in deep freezer (–80 °C) to prevent decomposition.

**Enzymatic deglycosylation of AMPARs expressed in HEK293T cells.**

GluA2 expressing HEK293T cells were labeled as described in “Two-step labeling of AMPARs in HEK293T cells.” The labeled cells were washed three times with PBS and lysed in PBS containing 1% triton X-100, 0.6% SDS, and 1% protease inhibitor cocktail for 30 min at 37 °C. The lysates were diluted (2.0-fold) in sodium phosphate buffer (50 mM, pH 7.5) containing 2% NP40 and 100 mM DTT. PNGase F (New England Biolabs) were used at 1,000 units/100  $\mu$ L of lysate and incubated overnight at 37 °C. The samples were subjected to western blotting analyses as described in “Two-step labeling of AMPARs in HEK293T cells.” In this experiment, after western blotting using anti-F1 antibody, the membrane was stripped with stripping buffer (250 mM glycine (pH = 2.5) and 1% SDS) and reprobed with the anti-GluA2/3 antibody

**Immunodepletion assays for quantifying labeling efficiency in HEK293T cells.**

GluA2 expressing HEK293T cells were labeled as described in “Two-step labeling of AMPARs in HEK293T cells.” The labeled cells were lysed by RIPA buffer without SDS. Anti-fluorescein antibody (abcam, ab19491, 1:50) was added for 3-4 h at 4 °C and centrifuged (1,200 g, 4 °C) for 10 min. A small portion of the supernatant was collected as the input. Protein A Sepharose (abcam, ab193256) (0.5  $\mu$ L/ $\mu$ L of lysate) was added to the supernatant and incubated at 4 °C overnight. Resins were then pelleted by centrifugation (500 g, 4 °C) for 5 min and the supernatant was collected. The labeling efficacy was determined by western blotting analysis. The target bands were manually selected, and the intensity were calculated with ImageJ software, background intensity was manually subtracted by selecting a region with no bands around the target bands. The labeling efficacy were calculated from band intensity of Sup. and input. The immunodetection of  $\beta$ -actin was performed with a mouse anti- $\beta$ -actin antibody (Abcam, ab8226, 1:3,000) and anti-mouse IgG HRP (CST, 7074S, 1:3,000). The immunodetection of F1-labeled GluA2 was performed with a rabbit anti-fluorescein antibody (abcam, ab19491, 1:3,000) and VeriBlot for IP Detection Reagent

## *Chapter 1*

HRP-conjugated (abcam, ab131366, 1:500). The immunodetection of GluA2 was performed with a rabbit anti-GluA2/3 antibody (Millipore, 07-598, 1:3,000) and VeriBlot for IP Detection Reagent HRP-conjugated (abcam, ab131366, 1:500).

### **Fluorescence Ca<sup>2+</sup> imaging.**

HEK293T cells transfected Ca<sup>2+</sup>-permeable GluA2 (GluA2<sup>flip(Q)</sup>) were labeled with 2  $\mu$ M of CAM2(TCO) in the culture medium at 37 °C for 4 h. The labeled cells were loaded with the 5  $\mu$ M calcium-indicator Fura-2 AM(Dojindo) for 20 min in the culture medium and then 1  $\mu$ M Tz(Fl) or Tz(Ax488) was treated for 5 min in HBS at room temperature. The cells not labeled was utilized as the control. For the fluorescence Ca<sup>2+</sup> imaging, 100  $\mu$ M CTZ (TCI) was added to the cells before the addition of glutamate to block the desensitization. Fluorescence images were obtained using fluorescence microscope (IX71, Olympus) equipped with a 20 $\times$  objective, complementary metal-oxide semiconductor (CMOS) camera (ORCA-flash 4.0, Hamamatsu Photonics) under xenon-lamp illumination, and analyzed with a video imaging system (AQUACOSMOS, Hamamatsu Photonics) according to the manufacture's protocol. The cells were alternately excited with 340 and 380 nm light, and the emitted fluorescence ratio of 340/380 nm was determined from the images.

### **Confocal live cell imaging of labeled AMPARs in HEK293T cells.**

HEK293T cells were co-transfected with GluA2<sup>flip(Q)</sup> and mCherry-F as a transfection marker. First step labeling was performed as describe in "Two-step labeling of AMPARs in HEK293T cells." For the second step labeling, after removal of the culture medium, 100 nM Tz(Ax488) was treated for 5 min in HBS (20 mM HEPES, 107 mM NaCl, 6 mM KCl, 2 mM CaCl<sub>2</sub>, and 1.2 mM MgSO<sub>4</sub> at pH 7.4) at room temperature and washed three times with HBS. Confocal live imaging was performed with a confocal microscope (LSM900, Carl Zeiss) equipped with a 63 $\times$ , numerical aperture

(NA) = 1.4 oil-immersion objective. Fluorescence images were acquired by excitation at 405, 488, 561, or 640 nm derived from diode lasers.

For studying the reaction kinetics of tetrazine ligation to cell-surface AMPARs, after first step labeling, cells were then incubated with 300 nM Tz(Ax488) at room temperature and imaged at specified time points by confocal microscopy. To quantify the fluorescence intensity of the membrane at each time point, mCherry-F positive cells ( $n = 6$ ) were selected and the average signal intensity of ROIs set on the membrane was calculated by ZEN blue software (Carl Zeiss). After subtracting background fluorescence, the averaged membrane intensity was defined as  $F$  at each time point ( $F_{MAX}$  was defined as  $F$  at 20 min). The membrane intensity was fitted with KaleidaGraph (Synergy software) using following equation (1):  $F = a + b(1 - e^{-ct})$ .

#### **Fluorescent spectra measurements.**

Fluorescence spectra were measured with a Shimadzu RF-6000 fluorescence spectrometer using a quartz cell with  $0.2 \times 1.0$  cm path length at excitation wavelengths of 610 nm (for Alexa 647 and SeTau-647) at room temperature. Tz probes were dissolved in PBS at a concentration of 100 nM and their fluorescence was measured (TCO(-)). Subsequently, a 10-fold excess of TCO-PEG4-COOH was added into the quartz cell and incubated for 10 min at room temperature, after which the fluorescence spectrum was measured (TCO(+)).

#### **Comparison of photostability between Ax647 and ST647 labeled on AMPARs.**

For photostability study of Ax647 and ST647 labeled on AMPARs, HEK293T cells were co-transfected with GluA2 and EGFP-F as a transfection marker. GluA2-expressing HEK293T cells were treated with 2  $\mu$ M CAM2(TCO) in the culture medium at 37 °C for 4 h. After removal of the culture medium, 100 nM Tz(Ax647) or Tz(ST647) was treated for 5 min in HBS at room temperature and washed 3 times with

HBS. Confocal live imaging was performed with a confocal microscope. Fluorescence images were acquired by excitation at 640 nm for Alexa 647 and SeTau-647 derived from diode lasers (laser power: 20.0%).

### Statistics and reproducibility.

All graphs were generated using Microsoft Excel. All data are expressed as mean  $\pm$  s.e.m. I accumulated the data for each condition from at least three independent experiments. I evaluated statistical significance with Student's *t*-test for comparisons between two mean values. A value of  $P < 0.05$  was considered significant.

### 1-5, Reference

1. Brecht, D. S. & Nicoll, R. A. AMPA receptor trafficking at excitatory synapses. *Neuron* **40**, 361–379 (2003).
2. Diering, G. H. & Huganir, R. L. The AMPA receptor code of synaptic plasticity. *Neuron* **100**, 314–329 (2018).
3. Cravatt, B. F., Wright, A. T. & Kozarich, J. W. Activity-based protein profiling: from enzyme chemistry to proteomic chemistry. *Annu. Rev. Biochem.* **77**, 383–414 (2008).
4. Fehrentz, T., Schönberger, M. & Trauner, D. Optochemical genetics. *Angew. Chem. Int. Ed.* **50**, 12156–12182 (2011).
5. Tsukiji, S., Miyagawa, M., Takaoka, Y., Tamura, T. & Hamachi, I. Ligand-directed tosyl chemistry for protein labeling in vivo. *Nat. Chem. Biol.* **5**, 341–343 (2009).
6. Tamura, T. *et al.* Rapid labelling and covalent inhibition of intracellular native proteins using ligand-directed *N*-acyl-*N*-alkyl sulfonamide. *Nat. Commun.* **9**, 1870 (2018).
7. Fujishima, S. H., Yasui, R., Miki, T., Ojida, A. & Hamachi, I. Ligand-directed acyl imidazole chemistry for labeling of membrane-bound proteins on live cells. *J. Am.*



- Chem. Soc.* **134**, 3961–3964 (2012).
8. Miki, T. *et al.* LDAI-based chemical labeling of intact membrane proteins and its pulse-chase analysis under live cell conditions. *Chem. Biol.* **21**, 1013–1022 (2014).
  9. Wakayama, S. *et al.* Chemical labelling for visualizing native AMPA receptors in live neurons. *Nat. Commun.* **8**, 14850 (2017).
  10. Sekine-Aizawa, Y. & Huganir, R. L. Imaging of receptor trafficking by using  $\alpha$ -bungarotoxin-binding-site- tagged receptors. *Proc. Natl. Acad. Sci. U. S. A.* **101**, 17114–17119 (2004).
  11. Kanda, H. & Gu, J. G. Effects of cold temperatures on the excitability of rat trigeminal ganglion neurons that are not for cold sensing. *J. Neurochem.* **141**, 532–543 (2017).
  12. Taberero, A. *et al.* Albumin promotes neuronal survival by increasing the synthesis and release of glutamate. *J. Neurochem.* **81**, 881–891 (2002).
  13. Atabay, C., Cagnoli, C. M., Kharlamov, E., Ikonovic, M. D. & Manev, H. Removal of serum from primary cultures of cerebellar granule neurons induces oxidative stress and DNA fragmentation: Protection with antioxidants and glutamate receptor antagonists. *J. Neurosci. Res.* **43**, 465–475 (1996).
  14. Blackman, M. L., Royzen, M. & Fox, J. M. Tetrazine ligation: Fast bioconjugation based on inverse-electron-demand Diels-Alder reactivity. *J. Am. Chem. Soc.* **130**, 13518–13519 (2008).
  15. Devaraj, N. K., Weissleder, R. & Hilderbrand, S. A. Tetrazine-based cycloadditions: Application to pretargeted live cell imaging. *Bioconjug. Chem.* **19**, 2297–2299 (2008).
  16. Oliveira, B. L., Guo, Z. & Bernardes, G. J. L. Inverse electron demand Diels-Alder reactions in chemical biology. *Chem. Soc. Rev.* **46**, 4895–4950 (2017).
  17. Ritchie, T. J. & Macdonald, S. J. F. The impact of aromatic ring count on compound developability - are too many aromatic rings a liability in drug design?

- Drug Discov. Today* **14**, 1011–1020 (2009).
18. Devaraj, N. K., Hilderbrand, S., Upadhyay, R., Mazitschek, R. & Weissleder, R. Bioorthogonal turn-on probes for imaging small molecules inside living cells. *Angew. Chem. Int. Ed.* **49**, 2869–2872 (2010).
  19. Liu, D. S. *et al.* Diels-alder cycloaddition for fluorophore targeting to specific proteins inside living cells. *J. Am. Chem. Soc.* **134**, 792–795 (2012).
  20. Beliu, G. *et al.* Bioorthogonal labeling with tetrazine-dyes for super-resolution microscopy. *Commun. Biol.* **2**, 261 (2019).
  21. Takeuchi, Y., Morise, J., Morita, I., Takematsu, H. & Oka, S. Role of site-specific N-glycans expressed on GluA2 in the regulation of cell surface expression of AMPA-type glutamate receptors, *PLoS ONE* **10**, e0135644 (2015).
  22. Podgorski, K., Terpetschnig, E., Klochko, O. P., Obukhova, O. M. & Haas, K. Ultra-bright and -stable red and near-infrared squaraine fluorophores for in vivo two-photon imaging. *PLoS One* **7**, (2012).
  23. Tsunoyama, T. A. *et al.* Super-long single-molecule tracking reveals dynamic-anchorage-induced integrin function. *Nat. Chem. Biol.* **14**, 497–506 (2018).

## **Chapter 2**

### **Quantification of AMPA receptor trafficking by ligand-directed two-step labeling**

#### **Abstract**

In this chapter, I analyzed the distribution and trafficking of AMPARs by ligand-directed two-step labeling. This method reveals some features of AMPARs in neurons, such as a surface expression level in the synaptic and non-synaptic region, long lifetime compared with AMPARs expressed in HEK293T cells, and rapid recycling kinetics. By using this method, I succeeded in the analysis of endogenous surface-AMPARs distribution and trafficking under cell-friendly conditions, which was not possible with the conventional biochemical and molecular biological method. Thus, ligand-directed two-step labeling may be a versatile tool for investigating the physiological and pathophysiological roles of AMPARs in neurons.

## **2-1, Introduction**

To analyze membrane protein localizations and trafficking, biochemical approaches, such as surface biotinylation assays or related methods, have been widely used<sup>1-3</sup>. Although the biochemical methods are also powerful for the analysis of AMPAR trafficking, cell-surface proteins are randomly labeled with biotin using these methods. As a result, purification of biotin-labeled AMPAR is required, which hampers quantitative analyses of trafficking. In contrast, to selectively visualize glutamate receptors, fluorescent proteins are fused to the receptors using genetically encoded approaches. For example, a pH-sensitive variant of GFP (super-ecliptic pHluorin [SEP]) can be fused to the extracellular region of receptors to visualize cell-surface receptors in live neurons<sup>4,5</sup>. Instead of fluorescent proteins, protein tags such as SNAP- or Halo-tags are fused to the receptors for the covalent labeling of small chemical probes at the time that the probes are added<sup>6-8</sup>. The downsizing of these protein tags has been successfully demonstrated by using a short peptide tag (1–3 kDa) and its probe pair<sup>9-11</sup>. More recently, genetic code expansion in combination with bioorthogonal click chemistry has been reported for the fluorescent labeling of glutamate receptors in HEK293T cells, in which chemical probes are covalently attached to the side chain of an unnatural amino acid residue<sup>12,13</sup>. These genetically encoded approaches have been widely used in trafficking studies of AMPARs. However, in most cases, these methods largely rely on the overexpression of target AMPAR subunits. Given the formation of hetero tetramers consisting of different subunits in AMPARs, the overexpression of a single AMPAR subunit may interfere with the localization and/or trafficking of native AMPARs in neurons.

To overcome these limitations, I analyzed the localization and trafficking of endogenous AMPARs cell-friendly conditions by ligand-directed two-step labeling.

## 2-2, Results and discussion

### 2-2-1, Analyses of AMPAR trafficking in HEK293T cells.

Once I had a potential labeling method for cell-surface AMPARs under cell culture conditions, I analyzed receptor trafficking using both live imaging and biochemical approaches. First, I analyzed cell-surface AMPAR trafficking in HEK293T cells using confocal live imaging. After incubating the cells with CAM2(TCO) under physiological temperature in culture medium, Tz(Ax488) was added to the culture medium to selectively visualize cell-surface AMPARs and cells were incubated for each period (0–8 h) (Fig. 1a). As shown in Fig. 1b, the labeled fluorescence on the cell-surface decreased after incubation at 37 °C. Fluorescent granules were instead observed in the intracellular area, and most of the fluorescent signals were from intracellular granules after 8 h of incubation. The half-time of cell-surface AMPARs ( $t_{1/2}^{\text{surface}}$ ), which includes both the remaining and recycled fractions, was calculated to be  $5.7 \pm 0.7$  h from the fluorescent intensity on the cell-surface (Fig. 1b). In addition, the intracellular punctate signals merged with a fluorescent lysosome marker (LysoTracker) after 8 h of incubation, suggesting that internalized AMPARs were transported to lysosomes (Fig. 1c). Quantitative analyses of the fates of cell-surface AMPARs were examined using biochemical approaches. To quantify the  $t_{1/2}^{\text{surface}}$  of AMPARs, HEK293T cells were incubated for each period (0–36 h) after treatment with CAM2(TCO) (path-1 in Fig. 2a). Next, Tz(Fl) was added for the selective modification of fluorescein to cell-surface AMPARs. Using western blotting of the cell lysate, the  $t_{1/2}^{\text{surface}}$  of AMPARs was determined to be  $5.3 \pm 0.3$  h (Fig. 2b), which was similar to the value that was determined using confocal imaging (Fig. 1b). The half-time of the degradation ( $t_{1/2}^{\text{life}}$ ) of cell-surface receptors was evaluated by modifying the protocols, where Tz(Fl) was added after CAM2(TCO) labeling (path-2 in Fig. 2a). The cells were then incubated for each period (0–36 h), and the cell lysates were subjected to western blotting. As shown in Fig. 2c,  $t_{1/2}^{\text{life}}$  was determined to be  $8.1 \pm 0.7$  h, which was slightly longer than the

$t_{1/2}^{\text{surface}}$  of cell-surface AMPARs ( $p < 0.05$ ). Considering the colocalization of internalized AMPARs and lysosomes (Fig. 1c), the internalized AMPARs are likely decomposed via lysosomal degradation in HEK293T cells.

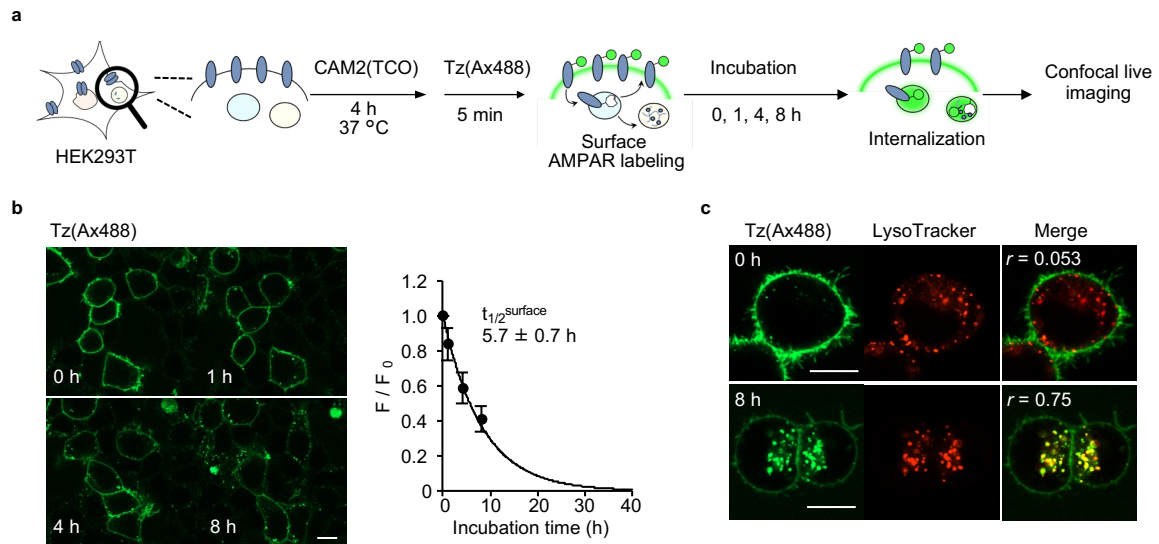


**Fig. 1 | Quantitative analyses of AMPAR trafficking in HEK293T cells using the two-step labeling under the physiological cell culture condition. (a)** Schematic illustration of trafficking analyses of cell-surface AMPARs by confocal microscopy. **(b)** Time-lapse confocal imaging of HEK293T cells after two-step labeling using CAM2(TCO) and Tz(Ax488). The HEK293T cells were transfected with GluA2<sup>flip(Q)</sup>. In left, confocal images are shown. Scale bars, 10  $\mu\text{m}$ . In right, time-course of the fluorescent intensity from the cell-surface is shown ( $n = 3$  biological replicates). [CAM2(TCO)] = 2  $\mu\text{M}$ , [Tz(Ax488)] = 0.1  $\mu\text{M}$ . **(c)** Co-staining of labeled AMPARs with LysoTracker<sup>TM</sup>. The labeled HEK293T cells were incubated with LysoTracker<sup>TM</sup> Red DND-99 immediately after Tz(Ax488) labeling (upper panel) or subsequent 8 h incubation at 37  $^{\circ}\text{C}$  (lower panel), and confocal live imaging was performed. Pearson's correlation coefficients ( $r$ ) are shown in the image. Scale bars, 10  $\mu\text{m}$ .

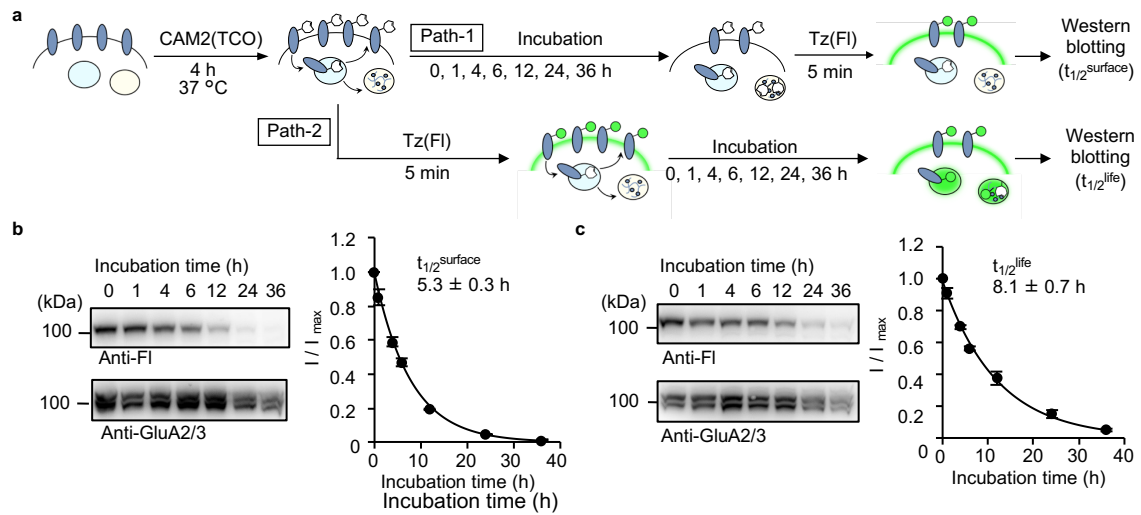


**Fig. 2 | Determination  $t_{1/2}^{surface}$  or  $t_{1/2}^{life}$  of AMPARs by western blotting.** (a) Schematic illustration of the procedure is shown. In (b) and (c),  $t_{1/2}^{surface}$  and  $t_{1/2}^{life}$  are determined, respectively. In left, representative results of western blotting are shown. In right, time-course of the labeled band is shown ( $n = 3$  biological replicates). [CAM2(TCO)] = 2  $\mu$ M, [Tz(Fl)] = 1  $\mu$ M.

**2-2-2, Analyses of AMPAR localization in HEK293T cells.**

I next determined the intracellular versus surface percentages of TCO-labeled AMPARs (TCO-AMPARs), which can provide valuable information regarding the fate of cell-surface AMPARs. To quantify these percentages, cell-surface AMPARs in HEK293T cells treated with CAM2(TCO) were selectively labeled with fluorescein by adding cell-impermeable Tz (Fl) to the medium under live cell conditions (path-1 in Fig. 3a). To label intracellular TCO-AMPARs, surface TCO-AMPARs were first masked with cell-impermeable Tz(Ax647) (path-2 in Fig. 3a). After lysis of the cells, Tz(Fl) was added to the cell lysate to label intracellular TCO-AMPARs. The whole-cell-labeling fraction, where both cell-surface and intracellular TCO-AMPARs were labeled with fluorescein, was prepared by adding Tz(Fl) after cell lysis (path-3 in Fig. 3a). Prior to these analyses, we first investigated whether the second step reaction using Tz(Fl) proceeds rapidly and/or selectively in cell lysate. Western blotting analyses revealed that the covalent modification of fluorescein was selective to AMPARs in cell lysate (Fig. 4), and the reaction was saturated after 15 min when either 0.1 or 0.3  $\mu$ M Tz(Fl) was added. The intracellular and cell-surface percentages of TCO-AMPARs after 4 h of incubation with CAM2(TCO) were analyzed using this protocol and determined to be  $4.1 \pm 0.9\%$  and  $94.4 \pm 3.3\%$ , respectively (Fig. 3b), indicating that intracellular TCO-AMPAR levels were quite low.



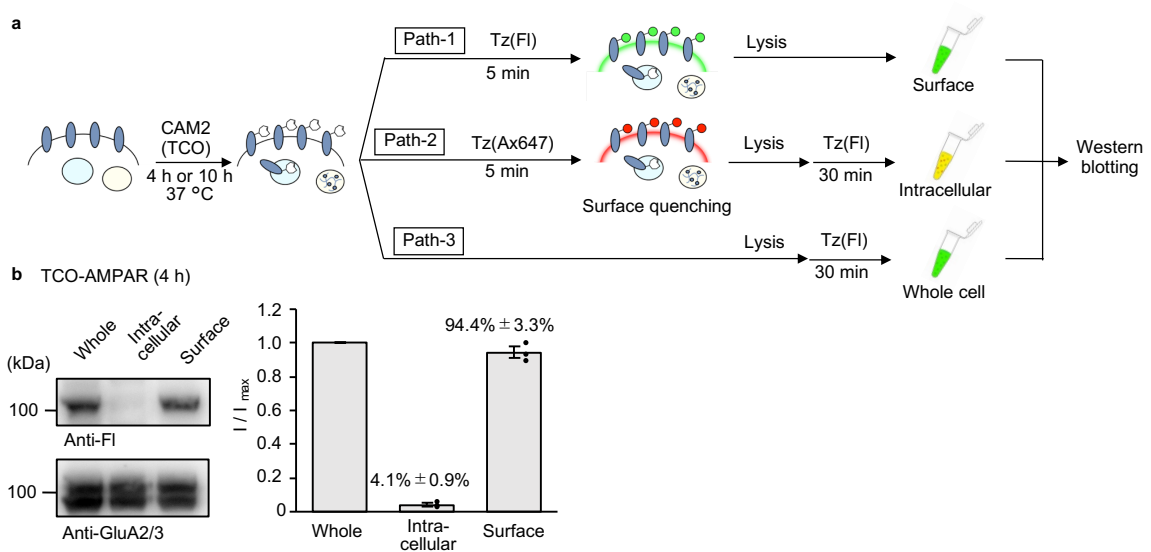


**Fig. 3 | Determination of TCO-labeled AMPARs on cell-surface, in intracellular area, or in whole-cell by western blotting. (a)** Schematic illustration of the procedure is shown. **(b)** Intracellular and surface ratio after CAM2(TCO) labeling for 4 h are determined. In left, representative results of western blotting are shown. In right, band intensities for cell-surface and intracellular labeling were analyzed, both of which were normalized by that for whole-cell labeling ( $n = 3$  biological replicates). [CAM2(TCO)] = 2  $\mu$ M, [Tz(Fl)] = 1  $\mu$ M. Data are represented as mean  $\pm$  s.e.m.

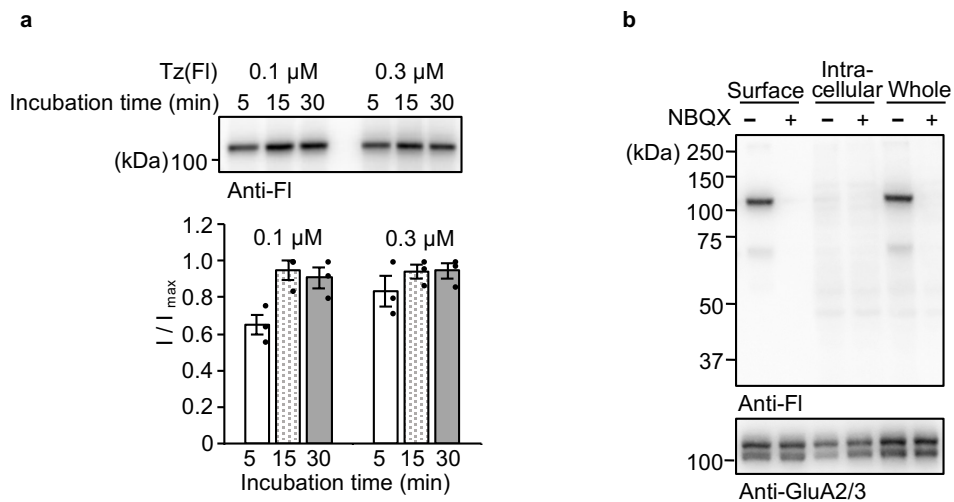


**Fig. 4 | Reaction kinetics of tetrazine ligation in cell lysates and a whole blot for surface, intracellular or whole-cell labeling in HEK293T cells. (a)** Reaction kinetics of tetrazine ligation in cell lysate evaluated by western blotting. After cell lysis of CAM2(TCO)-labeled HEK293T cells, each concentration of Tz(Fl) was added for 5, 15 or 30 min. Then, 10 μM TCO-PEG4-COOH was added for quenching Tz(Fl). This result indicates that the tetrazine ligation was saturated within 15 min (n =3 biological replicates). **(b)** Whole blot for surface, intracellular or whole-cell. The sample was prepared as described in Fig. 3b. Selective band corresponding to AMPAR was observed, which indicates high selectivity of the tetrazine ligation even in cell lysates. Data are represented as mean ± s.e.m

### 2-2-3, Rapid labeling of endogenous AMPARs in neurons.

I next examined the applicability of the bioorthogonal two-step labeling technique for the rapid modification of cell-surface AMPARs that are endogenously expressed in neurons. Primary cultured neurons from the cerebral cortex were incubated with CAM2(TCO) for 10 h under neuronal culture conditions, and Tz(FI) was then added for 5 min for cell-surface labeling. Western blotting analyses of the cell lysate showed a single strong band corresponding to the molecular weight of AMPARs (see lane 1 in Fig. 5a). This band was not detected in the co-presence of the competitive ligand NBQX, or in other control conditions (see lanes 2–4 in Fig. 5a). As observed with the AMPARs expressed in HEK293T cells, smeared bands were detected using anti-GluA2 antibodies; the anti-FI band corresponded to the highest band in the smeared anti-GluA2 signals. After the removal of *N*-linked sugars by PNGase treatment, the smeared anti-GluA2 bands converged into a single lower band, which merged with the anti-FI signal (Fig. 5b). These results suggest that the highly glycosylated fraction of endogenous AMPARs were selectively labeled with fluorescein by the rapid labeling. Among the AMPAR subunits (GluA1–4), GluA1, GluA2, and GluA3 are highly expressed in cultured cortical neurons<sup>14</sup>. I next examined the efficacy of our methods for visualizing tetrameric AMPARs by quantifying the remaining unlabeled GluA2 fraction. As shown in Fig. 6a,  $44 \pm 4\%$  of GluA2-containing AMPARs were recognized by the two-step labeling method. Similarly, I calculated that  $37 \pm 7\%$  of GluA1- and  $43 \pm 5\%$  of GluA3-containing AMPARs were recognized. However, considering the heterotetrameric formation of AMPAR subunits, we also needed to examine whether each subunit was covalently labeled with the probe or not. In this context, the immunoprecipitation assay in the denatured condition revealed that GluA2 and GluA3, but not GluA1, were covalently labeled with CAM2(TCO) (Fig. 6b). This selectivity is consistent with our previous results in HEK293T cells<sup>15</sup>. With regard to the efficacy of CAM2(TCO) labeling, the time-course of the labeling clearly indicated that chemical

labeling occurred more efficiently at 37 °C than in the previous condition at 17 °C (Fig. 7a). In addition, the concentration dependency of CAM2(TCO) revealed the EC<sub>50</sub> value ( $0.90 \pm 0.10 \mu\text{M}$ ) of two-step labeling at 37 °C in neurons (Fig. 7b).

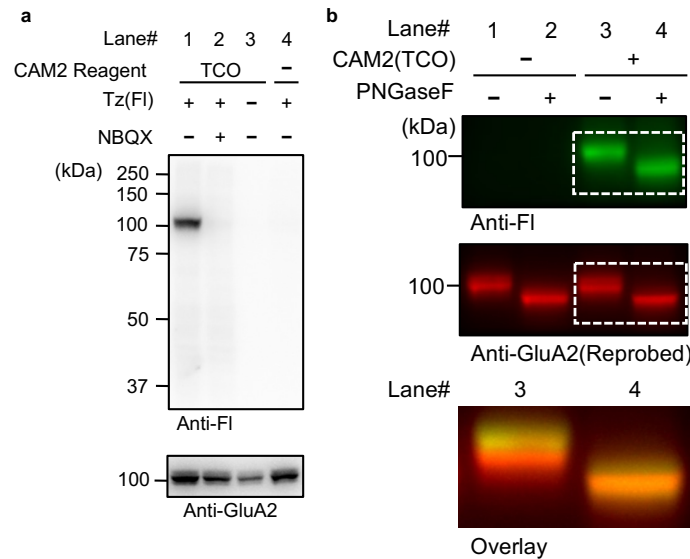


**Fig. 5 | The two-step labeling of cell-surface AMPARs endogenously expressed in neurons.** (a) Western blotting analyses of cortical neurons after the two-step labeling. Primary cultured cortical neurons were treated with 2  $\mu\text{M}$  CAM2(TCO) for 10 h followed by the addition of 1  $\mu\text{M}$  Tz(FI) for 5 min in the presence or absence of 50  $\mu\text{M}$  NBQX in culture medium at 37 °C. The cell lysates were analyzed by western blotting using anti-fluorescein or anti-GluA2 antibody. (b) Lower image shows the overlay of anti-FI image and anti-GluA2 image for lane #3 and #4. Primary cortical neurons were treated with 2  $\mu\text{M}$  CAM2(TCO) for 10 h followed by the addition of 1  $\mu\text{M}$  Tz(FI) for 5 min. PNGase F (1,000 units / 100  $\mu\text{L}$ ) was added to the cell lysate.

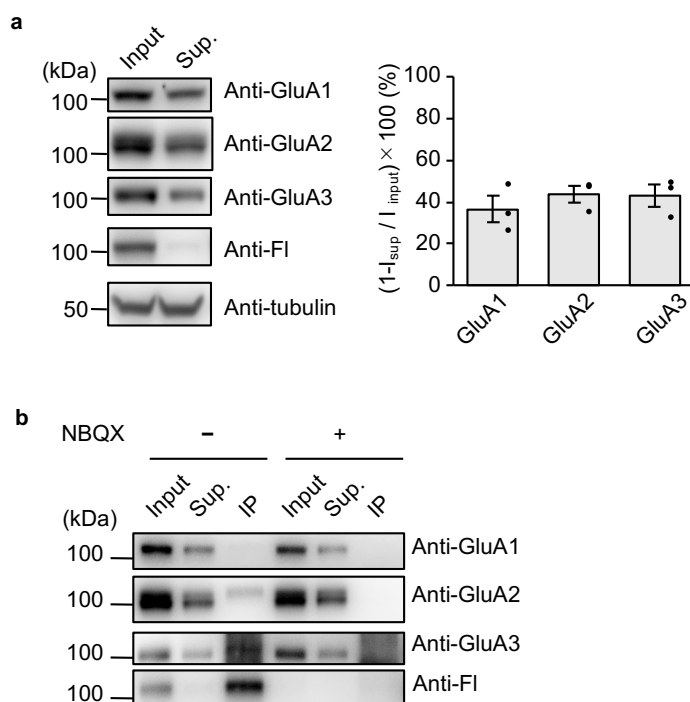


**Fig. 6 | Efficiency and subunit selectivity of the labeling in neurons. (a)** Quantification of labeling efficiency of AMPARs on cell-surface by immunodepletion assay in neurons. Cultured cortical neurons were labeled with 2  $\mu$ M CAM2(TCO) for 10 h and 1  $\mu$ M Tz(FI) for 5 min at 37  $^{\circ}$ C. Left, western blotting analyses of the cell lysate (Input) and supernatant (Sup.) after immunoprecipitation using anti-fluorescein antibody. Anti-tubulin was utilized as a loading control. Right, quantification of labeling efficiency from band intensity of Sup. and Input ( $n = 3$  biological replicates). **(b)** Immunoprecipitation of AMPAR subunits under denatured conditions. Cultured cortical neurons were labeled with 2  $\mu$ M CAM2(TCO) for 4 h and 1  $\mu$ M Tz(FI) for 5 min at 37  $^{\circ}$ C. After cell lysis, immunoprecipitation was conducted under denatured condition where tetrameric formation of AMPARs are collapsed. For details, see Methods. Data are represented as mean  $\pm$  s.e.m.

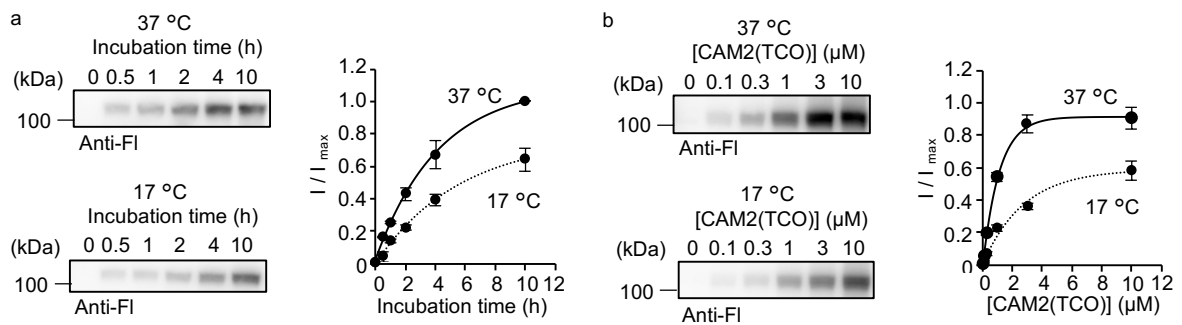


**Fig 7 | Reaction time and concentration dependency of CAM2(TCO) labeling to AMPARs in neuron. (a)** Time course of two-step labeling. Left, representative result of western blotting is shown. Right, time-course of the labeled band are shown ( $n = 3$  biological replicates). Primary cultured cortical neurons were treated with  $2 \mu\text{M}$  of CAM2(TCO) at  $37 \text{ }^\circ\text{C}$  or  $17 \text{ }^\circ\text{C}$  for each period followed by the addition of  $1 \mu\text{M}$  Tz(FI) for 5 min. **(b)** Concentration dependency of two-step labeling. Left, representative result of western blotting is shown ( $n = 3$  biological replicates). Right, concentration-dependency of the labeled band are shown. Primary cultured cortical neurons were treated with each concentration of CAM2(TCO) at  $37 \text{ }^\circ\text{C}$  or  $17 \text{ }^\circ\text{C}$  for 4 h followed by the addition of  $1 \mu\text{M}$  Tz(FI) for 5 min. Data are represented as mean  $\pm$  s.e.m

#### **2-2-4, Quantification of AMPAR localization in cultured neurons.**

Using the two-step labeling technique in primary hippocampal neurons, fluorescently labeled AMPARs were visualized by confocal microscopy. At 5 min after the addition of Tz(Ax488), confocal live imaging showed punctate fluorescent signals from the CAM2(TCO)-treated neurons, and these signals were not observed in neurons co-treated with NBQX (Fig. 8a). To characterize the fluorescent signals in detail, Tz(Ax488)-treated neurons were fixed with paraformaldehyde (PFA) and immunostained with anti-MAP2 or anti-PSD95 antibodies for dendritic or postsynaptic staining, respectively. As shown in Fig. 8b, labeled Alexa 488 signals were observed alongside the anti-MAP2 signals, and merged well with the anti-PSD95 signals. Considering the short incubation time with Tz (Ax488), the Alexa 488 signal likely corresponds to cell-surface AMPARs that are endogenously expressed in neurons.

Next, I quantified the surface distribution of AMPARs in neurons using fluorescence lifetime imaging microscopy (FLIM). In this method, the fluorescence decay curve in each pixel is analyzed by fitting it to a multi-exponential function, and the target fluorescence lifetime ( $\tau$ ) component can be extracted to quantify the fluorescence of interest without any background. Here, I used Tz(ST647) to visualize surface AMPARs because SeTau-647 has a unique fluorescence lifetime and high photostability<sup>16,17</sup>. The typical FLIM image for a lifetime fraction ( $\tau = 2.4 \pm 0.1$  ns) corresponding to SeTau-647 is shown in Fig. 8c, which revealed that surface AMPARs in spines are 3.3 times more concentrated than those in dendrites.

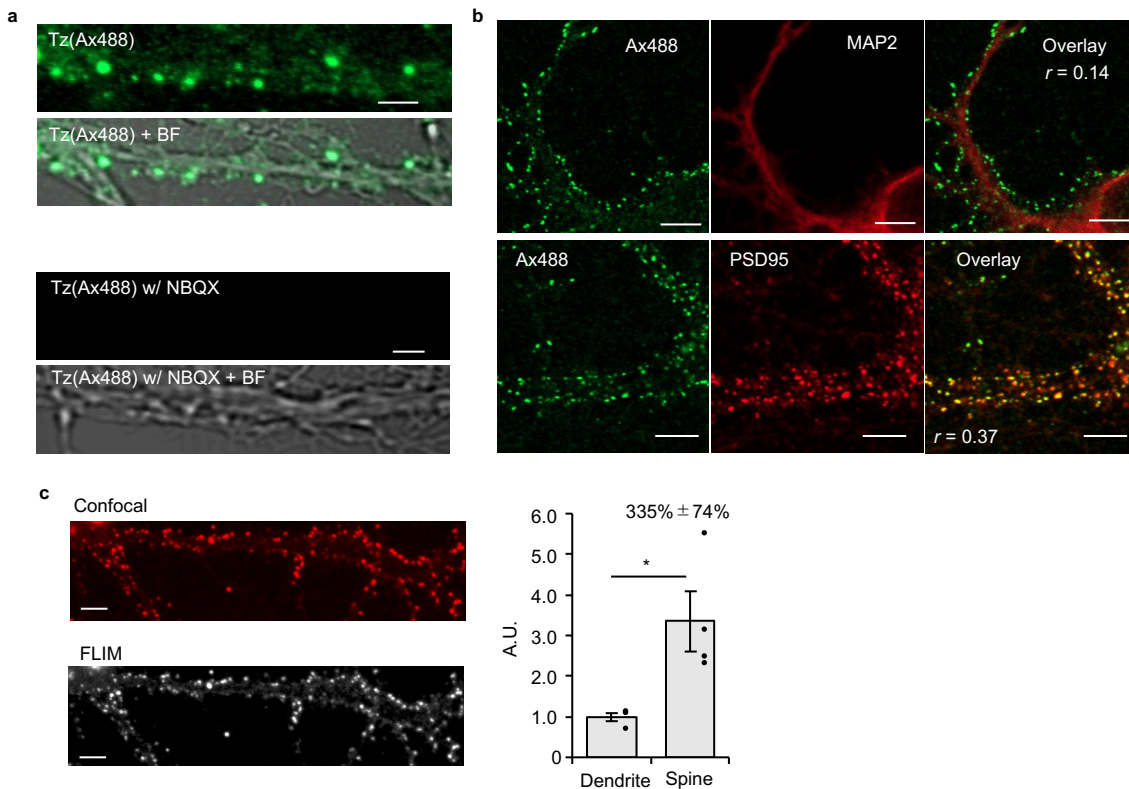


**Fig. 8 | Visualization of cell-surface AMPARs endogenously expressed in neurons.** (a) Confocal live imaging of the neurons labeled with 2  $\mu\text{M}$  CAM2(TCO) and 0.1  $\mu\text{M}$  Tz(Ax488). Labeling was conducted as described in a. Scale bars, 2  $\mu\text{m}$ . (b) Immunostaining of cortical neurons after the two-step labeling. Labeling was conducted as described in (a). The neurons were fixed, permeabilized, and immunostained using anti-MAP2 (upper) or anti-PSD95 antibody (lower). Scale bars, 5  $\mu\text{m}$ . Pearson's correlation coefficients ( $r$ ) are shown in the image. (c) FLIM imaging and analyses of cell-surface AMPARs in the neurons after the two-step labeling. In left, representative confocal image (upper) and FLIM image (lower) for a lifetime fraction ( $\tau = 2.4 \pm 0.1$  ns) are shown. Scale bars, 5  $\mu\text{m}$ . In right, FLIM intensities in spine and dendrite were analyzed ( $n = 4$  cells). [CAM2(TCO)] = 2  $\mu\text{M}$ , [Tz(ST647)] = 0.1  $\mu\text{M}$ . \*Significant difference ( $p < 0.05$  by two-sided Student's  $t$ -test.  $p = 0.048$ ). Data are represented as mean  $\pm$  s.e.m.



**2-2-5, Trafficking analyses of endogenous AMPARs in neurons**

AMPARs are dynamically regulated at synapses, which underlie activity-dependent neuronal plasticity. Molecular biology or biochemical methods, such as the genetic incorporation of fluorescent proteins, surface biotinylation assays, and metabolic incorporation of radioisotopes, have revealed the diffusion dynamics<sup>18</sup>, recycling process<sup>1</sup>, and half-life<sup>19,20</sup> of AMPARs, respectively. Although powerful, these methods are highly specialized for analyzing each process. However, I now have a rapid method to selectively label cell-surface AMPARs in neurons under physiological temperature in culture medium. I therefore applied the two-step labeling method to analyze AMPAR trafficking over a long period. Prior to analyzing the AMPAR trafficking, I examined the influence of the two-step labeling process on the viability of primary cultured neurons by comparing it with original CAM2 labeling. In immature neurons (day in vitro [DIV] 4), neither the original CAM2 labeling nor the two-step labeling affected neuronal viability after 24 h of labeling (Fig. 9a). However, in mature neurons (DIV 12), where AMPARs are highly expressed, viability was decreased after 3 h of labeling with the original CAM2 labeling, and neurons were severely damaged after 24 h of the original labeling (Fig. 9b). The main reason for the lowered viability may be ascribed to the experimental procedure rather than the CAM2 reagents, because similar neuronal damage was observed when the growth medium was exchanged for serum-free medium. In contrast, in the case of the two-step labeling method, where CAM2(TCO) was directly added into the growth medium at 37 °C, negligible damage was observed even after 24 h of the two-step labeling, indicating that this method is suitable for analyzing AMPARs over long periods in neurons. Besides, I examined the effects of CAM2(TCO) labeling on neuronal function. Neither the surface amount nor the synaptic fraction of AMPARs and NMDARs were affected by CAM2(TCO) labeling for 10 h (Fig. 10a and b). Association between GluA2 and the accessory protein, TARPy8 (ref.21) was also unaffected by CAM2(TCO) labeling (Fig. 10c). Although the homeostatic

## Chapter 2

phosphorylation of ERK and CREB was not significantly but slightly decreased, phosphorylation levels of AMPAR (GluA1) and NMDAR (GluN1) were not influenced by the CAM2(TCO) labeling (Fig. 10d).

I then analyzed the trafficking of endogenous AMPARs in neurons over a long period using the two-step labeling method. As described in the previous section, confocal microscopic imaging was able to clearly visualize cell-surface AMPARs in neurons in the two-step labeling method (Fig. 8a). However, synapses are very narrow (200–500 nm diameter), and it is thus difficult to analyze AMPAR trafficking in detail using optical microscopy. I therefore applied biochemical methods for analyzing the  $t_{1/2}^{\text{surface}}$  of AMPARs, including remaining and recycled components (Fig. 11a). As shown in Fig. 11b, the  $t_{1/2}^{\text{surface}}$  was calculated to be  $33.2 \pm 5.1$  h, which was markedly longer than the  $t_{1/2}^{\text{surface}}$  in HEK293T cells ( $5.3 \pm 0.3$  h). To explore the difference in the  $t_{1/2}^{\text{surface}}$  values, I focused on the trafficking of internalized AMPARs. I analyzed the intracellular and surface percentages of TCO-AMPARs after 10 h of incubation with CAM2(TCO). The intracellular percentage ( $10.3 \pm 1.7\%$ ) was markedly smaller than the surface percentage ( $90.4 \pm 0.6\%$ ) (Fig. 11c).

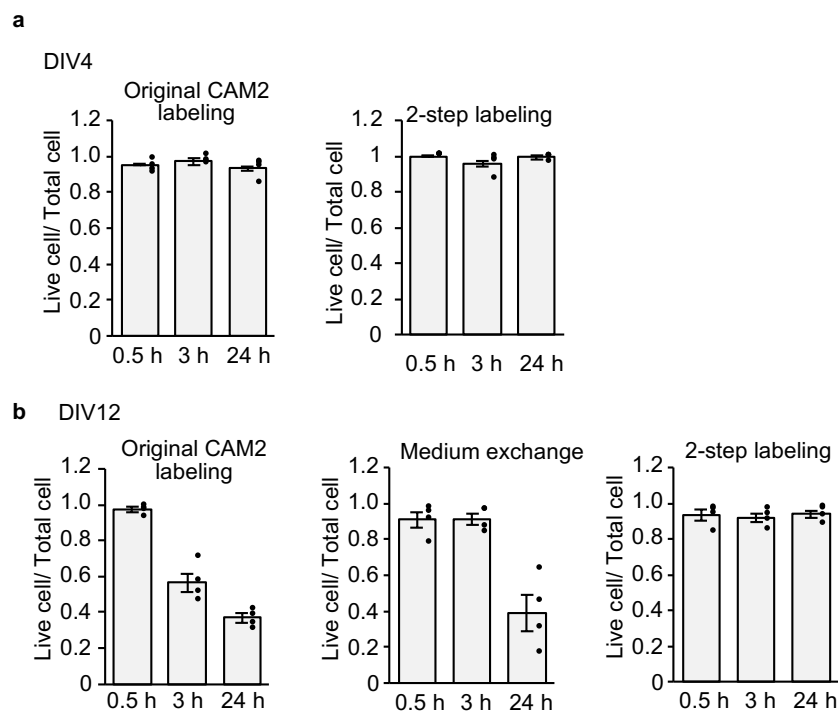
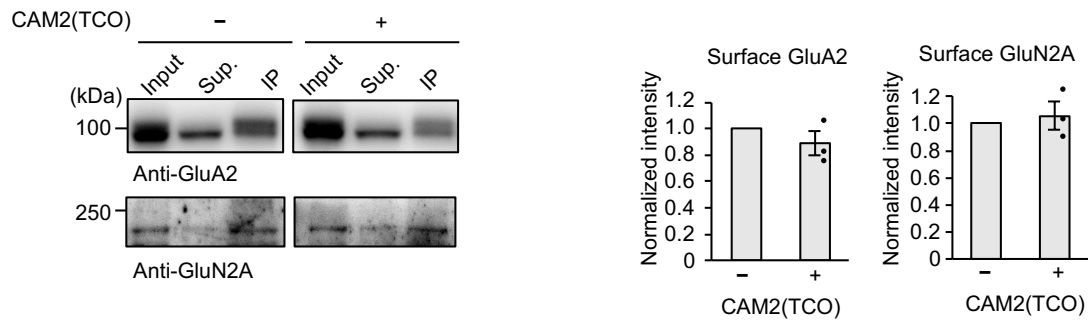


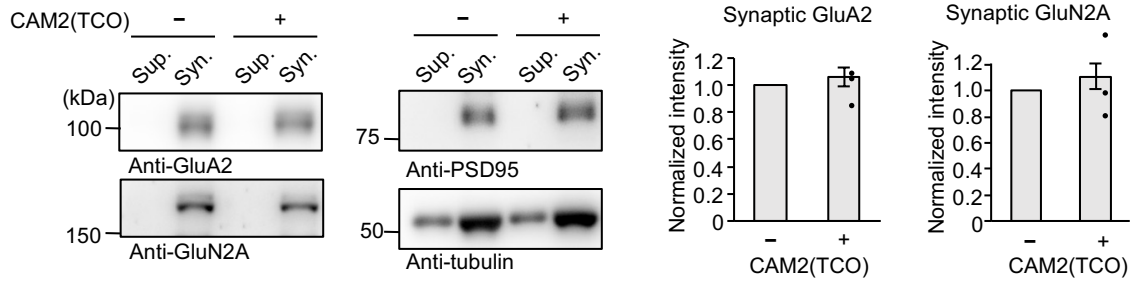
**Fig. 9 | Influence of two-step labeling process on the viability of cultured neurons.** (a, b) Effects of original CAM2 labeling process, medium exchange procedure into serum-free medium, two-step labeling process for immature cortical neurons (DIV4) in (a) or for mature cortical neurons (DIV12) in (b). Viability of neurons were evaluated by the Calcein AM Cell Viability Assay (n = 4 biological replicates). In immature neurons, viability of neurons was not affected by these processes. In mature neurons, viability of neurons was not affected by the two-step labeling process, even though live cells decreased after 3 h of original CAM2 labeling process or after 24 h of medium exchange procedure. Data are represented as mean  $\pm$  s.e.m.

## Chapter 2

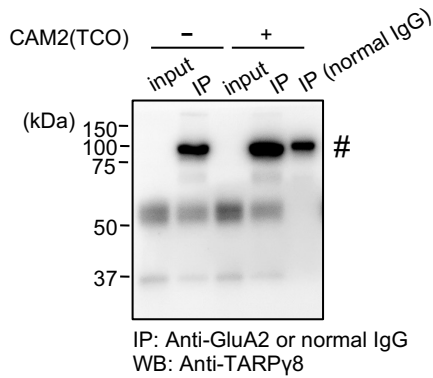
**a**



**b**



**c**



**d**

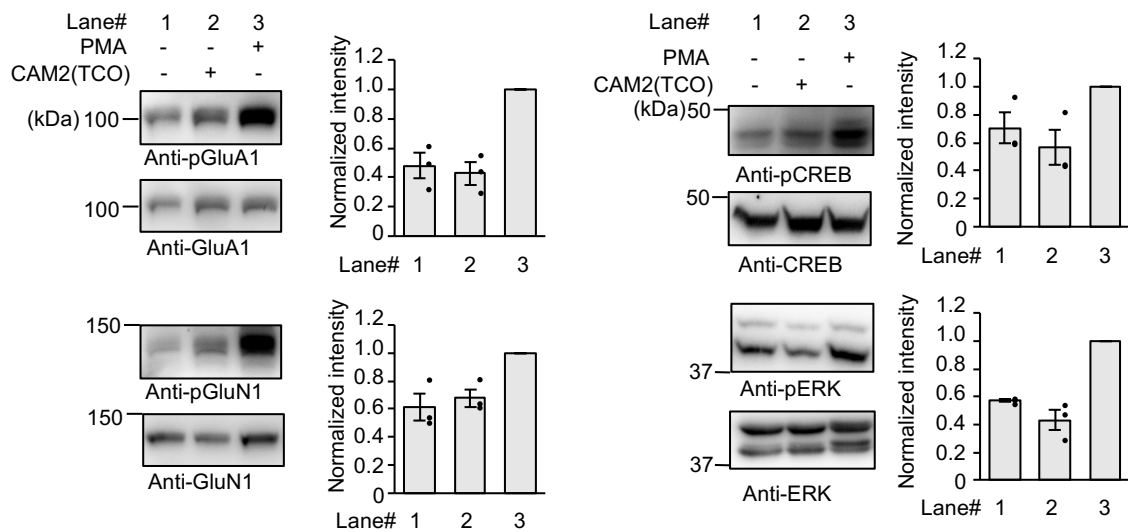


**Fig. 10 | Effect of CAM2(TCO) labeling on neuronal function.** **(a)** Surface biotinylation assay of cortical neurons after the two-step labeling. Cells were treated with 1 mg/mL sulfo-NHS-SS-biotin for 10 min at room temperature after two-step labeling. Western blotting analyses of the cell lysate (Input) and supernatant (Sup.) after affinity purification using NeutrAvidin agarose (n =3 biological replicates). **(b)** Effects of two-step labeling on the synaptosomal proteins. Synaptosome (Syn.) isolated using Syn-PER reagent and the supernatant (Sup.) was conducted western blotting (n =3 biological replicates). **(c)** Effects of CAM2(TCO) labeling on the interaction between AMPARs and TARP $\gamma$ 8. Primary hippocampal neurons were labeled with 2  $\mu$ M CAM2(TCO) and 1  $\mu$ M Tz(Fl). To analysis effect of CAM2(TCO) labeling on interaction of AMPARs and TARP $\gamma$ 8, coimmunoprecipitation assay was performed. Normal IgG was utilized as the control of anti-GluA2 antibody. TARP $\gamma$ 8 (around 50 kDa) was coimmunoprecipitated with anti-GluA2 antibody both in the presence or absence of CAM2(TCO). # is immunoprecipitated antibody band. **(d)** Effects of two-step labeling on constitutive phosphorylation. Primary cortical neurons were labeled with 2  $\mu$ M CAM2(TCO) and 1  $\mu$ M Tz(Fl). As a positive control, 1  $\mu$ M PMA (phorbol 12-myristate 13-acetate) was added for 10 min before cell lysis. Data are represented as mean  $\pm$  s.e.m.

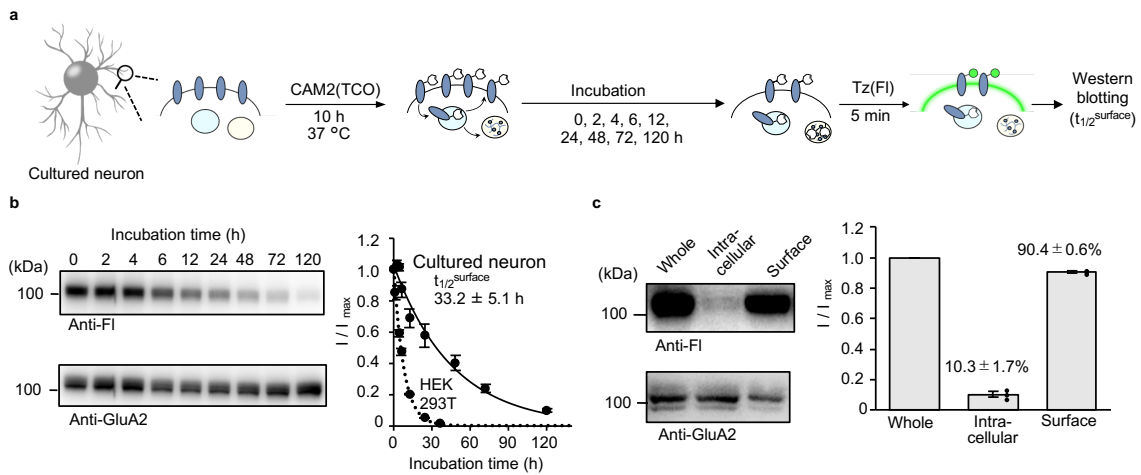


**Fig. 11 | Quantitative analyses of AMPAR trafficking in neurons using the two-step labeling under the physiological cell culture condition. (a)** Schematic illustration of the procedure for determining  $t_{1/2}^{\text{surface}}$  for AMPARs. **(b)** Determination of  $t_{1/2}^{\text{surface}}$  by western blotting. In left, representative results of western blotting are shown. In right, time-course of the labeled band is shown ( $n = 3$  biological replicates).  $[\text{CAM2(TCO)}] = 2 \mu\text{M}$ ,  $[\text{Tz(Fl)}] = 1 \mu\text{M}$ . **(c)** Determination of intracellular and surface ratio after CAM2(TCO) labeling for 10 h. In left, representative results of western blotting are shown. In right, band intensities for cell-surface and intracellular labeling were analyzed, both of which were normalized by that for whole-cell labeling ( $n = 3$  biological replicates).  $[\text{CAM2(TCO)}] = 2 \mu\text{M}$ ,  $[\text{Tz(Fl)}] = 1 \mu\text{M}$ .

**2-2-6, Trafficking analyses of endogenous AMPARs in neurons**

I next evaluated the recycling process of internalized AMPARs, as follows. The cultured neurons were labeled with CAM2(TCO) for 10 h in the culture medium at 37 °C, and Tz(F1) was then added to the culture medium for 5 min as a first pulse to mask the surface TCO-AMPARs (Fig. 12a). The neurons were further incubated for 15 min in the culture medium at 37 °C, and then Tz(Ax647) was added to the culture medium as a second pulse to label the recycled TCO-AMPARs. As shown in Fig. 12b, western blotting using anti-Alexa 647 antibodies clearly detected recycled AMPARs. The percentage was determined to be  $12.5 \pm 2.8\%$  compared with the surface AMPARs, suggesting that most of internalized AMPARs were recycled during this short period. In contrast, the recycled fraction was almost undetectable in HEK293T cells (Fig. 13). These data indicate that AMPARs are constantly recycled via endocytosis and exocytosis in neurons, which may be the molecular basis for the long lifetimes of AMPARs (Fig. 12c, d).

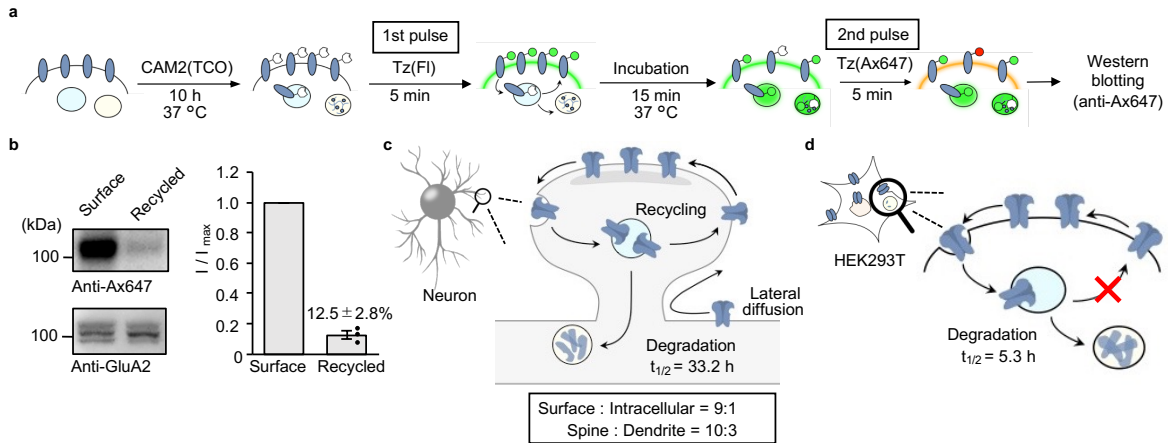


**Fig. 12 | Analyses of recycled AMPARs by pulse-chase-type analyses using the two-step labeling in neurons.** (a) Schematic illustration of pulse-chase-type analyses procedure. (b) Western blotting analyses of recycled AMPARs. In left, representative results of western blotting are shown. In right, exocytosed AMPARs were quantified, which were normalized by that for surface labeling (n = 3 biological replicates). [CAM2(TCO)] = 2  $\mu$ M, [Tz(FI) or Tz(Ax647)] = 1  $\mu$ M. (c, d) Trafficking and distribution of cell-surface AMPARs quantified by the two-step labeling in neuron (in c) and HEK293T cells (in d). Data are represented as mean  $\pm$  s.e.m.

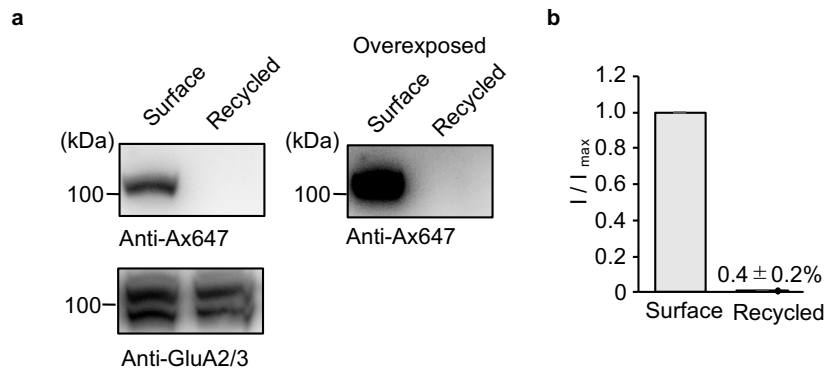


**Fig. 13 | Analyses of recycled AMPARs by pulse-chase-type analyses using the two-step labeling in HEK293T cells.** (a) Representative results of western blotting are shown. GluA2/3 was utilized as the loading control. In the right, overexposed image of the western blotting by anti-Ax647 antibody is shown. Recycled AMPARs were not detected even in this exposed image. (b) Quantification of recycled AMPARs. Intensity of recycled fraction was normalized by that for surface labeling (n = 3 biological replicates). This clearly indicates that recycling of AMPARs were not observed in HEK293T cells. Data are represented as mean  $\pm$  s.e.m.



### **2-3, Conclusion**

I have successfully analyzed trafficking and localization of AMPARs using ligand-directed two-step labeling in HEK293T cells and cultured neurons in culture medium and physiological temperature. Although the present study revealed that previous CAM2 labeling condition affects the viability of mature neurons after 24 h of labeling. In contrast, the present bioorthogonal two-step labeling method negligibly affected the cell viability of neurons. This method therefore allows the quantitative analysis of AMPAR trafficking for over 120 h after labeling. Here, I demonstrated that various kinds of chemical probes could be used to selectively and rapidly label endogenous cell-surface AMPARs in neurons using ligand-directed two-step labeling.

The selective labeling of SeTau-647, a middle-sized molecule with a long fluorescence lifetime and high photostability, allowed the quantitative analyses of cell-surface AMPAR distribution in neurons using FLIM. These analyses revealed a three-fold concentration of cell-surface AMPARs in spines compared with dendrites.

Thus, this method may be a versatile tool for investigating the physiological and pathophysiological roles of AMPAR trafficking in neurons.

## **2-4, Experimental Section**

### **General methods for biochemical and biological experiments.**

SDS-PAGE and western blotting were carried out using a BIO-RAD Mini-Protean III electrophoresis apparatus. Samples were applied to SDS-PAGE and electrotransferred onto polyvinylidene fluoride membranes (BIO-RAD), followed by blocking with 5% nonfat dry milk in Tris-buffered saline containing 0.05% Tween 20. Primary antibody was indicated in each experimental procedure, and anti-rabbit IgG-HRP conjugate (CST, 7074S, 1:3,000) or anti-mouse IgG-HRP conjugate (CST, 7076S, 1:3,000) was utilized as the secondary antibody. Chemiluminescent signals generated with ECL Prime (GE Healthcare) were detected with a Fusion Solo S imaging system (Vilber Lourmat).

### **Expression of AMPARs in HEK293T cells.**

HEK293T cells (ATCC) were cultured in Dulbecco's modified Eagle's medium (DMEM)-GlutaMAX (Invitrogen) supplemented with 10% dialyzed FBS (Invitrogen), penicillin (100 units/ml), and streptomycin (100 µg/ml), and incubated in a 5% CO<sub>2</sub> humidified chamber at 37 °C. Cells were transfected with a plasmid encoding rat GluA2 (GluA2<sup>flip(Q)</sup>) or the control vector pCAGGS (kindly provided by Dr. H. Niwa from RIKEN) using Lipofectamine 2000 (Invitrogen) according to the manufacturer's instructions, and subjected to labeling experiments after 36–48 h of the transfection.

### **Two-step labeling of AMPARs in HEK293T cells.**

For the first step labeling of AMPARs, HEK293T cells transfected with GluA2 were treated with 2 µM CAM2(TCO) in the absence or presence of 50 µM NBQX in the culture medium at 37 °C for 4 h. For the second step labeling, the culture medium was removed, and 1 µM Tz(Fl) in PBS was added for 5 min at room temperature. To quench excess Tz(Fl), 1 µM TCO-PEG4-COOH in PBS was added.

For western blot analyses of labeled AMPARs, labeled cells were washed three times with PBS, lysed with radio immunoprecipitation assay (RIPA) buffer containing 1% protease inhibitor cocktail (Nacalai tesque), and mixed with 5× Laemmli sample buffer containing 250 mM DTT. Western blotting analyses were performed as described in “General methods for biochemical and biological experiments.” The Fl-labeled GluA2 was detected using rabbit anti-fluorescein antibody (abcam, ab19491, 1:3,000). GluA2 was detected using a rabbit anti-GluA2/3 antibody (Millipore, 07-598, 1:3,000).

CAM2(TCO) and Tz-probes were stored in DMSO solution. The stock solutions were kept in deep freezer (−80 °C) to prevent decomposition.

### **Confocal live cell imaging of labeled AMPARs in HEK293T cells.**

HEK293T cells were co-transfected with GluA2<sup>flp(Q)</sup> and mCherry-F as a transfection marker. First step labeling was performed as describe in “Two-step labeling of AMPARs in HEK293T cells.” Confocal live imaging was performed with a confocal microscope (LSM900, Carl Zeiss) equipped with a 63×, numerical aperture (NA) = 1.4 oil-immersion objective. Fluorescence images were acquired by excitation at 405, 488, 561, or 640 nm derived from diode lasers. For trafficking analyses, after first step labeling, 100 nM Tz(Ax488) was added in DMEM-GlutaMAX for 5 min. The cells were washed three times in DMEM-GlutaMAX and incubated for 0, 1, 4, and 8 h in growth medium at 37 °C. Live cell imaging was performed with a confocal microscope. To quantify the fluorescence intensity of the membrane at each time point, mCherry-F positive cells were selected and the average signal intensity of ROIs set on the membrane was calculated by ZEN blue software after subtracting background fluorescence. The averaged membrane intensity was defined as  $F$  at each time point. The membrane intensity was fitted with KaleidaGraph using following equation (2):  $F = a + b \cdot e^{-ct}$ , and the offset value ( $a$ ) was set equal to zero. The  $t_{1/2}$  was defined as  $t_{1/2} = \ln(2)/c$ . For co-staining with LysoTracker Red DND-99 (Invitrogen), after first step

labeling, the cells were treated with 50 nM LysoTracker Red DND-99 for 30 min at 37 °C in culture medium, and then treated with 100 nM Tz(Ax488) in culture medium for 5 min. After washing three times with culture medium or subsequent incubation for 8 h, cells were imaged using a confocal microscope.

### **Half-life studies of AMPARs by western blotting in HEK293T cells.**

Schematic illustration of the experiments is shown in Fig. 2a. For determining  $t_{1/2}^{\text{surface}}$  (path-1 in Fig. 2a), first step labeling was conducted as described in “Two-step labeling of AMPARs in HEK293T cells.” After medium exchange for removal of the labeling reagents, the cells were incubated for 0, 1,4, 6, 12, 24, and 36 h. The cells were treated with 1  $\mu\text{M}$  Tz(Fl) in PBS for 5 min, and excess Tz(Fl) was quenched by addition of 1  $\mu\text{M}$  TCO-PEG4-COOH in PBS.

For determining  $t_{1/2}^{\text{life}}$  (path-2 in Fig. 2a), after first step labeling, cells were washed three times with culture medium and treated with 1  $\mu\text{M}$  Tz(Fl) in culture medium for 5 min. Excess Tz(Fl) was quenched by addition of 1  $\mu\text{M}$  TCO-PEG4-COOH in culture medium. Cells were then incubated for 0, 1,4, 6, 12, 24, and 36 h and washed three times with PBS. Cell lysis and western blotting were performed as described in “Two-step labeling of AMPARs in HEK293T cells.” The target bands were manually selected, and the intensity were calculated with Fusion software (Vilber Lourmat), background intensity was manually subtracted by cutting the minimal intensity in the selected area. The half-life was calculated by curve fitting using KaleidaGraph and following equation (3):  $I = a + b \cdot e^{-ct}$ , and the offset value ( $a$ ) was set equal to zero. The  $t_{1/2}$  was defined as  $t_{1/2} = \ln(2)/c$ .

### **Intracellular and surface ratio of labeled AMPARs in HEK293T cells.**

Schematic illustration of the experiments is shown in Fig. 3a. For determining labeled AMPARs on cell-surface (path-1 in Fig. 3a), after first step labeling as describe in

“Two-step labeling of AMPARs in HEK293T cells,” the cells were treated with 1  $\mu\text{M}$  Tz(Fl) for 5 min in PBS at room temperature. To quench excess Tz(Fl), 1  $\mu\text{M}$  TCO-PEG4-COOH in PBS was added and lysed with RIPA buffer containing 1% protease inhibitor cocktail for 30 min at 4  $^{\circ}\text{C}$ . For determining intracellular labeled AMPARs (path-2 in Fig. 3a), after first step labeling, 1  $\mu\text{M}$  Tz(Ax647) was treated for 5 min for masking of cell-surface TCO-labeled AMPARs. After cell lysis using RIPA buffer, the lysate was reacted with 0.3  $\mu\text{M}$  Tz(Fl) for 30 min at room temperature. Excess Tz(Fl) was quenched by addition of 1  $\mu\text{M}$  TCO-PEG4-COOH in the cell lysate. For preparing whole-cell-labeling fraction (path-3 in Fig. 3a), after first step labeling, the cells were lysed with RIPA buffer containing 1% protease inhibitor cocktail for 30 min at 4  $^{\circ}\text{C}$ . The lysate was reacted with 0.3  $\mu\text{M}$  Tz(Fl) for 30 min at room temperature. Excess Tz(Fl) was quenched by addition of 1  $\mu\text{M}$  TCO-PEG4-COOH in the cell lysate. Western blotting was performed as described in “Half-life studies of AMPARs by western blotting in HEK293T cells.” The target bands were manually selected, and the intensity were calculated with ImageJ software, background intensity was manually subtracted by selecting a region with no bands from the same lane. In more detail, the band intensity was determined as described below:

$$(\text{target intensity}) - (\text{target area}) = (\text{background area}) \times (\text{background intensity})$$

### **Reaction kinetics of Tz ligation in cell lysate.**

CAM2(TCO)-labeled HEK293T cells were lysed with RIPA buffer containing 1% protease inhibitor cocktail for 30 min at 4  $^{\circ}\text{C}$ , then the lysate was reacted with 0.1, 0.3  $\mu\text{M}$  Tz(Fl) for 5, 15, 30 min at room temperature. To quench excess Tz(Fl), 10  $\mu\text{M}$  TCO-PEG4-COOH was added. For western blotting analysis, after chemical labeling, cells were mixed with 5 $\times$  Laemmli sample buffer containing 250 mM DTT. The samples were applied to SDS-PAGE and electrotransferred onto PVDF membranes, followed by blocking with 5% nonfat dry milk in TBS containing 0.05% Tween 20. The

## *Chapter 2*

Fl-labeled GluA2 was detected by chemiluminescence analysis using rabbit anti-fluorescein antibody (abcam, ab19491, 1:3,000) and anti-rabbit IgG-HRP conjugate (CST, 7074S, 1:3,000). The immunodetection of GluA2 was performed with a rabbit anti-GluA2/3 antibody (Millipore, 07-598, 1:3,000) and anti-rabbit IgG-HRP conjugate (CST, 7076S, 1:3,000). The signal was generated with ECL Prime (GE Healthcare) and detected with Fusion Solo S imaging system (Vilber Lourmat).

### **Animals.**

Pregnant ICR mice and pregnant Sprague Dawley rats maintained under specific pathogen-free conditions were purchased from Japan SLC, Inc (Shizuoka, Japan). The animals were housed in a controlled environment ( $23 \pm 1$  °C, 12 h light/dark cycle) and had free access to food and water, according to the regulations of the Guidance for Proper Conduct of Animal Experiments by the Ministry of Education, Culture, Sports, Science, and Technology of Japan. All experimental procedures were performed in accordance with the National Institute of Health Guide for the Care and Use of Laboratory Animals, and were approved by the Institutional Animal Use Committees of Kyoto University or Nagoya University.

### **Preparation of primary cortical neuronal culture.**

Twenty-four-well plates (BD Falcon) were coated with poly-D-lysine (Sigma-Aldrich) and washed with sterile dH<sub>2</sub>O three times. Cerebral cortices from 16-day-old ICR mouse embryos were aseptically dissected and digested with 0.25 w/v% trypsin (Nacalai tesque) for 20 min at 37 °C. The cells were re-suspended in Neurobasal Plus medium supplemented with 10% FBS, penicillin (100 units/mL), and streptomycin (100 µg/mL) and filtered by Cell Strainer (100 µm, Falcon) and centrifuged at 1,000 rpm for 5 min. The cells were resuspended in Neurobasal Plus medium supplemented with 2% of B-27 Plus Supplement, 1.25 mM GlutaMAX I (Invitrogen), penicillin (100 units/mL),

and streptomycin (100 µg/mL) and plated at a density of  $2 \times 10^5$  cells on the 24-well plate. The cultures were maintained at 37 °C in a 95% air and 5% CO<sub>2</sub> humidified incubator. Culture medium was replaced every 3 or 4 days and the neurons were used at 12–15 DIV.

### **Two-step labeling of AMPARs in cultured neurons.**

To label endogenous AMPARs, 12 µM CAM2(TCO) in 100 µL of the culture medium with or without 300 µM NBQX was gently added to the cortical neurons cultured in 500 µL medium on 24-well plates to a final concentration of 2 µM CAM2(TCO) and 50 µM NBQX. The cells were incubated for 10 h at 37 °C. For the second step, the culture medium was removed and the cells were treated with 1 µM Tz(Fl) for 5 min in PBS at room temperature. To quench excess Tz(Fl), 1 µM TCO-PEG4-COOH in PBS was added. Western blot analyses of labeled AMPARs were performed as described in “Two-step labeling of AMPARs HEK293T cells.”

### **Glycosylation assay in neuron**

Primary cultures of cortical neurons were labeled as described in “Two-step labeling of AMPARs in cultured neurons”. The labeled cells were washed three times with PBS and lysed in PBS containing 1% triton X-100, 0.6% SDS and 1% protease inhibitor cocktail for 30 min at 37 °C. The lysates were diluted (2.0-fold) in sodium phosphate buffer (50 mM, pH 7.5) containing 2% NP40 and 100 mM DTT. PNGase F (New England Biolabs) were used at 1,000 units / 100 µL of lysate and incubated overnight at 37 °C. The samples were subjected to western blotting analyses as described in “Two-step labeling of AMPARs in HEK293T cells”. In this experiment, after western blotting using anti-Fl antibody, the membrane was stripped with stripping buffer (250 mM glycine (pH = 2.5) and 1% SDS) and reprobed with the anti-GluA2 antibody.

**Immunodepletion assays for quantifying labeling efficiency in cortical neurons.**

Primary cultures of cortical neurons were labeled as described in “Two-step labeling of AMPARs in cultured neurons”. The labeled cells were lysed by RIPA buffer without SDS. Anti-fluorescein antibody (abcam, ab19491, 1:50) was added for 3-4 h at 4 °C and centrifuged (1,200 g, 4 °C) for 10 min. A small portion of the supernatant was collected as the input. Protein A Sepharose (abcam, ab193256) (0.5  $\mu$ L/ $\mu$ L of lysate) was added to the supernatant and incubated at 4 °C overnight. Resins were then pelleted by centrifugation (500 g, 4 °C) for 5 min and the supernatant was collected. The labeling efficacy was determined by western blotting analysis. The target bands were manually selected, and the intensity were calculated with ImageJ software, background intensity was manually subtracted by selecting a region with no bands around the target bands. The labeling efficacy were calculated from band intensity of Sup. and input. Immunodetection of GluA1, GluA2, GluA3, Fl-labeled AMPARs and  $\beta$  III Tubulin was performed with a rabbit anti-GluA1 antibody (abcam, ab109450, 1:1000), a rabbit anti-GluA2 (abcam, abcam20673, 1:1000), a rabbit GluA3 (CST, 4676S, 1:1000), a rabbit anti-fluorescein antibody (abcam, ab19491, 1:3,000) and a rabbit  $\beta$  III Tubulin (abcam, ab18207, 1:1000). As a secondary antibody, VeriBlot for IP Detection Reagent HRP-conjugated (abcam, ab131366, 1:500) was used.

**Immunodepletion assays for labeling selectivity**

Primary cultures of cortical neurons were labeled with as described in “Two-step labeling of AMPARs in cultured neurons”. The labeled cells were lysed in lysis buffer (150 mM NaCl, 10 mM Na<sub>2</sub>HPO<sub>4</sub>, 2 mM EDTA, 1% triton X-100 and protease inhibitor) including 1% SDS to dissociate tetrameric AMPARs. The lysates were incubated for 30 min at 4 °C and then diluted 5-fold in lysis buffer without SDS. A part of the lysates was kept for western blotting as input. The remained lysates were incubated with rabbit anti-fluorescein antibody (abcam, ab19491, 1:50) for 3-5 h at 4 °C.



Antibody supplemented lysates were incubated for 3-5 h with pre-washed Protein A-sepharose (0.5  $\mu$ L/  $\mu$ L of lysate) at 4 °C. The supernatants were collected for western blotting as Sup. Resins were washed three times with cold lysis buffer containing and bound proteins were boiled in Laemlli buffer for 10 min. In western blotting, 20% of the input and Sup. proteins were loaded for SDS-PAGE. Western blotting was performed as described in “Two-step labeling of AMPARs in HEK293T cells”. Immunodetection of GluA1, GluA2, GluA3 and Fl-labeled AMPARs were performed with a rabbit anti-GluA1 antibody (abcam, ab109450, 1:1000), a rabbit anti-GluA2 (abcam, abcam20673, 1:1000), a rabbit GluA3 (CST, 4676S, 1:1000) and a rabbit anti-fluorescein antibody (abcam, ab19491, 1:3,000). As a secondary antibody, VeriBlot for IP Detection Reagent HRP-conjugated (abcam, ab131366, 1:500) was used.

#### **Time course and concentration-dependency of two-step labeling in cultured cortical neurons.**

Primary cultures of cortical neurons were prepared as described above and used at 12 DIV. To label endogenous AMPARs by two-step labeling method and to determine time course of two-step labeling, 12  $\mu$ M CAM2(TCO) in 100  $\mu$ L culture medium was gently added to the cortical neurons cultured in 500  $\mu$ L medium on 24-well plates to a final concentration of 2  $\mu$ M CAM2(TCO). The cells were incubated for 0, 0.5, 1, 2, 4, 10 h at 17 °C or 37 °C. The cells reacted at 17 °C were incubated in culture medium with 10 mM HEPES. For the second step labeling, the culture medium was removed and the cells were treated with 1  $\mu$ M Tz(Fl) for 5 min in Neurobasal Plus medium at room temperature. To quench excess Tz(Fl), 1  $\mu$ M TCO-PEG4-COOH in Neurobasal Plus medium was added. To determine dose-dependency of two-step labeling, 0, 0.6, 1.8, 6, 18, 60  $\mu$ M CAM2(TCO) in 100  $\mu$ L culture medium was gently added to the cortical neurons cultured in 500  $\mu$ L medium on 24-well plates to a final concentration of

## *Chapter 2*

0, 0.1, 0.3, 1, 3, 10  $\mu\text{M}$  CAM2(TCO). The cells were incubated for 4 h at 17 °C or 37 °C. The cells reacted at 17 °C were incubated in culture medium with 10 mM HEPES. For the second step labeling, the culture medium was removed and the cells were treated with 1  $\mu\text{M}$  Tz(Fl) for 5 min in Neurobasal Plus medium at room temperature. To quench excess Tz(Fl), 1  $\mu\text{M}$  TCO-PEG4-COOH in Neurobasal Plus medium was added. The samples were subjected to western blotting analyses as described in “Two-step labeling of AMPARs in HEK293T cells”.

### **Preparation of primary hippocampal neuronal culture.**

Glass bottom dishes (IWAKI) or coverslips (diameter, 13 mm, Matsunami) were coated with poly-D-lysine (Sigma-Aldrich) and washed with sterile dH<sub>2</sub>O three times. Hippocampi from 18-day-old Sprague Dawley rat embryos were aseptically dissected and digested with 0.25 w/v% trypsin (Nacalai tesque) for 20 min at 37 °C. The cells were re-suspended in Neurobasal Plus medium supplemented with 10% FBS, penicillin (100 units/mL) and streptomycin (100  $\mu\text{g}/\text{mL}$ ) and filtered by Cell Strainer (100  $\mu\text{m}$ , Falcon) and centrifuged at 1,000 rpm for 5 min. The cells were re-suspended in Neurobasal Plus medium supplemented with 2% of B-27 Plus Supplement, 1.25 mM GlutaMAX I (Invitrogen), penicillin (100 units/mL), and streptomycin (100  $\mu\text{g}/\text{mL}$ ) and plated at a density of  $2 \times 10^4$  cells on glass coverslips inside 24-well plates (BD Falcon) or glass bottom dishes. Cultures were maintained at 37 °C in a 95% air and 5% CO<sub>2</sub> humidified incubator. Culture medium was replaced every 7 days and the neurons were used at 16–18 DIV.

Live cell imaging of AMPARs in cultured neurons. To label endogenous AMPARs, 12  $\mu\text{M}$  CAM2(TCO) in 300  $\mu\text{L}$  of growth medium with or without 300  $\mu\text{M}$  NBQX was gently added to the hippocampal neurons cultured in 1.5 mL medium on glass bottom dishes to a final concentration of 2  $\mu\text{M}$  CAM2(TCO) and 50  $\mu\text{M}$  NBQX. After removal of the culture medium, neurons were treated with 100 nM Tz(Ax488) for

5 min in HBS at room temperature and washed three times with HBS. Confocal live imaging was performed with a confocal microscope.

**Immunostaining of cultured neurons after labeling.**

Primary cultures of hippocampal neurons were labeled by 2  $\mu$ M CAM2(TCO) and followed by 100 nM Tz(Ax488) as described above. The cells were fixed with 4% PFA in PBS at room temperature for 30 min and washed three times with PBS. PFA-fixed cells were permeabilized for 15 min with PBS containing 0.1% Triton X-100 at room temperature. The cells were washed three times in PBS and incubated in 10% normal goat serum for 1 h at room temperature. After blocking, the cells were incubated overnight at 4 °C with primary antibodies in PBS containing 1% normal goat serum. The cells were then washed three times with PBS and incubated for 1 h at room temperature with secondary antibodies in PBS containing 1% normal goat serum. The following primary antibodies were used: mouse anti-PSD95 (abcam, ab2723, 1:1,000) or rabbit anti-MAP2 (Millipore, AB5622, 1:1,000). Secondary antibodies were used goat anti-mouse Alexa 647 (abcam, ab150115, 1:1,000) and goat anti-rabbit Alexa633 (Invitrogen, A21070, 1:2,000). Imaging of immunostained hippocampal neurons was performed with a confocal microscope.

**Fluorescence lifetime imaging of AMPARs in cultured hippocampal neurons.**

Primary cultures of hippocampal neurons were labeled by 2  $\mu$ M CAM2(TCO), followed by 100 nM Tz(ST647) and fixed with 4% PFA in PBS. The cells were immunolabeled with PSD95 and MAP2 primary antibodies, and stained with Alexa488 and Alexa405 secondary antibodies, respectively. Confocal and lifetime imaging of immunostained hippocampal neurons was performed by TCS SP8 FALCON (Leica microsystems) equipped with a white light laser and 63 $\times$ , NA = 1.4 oil-immersion objective.

## Chapter 2

SeTau-647 was imaged using 640 nm exc. (laser power 100, emission collected at 653–700 nm, using 0–12.5 ns time gate).

FLIM images were processed in LAS X 3.5.5 software (Leica microsystems) to fit the lifetime decay curves using an n-exponential reconvolution model with the number of components that  $\chi^2$  value is closest to 1. In our data, a three-component fit was utilized. The component of the lifetime corresponding to SeTau-647 ( $\tau = 2.4 \pm 0.1$  ns) was used for calculating the intensity of FLIM images. The synaptic or dendritic region was selected ROI on PSD95 or MAP2 signals and the background intensities were subtracted by selecting a region of no cells.

### **Cell viability assay of matured and unmatured cultured cortical neurons.**

Primary cultures of cortical neurons were prepared as described above and used at 4 or 12 DIV. To label endogenous AMPARs by two-step labeling method, 12  $\mu$ M CAM2(TCO) in 100  $\mu$ L culture medium was gently added to the cortical neurons cultured in 500  $\mu$ L medium on 24-well plates to a final concentration of 2  $\mu$ M CAM2(TCO). The cells were incubated for 10 h at 37 °C and further incubated for 0, 2 h and 24 h at 37 °C. For the second step labeling, the culture medium was removed and the cells were treated with 1  $\mu$ M Tz(Fl) for 5 min in Neurobasal Plus medium at 37 °C. To quench excess Tz(Fl), 1  $\mu$ M TCO-PEG4-COOH in Neurobasal Plus medium was added.

To label endogenous AMPARs by original method, 2  $\mu$ M CAM2(Ax488) in culture medium with 10 mM HEPES and without B27 Plus supplement was added to the cortical neurons cultured on 24-well plates. The cells were incubated for 4 h at 17 °C, washed 3 times with HBS and further incubated for 0, 2 h and 24 h at 37 °C.

For cell viability assay, labeled cells were washed with HBS and incubated with 2  $\mu$ M Calcein AM (Dojindo) and 50  $\mu$ g/mL Hoechst33342 (Dojindo) in HBS for 15 min at 37 °C. Fluorescence live imaging was performed with a fluorescent microscope

(IX71, Olympus) equipped with a 20×, numerical aperture (NA) = 1.4 objective. Calcein positive cells were regarded as live cells, and total cell number were counted by Hoechst33342 fluorescence. The cell viability rate (live cell / total cell) was calculated according to the following formula: (Number of Calcein positive cells) / (Number of Hoechst33342 positive cells). The images were obtained four independent experiments. The ROI of these cells were manually selected using ImageJ software.

#### **Surface biotinylation assay.**

Primary cultures of cortical neurons were labeled as described in “Two-step labeling of AMPARs in cultured neurons”. The labeled or non-labeled cells were incubated with 1 mg/mL sulfo-NHS-SS-biotin (Dojindo) in the PBS (pH 8.0) for 10 min at room temperature. Cells were washed and quenched three times in TBS (10 mM, pH 8.0) and then lysed in RIPA buffer containing 1% protease inhibitor cocktail for 30 min at 4 °C. The lysates were incubated with NeutrAvidin Agarose (Thermo Scientific) at 4 °C for 3-5 h. A part of lysate was kept for western blotting as input. Bound proteins were eluted by Laemlli buffer including 250 mM DTT for 30 min at room temperature and unbound proteins were collected as supernatant. Western blotting was performed as described in “Two-step labeling of AMPARs in HEK293T cells”.

#### **Fractionation of synaptic proteins using Syn-PER reagents.**

Primary cultures of cortical neurons were labeled as described in “Two-step labeling of AMPARs in cultured neurons”. The labeled cells were collected with SynPER Synaptic Protein Extraction Reagent (Thermo Fisher Scientific) including protease inhibitor cocktail. Samples were centrifuged at 1,200×g for 10 min at 4 °C to remove the debris. The supernatants were centrifuged at 15,000×g for 20 min at 4 °C. Pellets containing the synaptosomal fraction were solubilized in Syn-PER reagent including protease inhibitor cocktail. The supernatants were collected for the control. Western blotting was

performed as described in “Two-step labeling of AMPARs in HEK293T cells”. Immunodetection of PSD95 and  $\beta$  III Tubulin was performed with a mouse anti-PSD95 antibody (abcam, ab2723, 1:1000) and a rabbit  $\beta$  III Tubulin (abcam, ab18207, 1:1000).

### **Western blotting for quantification of phosphorylated proteins.**

Primary cultures of cortical neurons were labeled as described in “Two-step labeling of AMPARs in cultured neurons”. The labeled cells were washed three times in cold PBS and lysed in RIPA buffer containing 1% protease inhibitor cocktail and 1% phosphatase inhibitor cocktail (Nacalai tesque) for 30 min at 4 °C. Non-labeled cells were treated 1  $\mu$ M PMA (funakoshi) for 10 min at room temperature as a positive control. Western blotting was performed as described in “Two-step labeling of AMPARs in HEK293T cells”. In this experiment, Bullet Blocking One for Western Blotting (Nacalai tesque) was used for membrane blocking. Immunodetection of GluA1, pGluA1, GluN1, pGluN1, ERK, pERK, CREB and pCREB was performed with a rabbit anti-GluA1(abcam, ab109450, 1:1000), rabbit anti-pGluA1(CST, 75574S, 1:1000), mouse anti-GluN1(Millipore, 05-432 1:1000), rabbit anti-pGluN1 (CST, 3381S, 1:500), rabbit anti-ERK (CST, 9102S, 1:1000), rabbit pERK(CST, 9101S, 1:1000), rabbit anti-CREB (CST, 9197S, 1:1000) and rabbit anti-pCREB (CST, 9198S, 1:500).

### **Half-life studies of endogenous AMPARs in cultured neurons.**

Schematic illustration of the experiments is shown in Fig. 11a. For determining  $t_{1/2}^{\text{surface}}$ , after first step labeling as describe in “Two-step labeling of AMPARs in cultured neurons,” the cells were incubated for 0, 2, 4, 6, 12, 24, 48, 72, and 120 h. For the second step, the culture medium was removed and the cells were treated with 1  $\mu$ M Tz(F1) for 5 min in PBS at room temperature. To quench excess Tz(F1), 1  $\mu$ M TCO-PEG4-COOH in PBS was added and washed three times with PBS. Cell lysis and western blotting were performed as described in “Two-step labeling of AMPAR in

HEK293T cells.” The immunodetection of GluA2 was conducted with a rabbit anti-GluA2 antibody (abcam, ab20673, 1:3,000). Quantification of the band intensity and calculation of the half-time was calculated described as in “Half-life studies of AMPARs by western blotting in HEK293T cells.”

### **Intracellular and surface ratio of labeled AMPARs in cultured neurons.**

Schematic illustration of the experiments is shown in Fig. 3a. For determining labeled AMPARs on cell-surface (path-1 in Fig. 3a), after first step labeling as describe in “Two-step labeling of AMPARs in cultured neurons,” the cells were treated with 1  $\mu$ M Tz(Fl) for 5 min in PBS at room temperature. To quench excess Tz(Fl), 1  $\mu$ M TCO-PEG4-COOH in PBS was added and lysed with RIPA buffer containing 1% protease inhibitor cocktail for 30 min at 4 °C.

For determining intracellular labeled AMPARs (path-2 in Fig. 3a), after first step labeling, 1  $\mu$ M Tz(Ax647) was treated for 5 min for masking of cell-surface TCO-labeled AMPARs. After cell lysis using RIPA buffer containing 1% protease inhibitor cocktail for 30 min at 4 °C, the lysate was reacted with 0.3  $\mu$ M Tz(Fl) for 30 min at room temperature. Excess Tz(Fl) was quenched by addition of 1  $\mu$ M TCO-PEG4-COOH in the cell lysate.

For preparing whole-cell-labeling fraction (path-3 in Fig. 3a), after first step labeling, the cells were lysed with RIPA buffer containing 1% protease inhibitor cocktail for 30 min at 4 °C. The lysate was reacted with 0.3  $\mu$ M Tz(Fl) for 30 min at room temperature. Western blotting was performed as described in “Two-step labeling of AMPARs in HEK293T cells.” Quantification of the band intensity and calculation of the ratio was conducted as described in “Intracellular and surface ratio of labeled AMPARs in HEK293T cells.”

### **Quantification of recycled AMPARs in cultured neurons.**

## *Chapter 2*

The first step labeling was performed as describe in “Two-step labeling of AMPARs in cultured neurons.” For the second step, the culture medium was removed and the cells were treated with 1  $\mu$ M Tz(Fl) for 5 min in the culture medium at 37 °C. To quench excess Tz(Fl), 1  $\mu$ M TCO-PEG4-COOH in the culture medium was added. After incubation at 37 °C for 15 min, recycled AMPARs were labeled with 1  $\mu$ M Tz(Ax647) for 5 min in PBS. To quench excess Tz(Ax647), 1  $\mu$ M TCO-PEG4-COOH in PBS was added. Cell lysis and western blotting were performed as described in “Two-step labeling of AMPARs in HEK293T cells” using anti-Alexa 647 antibody. Quantification of the band intensity and calculation of the ratio was conducted as described in “Intracellular and surface ratio of labeled AMPARs in HEK293T cells.” Anti-Alexa 647 antibody was prepared from the sera of a rabbit immunized with an antigen which was a conjugate of Alexa 647-NHS and KLH (Sigma), and the antibody was affinity-purified using Alexa 647-conjugated agarose. Alexa 647-conjugated agarose was prepared from CarboxyLink Coupling Resin (Thermo Fisher) and Alexa 647 NHS ester (Invitrogen). The anti-sera (1:2,000) or the purified antibody (1:1,000) was used for the western blotting.

### **Quantification of recycled AMPARs in HEK293T cells.**

GluA2-expressing HEK293T cells were labeled with 2  $\mu$ M CAM2(TCO) in culture medium in 37 °C for 4 h. For the second step, the culture medium was removed and the cells were treated with 1  $\mu$ M Tz(Ax647) for 5 min in the culture medium at 37 °C. To quench excess Tz(Ax647), 1  $\mu$ M TCO-PEG4-COOH in the culture medium was added. After incubation at 37 °C for 15 min, recycled AMPARs were labeled with 1  $\mu$ M Tz(Fl) for 5 min in PBS. To quench excess Tz(Fl), 1  $\mu$ M TCO-PEG4-COOH in PBS was added. Cell lysis and western blotting were performed as described in “Two-step labeling of AMPARs in HEK293T cells”. The target bands were manually selected, and



the intensity were calculated with ImageJ software, background intensity was manually subtracted by selecting a region with no bands around the target bands.

### **Statistics and reproducibility.**

All graphs were generated using Microsoft Excel. All data are expressed as mean  $\pm$  s.e.m. I accumulated the data for each condition from at least three independent experiments. I evaluated statistical significance with Student's *t*-test for comparisons between two mean values. A value of  $P < 0.05$  was considered significant.

### **2-5, Reference**

1. Ehlers, M. D. Reinsertion or degradation of AMPA receptors determined by activity-dependent endocytic sorting. *Neuron* **28**, 511–525 (2000).
2. Mammen, A. L., Huganir, R. L. & O'Brien, R. J. Redistribution and stabilization of cell surface glutamate receptors during synapse formation. *J. Neurosci.* **17**, 7351–7358 (1997).
3. Hanus, C. *et al.* Unconventional secretory processing diversifies neuronal ion channel properties. *eLife* **5**, 1–27 (2016).
4. Kopec, C. D., Li, B., Wei, W., Boehm, J. & Malinow, R. Glutamate receptor exocytosis and spine enlargement during chemically induced long-term potentiation. *J. Neurosci.* **26**, 2000–2009 (2006).
5. Tanaka, H. & Hirano, T. Visualization of subunit-specific delivery of glutamate receptors to postsynaptic membrane during hippocampal long-term potentiation. *Cell Rep.* **1**, 291–298 (2012).
6. Keppler, A. *et al.* A general method for the covalent labeling of fusion proteins with small molecules in vivo. *Nat. Biotechnol.* **21**, 86–89 (2003).
7. Los, G. V. *et al.* HaloTag: A novel protein labeling technology for cell imaging and protein analysis. *ACS Chem. Biol.* **3**, 373–382 (2008).

## Chapter 2

8. Hirayama, S., Hori, Y., Benedek, Z., Suzuki, T. & Kikuchi, K. Fluorogenic probes reveal a role of GLUT4 *N*-glycosylation in intracellular trafficking. *Nat. Chem. Biol.* **12**, 853–859 (2016).
9. Griffin, B. A., Adams, S. R. & Tsien, R. Y. Specific covalent labeling of recombinant protein molecules inside live cells. *Science* **281**, 269–272 (1998).
10. Chen, I., Howarth, M., Lin, W. & Ting, A. Y. Site-specific labeling of cell surface proteins with biophysical probes using biotin ligase. *Nat. Methods* **2**, 99–104 (2005).
11. Nonaka, H., Fujishima, S. H., Uchinomiya, S. H., Ojida, A. & Hamachi, I. Selective covalent labeling of tag-fused GPCR proteins on live cell surface with a synthetic probe for their functional analysis. *J. Am. Chem. Soc.* **132**, 9301–9309 (2010).
12. Neubert, F. *et al.* Bioorthogonal click chemistry enables site-specific fluorescence labeling of functional NMDA receptors for super-resolution imaging. *Angew. Chem. Int. Ed.* **130**, 16602–16607 (2018).
13. Tsai, Y. H., Essig, S., James, J. R., Lang, K. & Chin, J. W. Selective, rapid and optically switchable regulation of protein function in live mammalian cells. *Nat. Chem.* **7**, 554–561 (2015).
14. Janssens, N. & Lesage, A.S.J. Glutamate receptor subunit expression in primary neuronal and secondary glial cultures. *J. Neurochem.* **77**, 1457–1474 (2001).
15. Wakayama, S. *et al.* Chemical labelling for visualizing native AMPA receptors in live neurons. *Nat. Commun.* **8**, 14850 (2017).
16. Podgorski, K., Terpetschnig, E., Klochko, O. P., Obukhova, O. M. & Haas, K. Ultra-bright and -stable red and near-infrared squaraine fluorophores for in vivo two-photon imaging. *PLoS One* **7**, (2012).
17. Tsunoyama, T. A. *et al.* Super-long single-molecule tracking reveals dynamic-anchorage-induced integrin function. *Nat. Chem. Biol.* **14**, 497–506

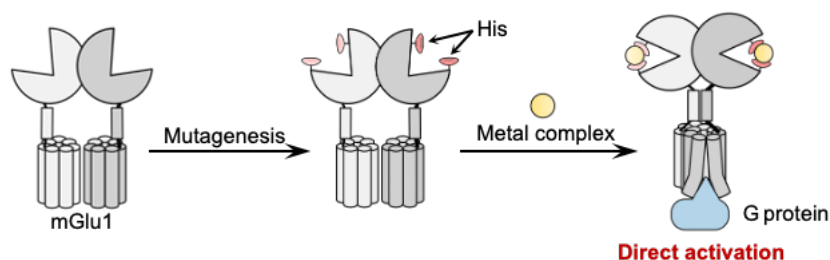
- (2018).
18. Ashby, M. C., Maier, S. R., Nishimune, A. & Henley, J. M. Lateral diffusion drives constitutive exchange of AMPA receptors at dendritic spines and is regulated by spine morphology. *J. Neurosci.* **26**, 7046–7055 (2006).
  19. O'Brien, R. J. *et al.* Activity-dependent modulation of synaptic AMPA receptor accumulation. *Neuron.* **21**, 1067–1078 (1998).
  20. Archibald, K., Perry, M. J., Molnár, E. & Henley, J. M. Surface expression and metabolic half-life of AMPA receptors in cultured rat cerebellar granule cells. *Neuropharmacol.* **37**, 1345–1353 (1998).
  21. Tomita, S., Fukata, M., Nicoll, R. A. & Brecht, D. S. Dynamic interaction of stargazin-like TARPs with cycling AMPA receptors at synapses. *Science* **303**, 1508–1511 (2004).

## Chapter 3

### Coordination chemogenetics for activation of GPCR-type glutamate receptors in brain tissue

#### Abstract

Direct activation of cell-surface receptors is highly desirable for elucidating the physiological roles of receptors. However, subtype-selective ligands are very limited because of the high homology among receptor subtypes. A potential approach for selective activation of a receptor subtype is chemogenetics, in which both point mutagenesis of the receptors and designed ligands are used. However, ligand-binding properties are affected in most current methods. Here, I developed a chemogenetic method for direct activation of metabotropic glutamate receptor 1 (mGlu1), which plays essential roles in cerebellar functions in the brain. A mGlu1 mutant, mGlu1(N264H), that was directly activated by palladium complexes was identified by screening assay. Notably, a palladium complex showing low cytotoxicity successfully activated mGlu1 in mGlu1(N264H) knock-in mice, revealing that activation of endogenous mGlu1 is sufficient to evoke the critical cellular mechanism of synaptic plasticity, a basis of motor learning in the cerebellum.



### 3-1, Introduction

Cell-surface receptors have indispensable roles in transmitting extracellular information into cells. Most receptors belong to protein families composed of highly homologous subtypes, each with unique physiological functions. In elucidating the roles of each receptor subtype, it is highly desirable to develop activators that selectively target a particular subtype. However, the high homology of the orthosteric ligand-binding site hampers the development of subtype-selective agonists<sup>1,2</sup>. Instead, researchers have focused on positive allosteric modulators (PAMs)<sup>3</sup>, which increase the efficacy of endogenous ligands by binding to an allosteric site as subtype-selective ligands. Although PAMs represent potentially powerful therapeutic agents to increase the efficacy of receptors in situations where the concentration of endogenous ligands is reduced, researchers should be careful when using PAMs to clarify the physiological functions of receptors. Given the non-uniform concentration of endogenous ligands such as neurotransmitters in tissues<sup>4</sup>, the effects of a PAM may reflect the concentration of the ligands rather than the receptor function. Thus, direct activators with high subtype-selectivity are ideal for understanding the physiological roles of the target receptor.

A potential method for direct activation of target receptors would be chemogenetics, in which proteins are genetically engineered to interact with the designed ligand selectively<sup>5</sup>. Designer receptors exclusively activated by designer drugs (DREADDs), which have low constitutive activity and high selectivity to an artificial ligand, clozapine-*N*-oxide, have been developed by directed molecular evolution of muscarinic acetylcholine receptors<sup>6</sup>. In association with improving the designed ligands, DREADDs are powerful tools to control cellular signaling of target cells in tissues or living animals<sup>7,8</sup>. Although powerful for manipulating cellular signals, this method is not suitable for understanding the physiological roles of each receptor subtype because engineered receptors lacking affinity to endogenous ligands need to be ectopically

expressed. Thus, developing new chemogenetic methods to directly activate receptor subtypes with synthetic ligands without affecting the original receptor function is highly desirable. As a potential approach, our group have recently reported a chemogenetic method using coordination chemistry for the AMPAR and metabotropic mGlu1, which belong to ionotropic and metabotropic glutamate receptors, respectively<sup>9,10</sup>. In this method, structure-based incorporation of coordinating amino acid residues as allosteric sites into glutamate receptors allowed metal-complex-associated activation of glutamate receptors in HEK293 cells or cultured neurons. Although useful for chemogenetic activation of these receptors, the chemogenetic coordination acted as a PAM, which increased the affinity of glutamate to the receptors.

In this chapter, I developed a direct activation method of mGlu1 by chemogenetics, termed dA-CBC (direct-activation via coordination-based chemogenetics). In the engineered receptor, Pd(bpy) [Pd(bpy)(NO<sub>3</sub>)<sub>2</sub>; bpy, 2,2'-bipyridine] directly activated the mGlu1 mutant without potentiating the affinity of glutamate. I also designed a derivative of Pd(bpy) with low toxicity to neurons. In mice with the mGlu1 mutation, the newly developed palladium complex successfully induced downstream signals of mGlu1 in acute cerebellar slices of the mice. Notably, the palladium complex evoked synaptic plasticity such as long-term depression (LTD), a putative cellular model of information storage for motor learning in the cerebellum of mammals. Thus, dA-CBC revealed that activation of mGlu1 is sufficient to evoke a critical cellular mechanism of memory in the cerebellum.

## 3-2, Result and Discussion

### 3-2-1, Screening the direct-activator-type mGlu1 mutant by dA-CBC.

mGlu1, with a large extracellular and a 7-transmembrane (7TM) domain, belongs to the class C G-protein coupled receptor (GPCR) family. The extracellular domain is composed of a Venus Flytrap (VFT) domain and a cysteine-rich domain (CRD) for glutamate binding and as a semi-rigid linker, respectively (Fig. 1a)<sup>11</sup>. Glutamate binding to the VFT domain induces closure of the domain in the mGlu1 homodimer, which is transmitted to the 7TM domain via CRD for receptor activation (Fig. 1a). I reported chemogenetic methods previously for allosteric activation of glutamate receptors by regulating the open and closed form of the VFT domain using metal coordination, termed on-cell coordination chemistry (OcCC). I identified a mGlu1 mutant, mGlu1(P58H/N264H), whose glutamate-induced responses were allosterically activated by Pd(bpy) (Fig. 1b, top). In the mutant, 1  $\mu$ M of glutamate, which is insufficient for receptor activation, successfully induced intracellular signals in the presence of Pd(bpy). Importantly, the mGlu1 mutant was activated by Pd(bpy) even in the absence of glutamate, which guided the hypothesis that the introduction of histidine mutations in appropriate positions should induce direct activation of the mGlu1 by metal coordination without potentiating the affinity of glutamate (Fig. 1b, bottom). This strategy is termed dA-CBC, and our previous OcCC is renamed A-CBC (activation via coordination-based chemogenetics).

Here, I prepared seven mGlu1 mutants with two histidine mutations on both upper and lower lobes at the entrance of the VFT domain (Fig. 1c). The mutation sites, which are not involved in glutamate binding, were selected to minimize the influence on receptor function and based on structural information available for open (*i.e.*, apo) and closed (*i.e.*, glutamate-binding) conformations<sup>12,13</sup>. I hypothesized that domain closure occurs by metal coordination instead of glutamate binding when the mutated histidines work as a bidentate chelator for metal ions or complexes. mGlu1 is a Gq-coupled GPCR,

which elevates the intracellular  $\text{Ca}^{2+}$  concentration ( $[\text{Ca}^{2+}]_i$ ) via phospholipase C (PLC) activation. Receptor activation was evaluated by monitoring  $[\text{Ca}^{2+}]_i$  changes using a fluorescent  $\text{Ca}^{2+}$  indicator, Fura-2, after treatment with 10  $\mu\text{M}$  metal ions ( $\text{Ni}^{2+}$ ,  $\text{Cu}^{2+}$ ,  $\text{Zn}^{2+}$ ,  $\text{Cd}^{2+}$  or  $\text{Pd}^{2+}$ ) or a metal complex (Pd(bpy)) in HEK293 cells transfected with each mGlu1 mutant (Fig. 2a). The 1st screening identified five mutants (P57H/N264H, P58H/N264H, A59H/N264H, E60H/N264H, K61H/N264H) that were prominently activated by Pd(bpy) (Fig. 1d, e and Fig. 2b). Although  $\text{Pd}^{2+}$  also activated three mutants (P58H/N264H, E60H/N264H, K61H/N264H), the obtained  $\Delta$ ratio values were not that high when compared with those by Pd(bpy). Other metal ions ( $\text{Ni}^{2+}$ ,  $\text{Cu}^{2+}$ ,  $\text{Zn}^{2+}$  or  $\text{Cd}^{2+}$ ) failed to activate these mGlu1 mutants. I selected three mutants (P58H/N264H, A59H/N264H, K61H/N264H) as hit mutants from the 1st screening because these three mutants showed intact glutamate-induced responses and prominent Pd(bpy)-induced responses (Fig. 1e). The calculated half-maximal effective concentration ( $\text{EC}_{50}$ ) values of Pd(bpy) were 1.2–3.8  $\mu\text{M}$  for the three mutants (Fig. 1f). The dose-dependency of glutamate-evoked responses was not affected significantly in these mutants when compared with that of wild-type (WT) mGlu1 (Fig. 3), indicating that introduction of these histidine mutations did not affect the original receptor function of mGlu1.



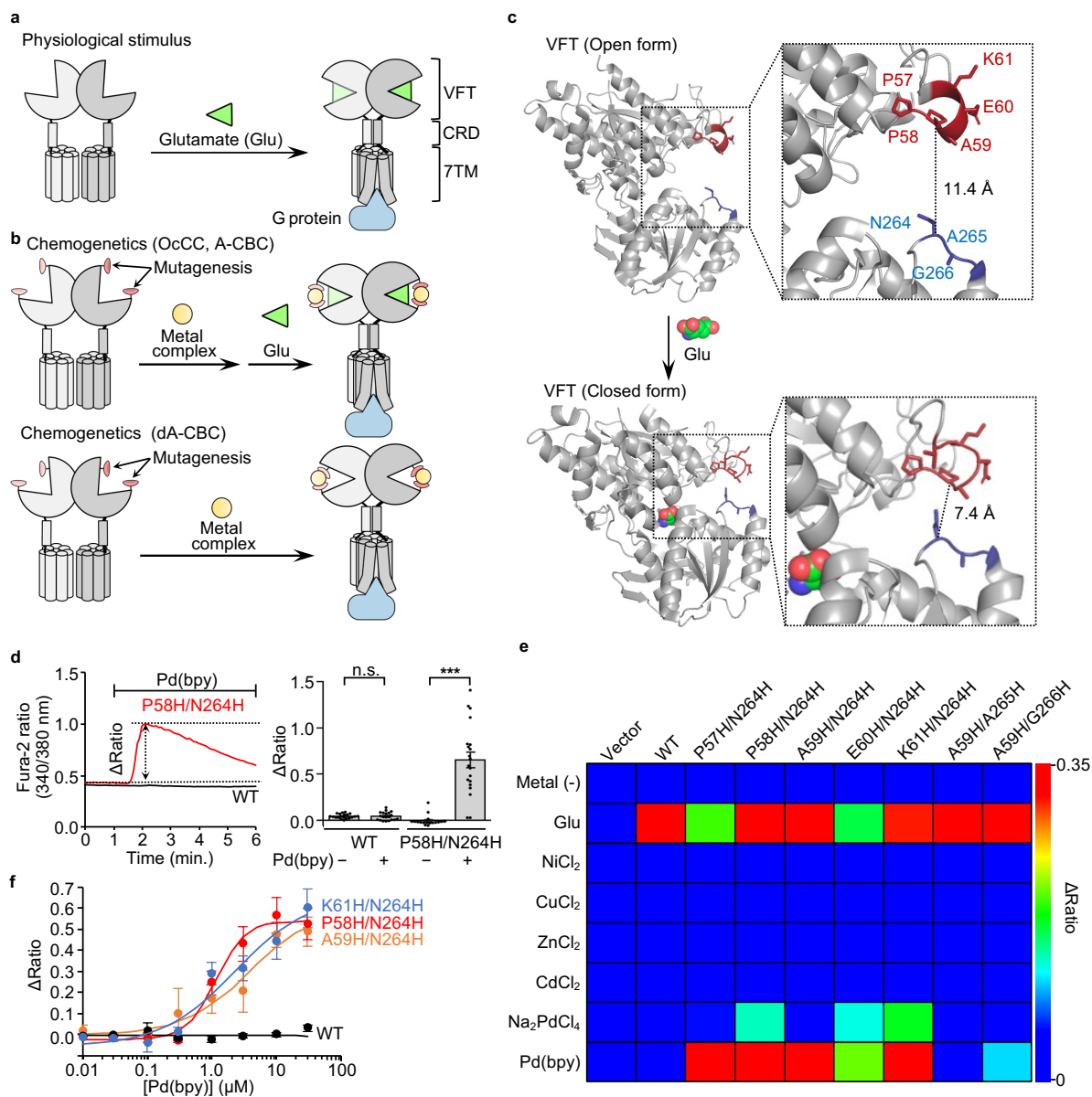


**Fig. 1 | Screening of the direct-activation-type mGlu1 mutants.** (a) Schematic illustration of glutamate-induced conformational changes of mGlu1. (b) Schematic illustration of the coordination-based chemogenetics (CBC). Upper: allosteric activation of mGlu1 by A-CBC (OcCC in the previous terminology). Bottom: direct activation of mGlu1 by dA-CBC. (c) Conformational change of the VFT on the glutamate binding. Upper: open form in the apo state (Protein Data Bank (PDB) 1EWT). Lower: closed form in the glutamate-binding state (PDB 1EWK). The mutation sites at the upper and lower lobes are highlighted in red and blue. (d) Pd(bpy)-induced mGlu1 responses in HEK293 cells. Left: representative trace of  $\text{Ca}^{2+}$  response induced by 10  $\mu\text{M}$  of Pd(bpy) in HEK293 cells transfected with the plasmid of mGlu1 P58H/N264H mutant (red) or WT mGlu1 (black). The  $\Delta$ ratio is defined as the difference between the maximum and the initial ratio values. Right: averaged  $\Delta$ ratio in the presence or absence of 10  $\mu\text{M}$  of Pd(bpy). (n = 20). \*\*\*Significant difference ( $P < 0.001$ , two-tailed Welch's  $t$ -test). n.s.,

### Chapter 3

not significant ( $P > 0.05$ ). **(e)** The heatmap shows the averaged  $\Delta$ ratio induced by 10  $\mu$ M glutamate, metal ions, or a metal complex. See Fig. 2b for each data. **(f)** Concentration-dependent curves for Pd(bpy) in HEK293 cells expressing mGlu1 WT (black), P58H/N264H (red), A59H/N264H (orange) or K61H/N264H (blue). (n = 20).  $EC_{50}$  values were 1.2, 3.8, and 2.3  $\mu$ M for P58H/N264H, A59H/N264H, and K61H/N264H, respectively.

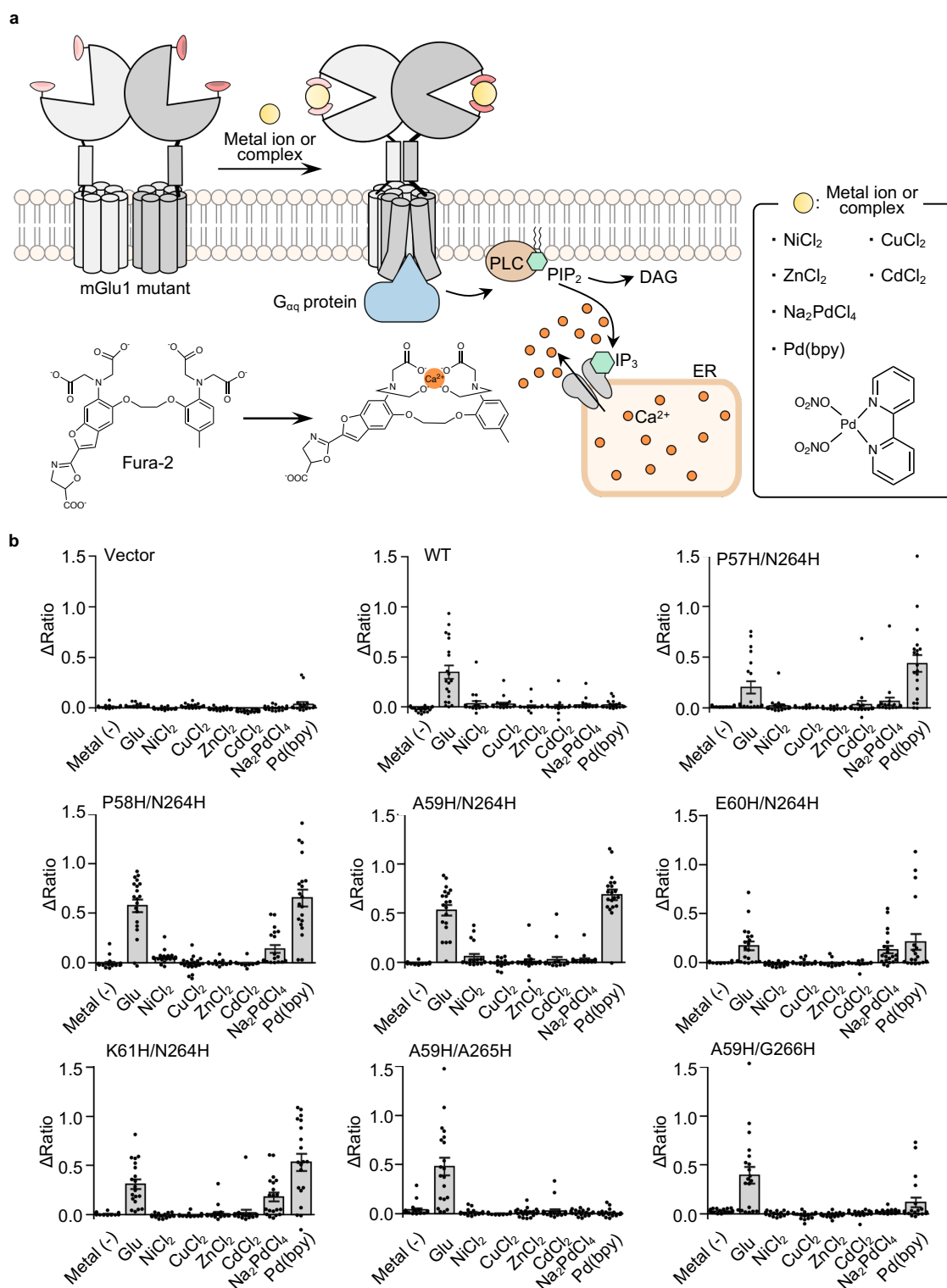


**Fig. 2 | Screening assay for mGlu1 double mutants with metal ions and a metal complex. (a)** Schematic illustrations of detection of  $[Ca^{2+}]_i$  changes after activation of Gq-coupled mGlu1 using Fura-2. **(b)** Averaged  $\Delta$ ratio induced by 10  $\mu$ M of glutamate, metal ions, or metal complex. Data are presented as mean  $\pm$  s.e.m.

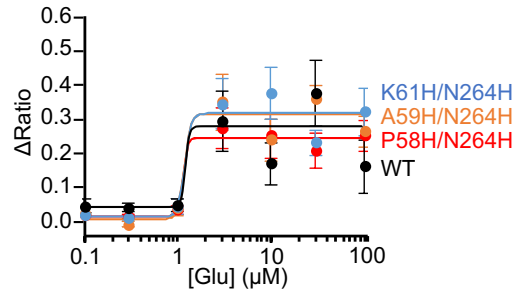


**Fig. 3 | Concentration-dependent curves of glutamate for hit mutants or WT mGlu1.** Concentration-dependent curves for glutamate in HEK293 cells expressing mGlu1 WT (black), P58H/N264H (red), A59H/N264H (orange) or K61H/N264H (blue). (n = 20). Data are presented as mean  $\pm$  s.e.m.

### 3-2-2, 2nd Screening for dA-CBC of mGlu1

Although hit mutants and Pd(bpy) pairs were obtained, it was unclear whether Pd(bpy) acts as a direct activator or an activator coupled with PAM activity (*i.e.*, ago-PAM)<sup>2</sup> for the mGlu1 mutants. Then, in the next step (*i.e.*, 2nd screening), I aimed to find mGlu1 mutants activated by Pd(bpy) directly without potentiating the affinity of glutamate. To evaluate the PAM effect selectively by excluding the direct activation effect of Pd(bpy), I used a mGlu1-selective orthosteric antagonist, LY367385 (ref. 14), which competitively binds with glutamate to the VFT domain (Fig. 4a). As shown in Fig. 4b and 4c, pretreatment with LY367385 suppressed glutamate-induced responses. Importantly, 10  $\mu$ M LY367385 also inhibited Pd(bpy)-induced Ca<sup>2+</sup> responses in the mGlu1(P58H/N264H) mutant (Fig. 4d and 4e), which showed that direct activation of Pd(bpy) can be suppressed by the orthosteric antagonist. Then, I directly evaluated the positive allosteric effect of Pd(bpy) for the glutamate-induced response by pretreatment with LY367385 (Fig. 4f). The dose-dependent glutamate-induced responses of the hit mutants were obtained even in the presence of LY367385, and the positive allosteric effect of Pd(bpy) was largely different among these mutants (Fig. 4g). The EC<sub>50</sub> values of glutamate were shifted to the left for the P58H/N264H or K61H/N264H mutant (Fig.4g). In contrast, a prominent shift of the EC<sub>50</sub> value was not observed for the A59H/N264H mutant, indicating that the A59H/N264H mutant was activated by Pd(bpy) without potentiating glutamate affinity. In contrast, Pd(bpy) acted as ago-PAM for P58H/N264H and K61H/N264H mutants. Thus, the screening results identified the A59H/N264H mutant and Pd(bpy) as a hit pair for dA-CBC of mGlu1.

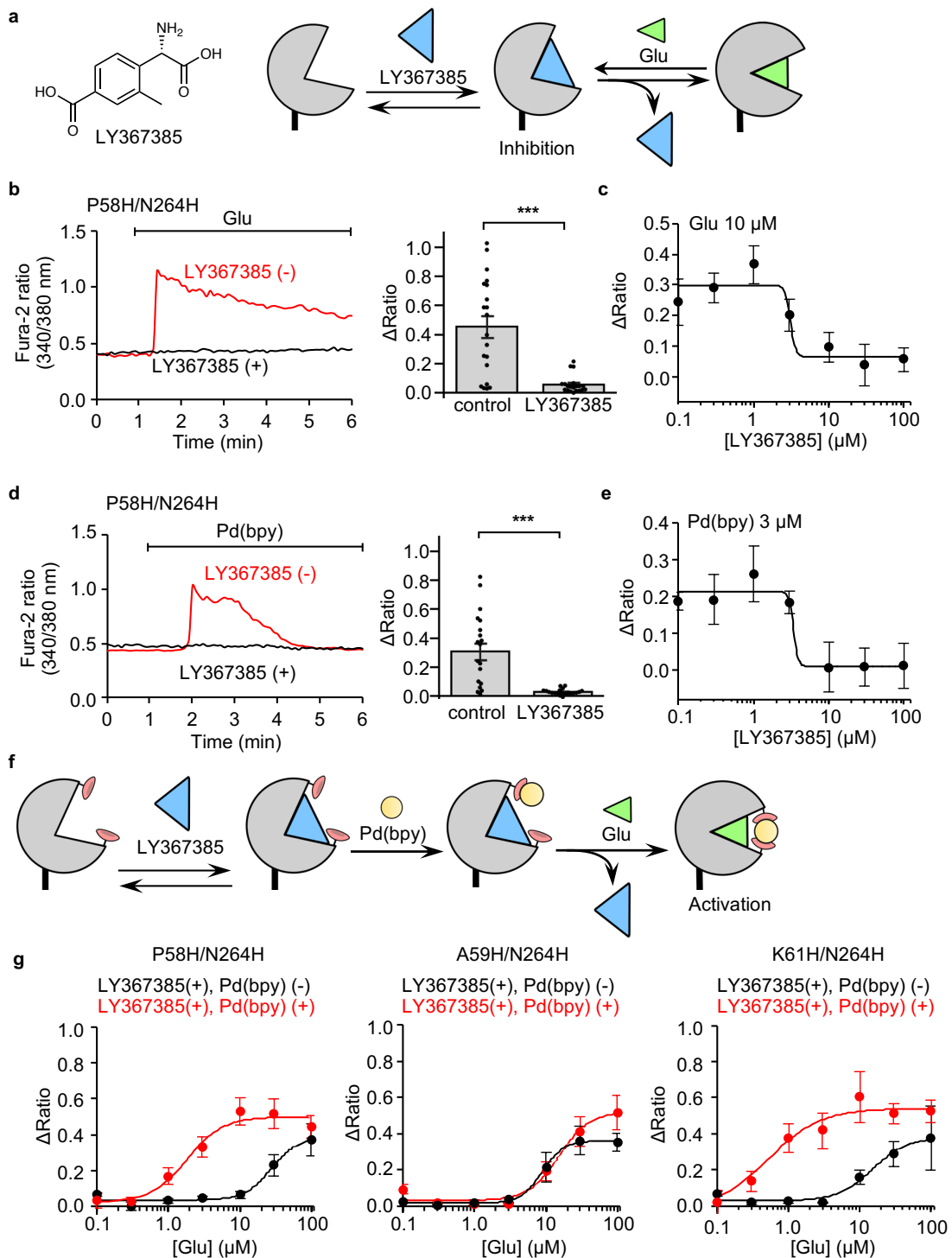


**Fig. 4 | Evaluation of positive allosteric effects of the Pd(bpy) for mGlu1 mutants by co-treatment of competitive antagonist, LY367385. (a)** Schematic illustrations of competitive inhibition of mGlu1 using LY367385. **(b, c)** Inhibition of the 10  $\mu\text{M}$  glutamate-induced responses using LY367385 in HEK293 cells transfected with the plasmid of mGlu1 P58H/N264H mutant. In **b**, representative traces of  $\text{Ca}^{2+}$  response with (black) or without (red) 10  $\mu\text{M}$  LY367385 are shown ( $n = 20$ ), and averaged  $\Delta\text{Ratio}$  is shown in the right. \*\*\*Significant difference ( $P < 0.001$ , two-tailed Welch's  $t$ -test). In **c**, a concentration dependent curve of LY367385 for the inhibition of 10  $\mu\text{M}$

glutamate-induced response is shown. (n = 20). **(d, e)** Inhibition of the 3  $\mu\text{M}$  Pd(bpy)-induced responses using LY367385 in HEK293 cells transfected with the plasmid of mGlu1 P58H/N264H mutant. In **d**, representative traces of  $\text{Ca}^{2+}$  response with (black) or without (red) 10  $\mu\text{M}$  LY367385 are shown (n = 20), and averaged  $\Delta\text{ratio}$  is shown in the right. \*\*\*Significant difference ( $P < 0.001$ , two-tailed Welch's  $t$ -test). In **e**, a concentration-dependent curve of LY367385 for the inhibition of 3  $\mu\text{M}$  Pd(bpy)-induced response is shown. (n = 20). **(f)** Schematic illustrations of the evaluation of positive allosteric effect of Pd(bpy) for glutamate-induced responses in the presence of LY367385. **(g)** Evaluation of the positive allosteric effect of Pd(bpy) to the mGlu1 mutants. Effects of 3  $\mu\text{M}$  Pd(bpy) on the concentration-dependency of the glutamate-responses were examined in the presence of 10  $\mu\text{M}$  LY367385 in HEK293 cells expressing the hit mutants (P58H/N264H, A59H/N264H, K61H/N264H). (n = 20). Data are presented as mean  $\pm$  s.e.m.

### 3-2-3, Direct activation mechanism of the mGlu1 mutant by dA-CBC.

I next investigated the activation mechanism of the mGlu1 A59H/N264H mutant. The corresponding single mutants (A59H and N264H mutants) were prepared to examine the bidentate coordination of Pd(bpy) to both histidine residues. As shown in Fig. 5a, Pd(bpy) failed to activate the A59H mutant. In contrast, the N264H mutant was unexpectedly activated by Pd(bpy). In both mutants, glutamate responses were intact, suggesting that receptor function was unaffected by the mutations (Fig. 5b). Regarding other Pd(bpy)-responsive mutants (P58H/N264H and K61H/N264H), the corresponding single mutants (P58H and K61H) failed to be activated by Pd(bpy) (Fig. 5a). These results indicate that the single N264H mutation is sufficient for the chemogenetic activation of mGlu1.

Considering the putative activation mechanism of dA-CBC (Fig. 1b, bottom), a coordination partner of the N264H mutation for Pd(bpy) binding is required on the upper lobe of the VFT domain. I found four coordinating amino acid residues (H54, H55, E60, H111) within 15 Å from the N264 residue in the crystal structure of the closed-form of the VFT domain (Fig. 5c and Table 1). These candidate amino acids were exchanged to phenylalanine or alanine in the N264H mutant, and Pd(bpy)-induced responses were examined for these mutants. As shown in Fig. 5d, the H54F/N264H and H55F/N264H mutant failed to be activated by Pd(bpy). However, glutamate-induced responses were also lost in the H54F/N264H mutant but not the H55F/N264H mutant. Given that H54 interacts with D107 in the crystal structure<sup>12</sup>, substituting this residue is likely to be lethal for receptor activity in the H54F/N264H mutant. Collectively, although the involvement of H54 cannot be excluded, endogenous H55 is probably the coordination partner of the N264H mutation for Pd(bpy)-induced chemogenetic activation. The EC<sub>50</sub> value of Pd(bpy) for the N264H mutant was 1.6 μM, and glutamate-induced responses were unaffected by the N264H mutation (Fig. 6a, b). Importantly, the dose-dependency of the glutamate-induced responses in the presence of



LY367385 was unaffected in the presence of Pd(bpy), indicating that the affinity of glutamate was not potentiated by Pd(bpy) in the mGlu1(N264H) mutant (Fig. 6c). Thus, the single point mutation (N264H) is sufficient for the direct activation of mGlu1 by Pd(bpy).

The chemogenetic activation of the mGlu1(N264H) mutant in HEK293 cells was examined in more detail. Western blotting indicated that the total expression level of the N264H mutant was comparable to that of WT mGlu1 (Fig. 6d). A newly designed mGlu1-selective fluorescent probe, FITM-Cy3, was designed to quantify the expression level of mGlu1 on the cell-surface under live-cell conditions (Fig. 6e). FITM, a negative allosteric modulator (NAM) of mGlu1<sup>15</sup>, which binds to the 7TM domain<sup>16</sup>, was conjugated with an anionic fluorescent dye, sulfo-Cy3, to obtain FITM-Cy3. Confocal live imaging clearly showed that FITM-Cy3 visualizes surface mGlu1 with a dissociation constant ( $K_d$ ) of 6.8 nM in HEK293 cells (Fig. 7), and FITM-Cy3 clarified that surface expression of the N264H mutant was comparable to that of WT mGlu1 (Fig. 6f). I also examined reversibility and selectivity of the Pd(bpy)-induced activation of mGlu1. As shown in Fig. 8, repeated  $[Ca^{2+}]_i$  increases were observed after washing out Pd(bpy) in the culture medium. The Pd(bpy)-induced mGlu1 responses were inhibited by LY367375 or FITM, which binds to the VFT or 7TM domain of mGlu1, respectively (Fig. 9a, b). Moreover, U73122, a PLC inhibitor, suppressed the Pd(bpy) induced response (Fig. 9c), which indicates that Pd(bpy) activates the conventional Gq-pathway of mGlu1. Thus, I can directly and reversibly activate mGlu1 and its downstream signal pathways with minimal disturbance of the receptor function by using a pair of Pd(bpy) and single-point mutagenesis (N264H) of mGlu1 in the dA-CBC method.

**Table 1 | Distance (Å) between  $\alpha$ -carbon atoms estimated by the crystal structure of mGlu1 open form (PDB 1EWT) and closed form (PDB 1EWK).**

	H54-N264	H55-N264	E60-N264	H111-N264
Apo	20.1	16.3	16.8	17.4
Glutamate binding	13.9	10.2	10.4	10.9

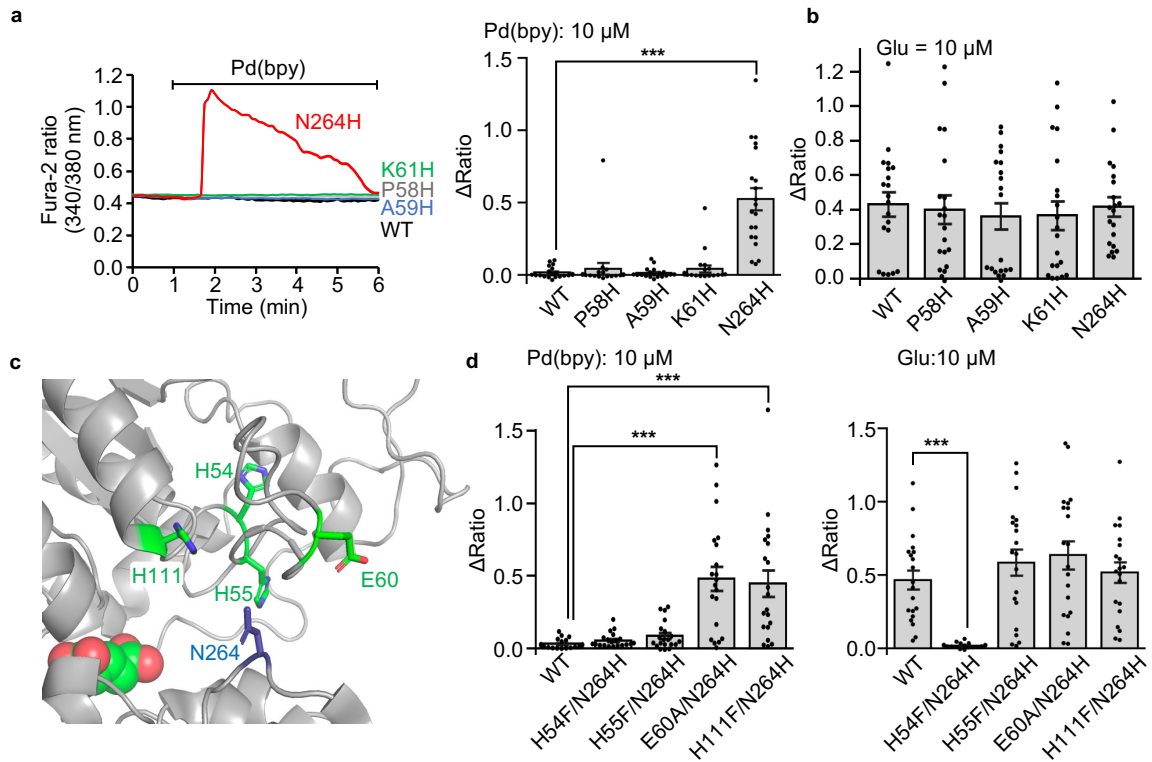


**Fig. 5 | Mechanism of direct activation of the mGlu1 mutant by dA-CBC.** (a) Pd(bpy)-induced mGlu1 responses in HEK293 cells expressing the mGlu1 mutant. Left: representative traces of  $\text{Ca}^{2+}$  responses induced by  $10 \mu\text{M}$  of Pd(bpy) in HEK293 cells expressed with the mGlu1 N264H (red), P58H (grey), A59H (blue), or K61H (green) mutants. Right: averaged  $\Delta\text{Ratio}$ . ( $n = 20$ ). (b) Glutamate-induced mGlu1 responses were evaluated in HEK293 cells expressed with WT mGlu1, mGlu1(P58H), mGlu1(A59H), mGlu1(K61H), or mGlu1(N264H) mutant. ( $n = 20$ ). (c) Mutated coordinating amino acid residues within  $15 \text{ \AA}$  from N264 in the crystal structure of the VFT domain (PDB 1EWK). (d) Averaged  $\Delta\text{Ratio}$  induced by  $10 \mu\text{M}$  Pd(bpy) (left) and  $10 \mu\text{M}$  glutamate (right). ( $n = 20$ ). \*\*\*Significant difference ( $P < 0.001$ , One-way ANOVA with Dunnet's test). Data are presented as mean  $\pm$  s.e.m.

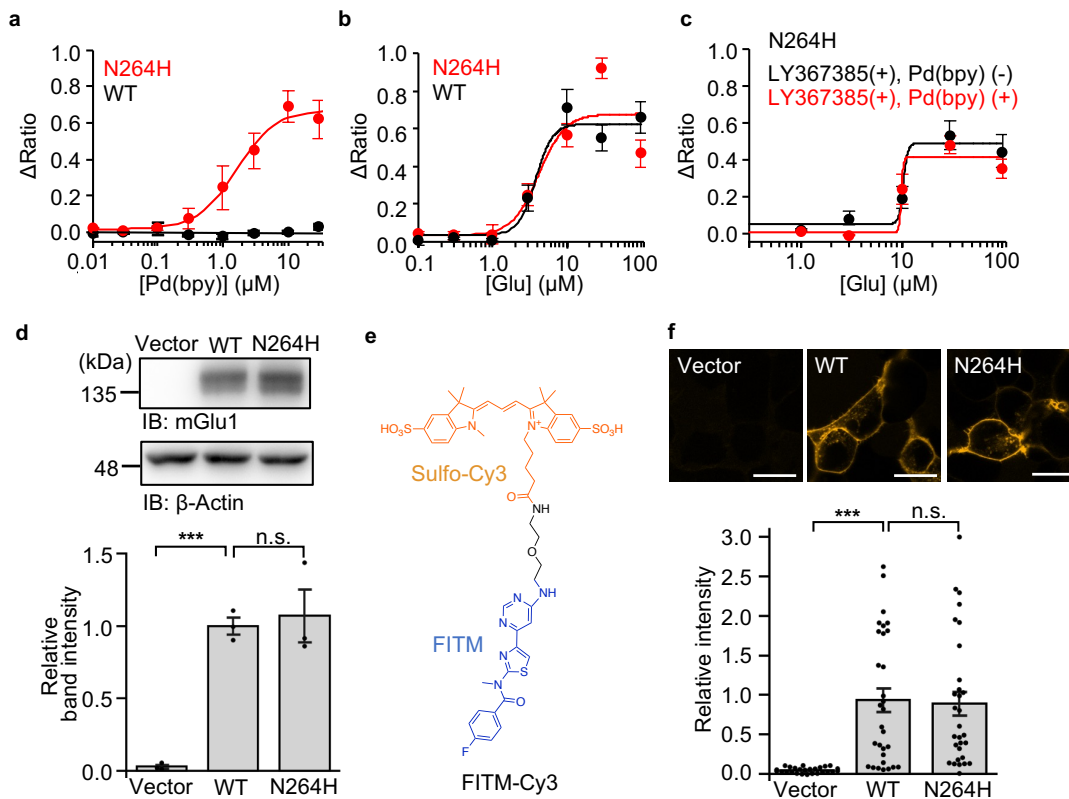


**Fig. 6 | Characterization of mGlu1 N264H mutant.** (a, b) Concentration-dependent curves for Pd(bpy) (in a) and glutamate (in b) in HEK293 cells expressing mGlu1(N264H) or WT mGlu1. (n = 20). (c) Evaluation of the positive allosteric effect of Pd(bpy) to the mGlu1(N264H) mutant. Effect of 3 μM Pd(bpy) on the concentration-dependency of the glutamate-responses in the presence of 10 μM LY367385 in HEK293 cells expressing mGlu1(N264H) is shown. (n = 20). (d) Evaluation of the protein expression level of mGlu1(N264H) by western blotting. (n = 3, biologically independent experiments). \*\*\*Significant difference ( $P < 0.001$ , One-way ANOVA with Dunnet's test). n.s., not significant ( $P > 0.05$ ). (e) Chemical structure of FITM-Cy3, a fluorescent probe for mGlu1. (f) Evaluation of the cell-surface expression of mGlu1(N264H) by live imaging using FITM-Cy3. Upper: Representative confocal images of the HEK293 cells transfected with WT mGlu1, mGlu1(N264H), or vector control after addition of 1 μM FITM-Cy3. Lower: quantification of fluorescent intensity on the cell-surface. (n = 30). Scale bars, 20 μm. \*\*\*Significant difference ( $P < 0.001$ , One-way ANOVA with Dunnet's test). n.s., not significant ( $P > 0.05$ ).

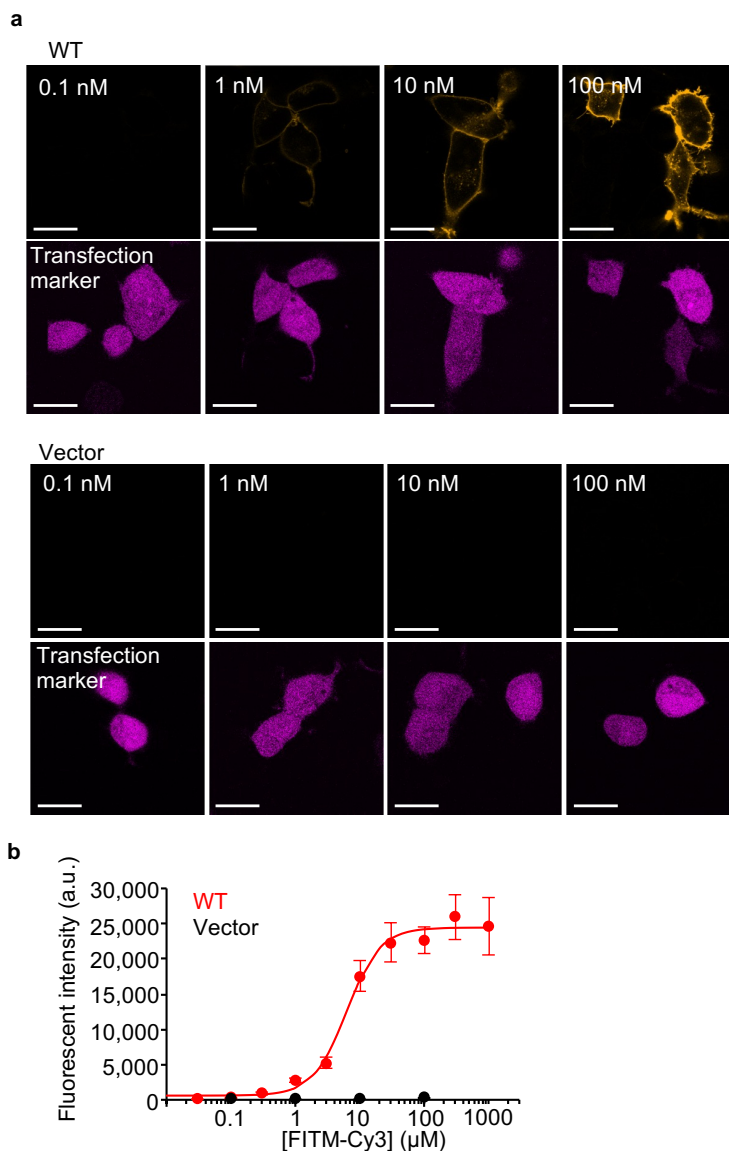


**Fig. 7 | Evaluation of the affinity of FITM-Cy3 to mGlu1 WT by confocal microscopy. (a)** Confocal live imaging of surface mGlu1 using various concentrations of FITM-Cy3 (upper) and transfection marker (lower) in HEK293 cells expressing WT mGlu1 or the control vector. iRFP670 was utilized as a transfection marker. **(b)** Concentration-dependent curves for fluorescent intensity of FITM-Cy3 in HEK293 cells expressing WT mGlu1 (red) and vector control (black) ( $n = 26\text{--}118$ ). The  $K_d$  value of FITM-Cy3 to WT mGlu1 on the cell-surface was determined to be  $6.8 \pm 2.7$  nM ( $n = 3$ , biologically independent experiments). Data are presented as mean  $\pm$  s.e.m.

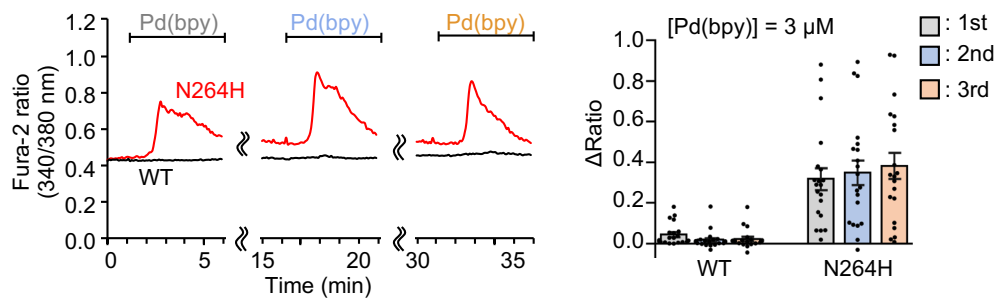


**Fig. 8 | The  $\text{Ca}^{2+}$  response induced by the repetitive treatment of 3  $\mu\text{M}$  Pd(bpy).** Left: representative trace of the  $\text{Ca}^{2+}$  response induced by 3  $\mu\text{M}$  Pd(bpy) in HEK293 cells expressing WT mGlu1(black) or mGlu1(N264H) (red). Pd(bpy) was treated repetitively after washing the cells with the culture medium and measurement buffer for 10 min. Right: averaged  $\Delta\text{Ratio}$  induced by 3  $\mu\text{M}$  Pd(bpy). (n = 20). Data are presented as mean  $\pm$  s.e.m.

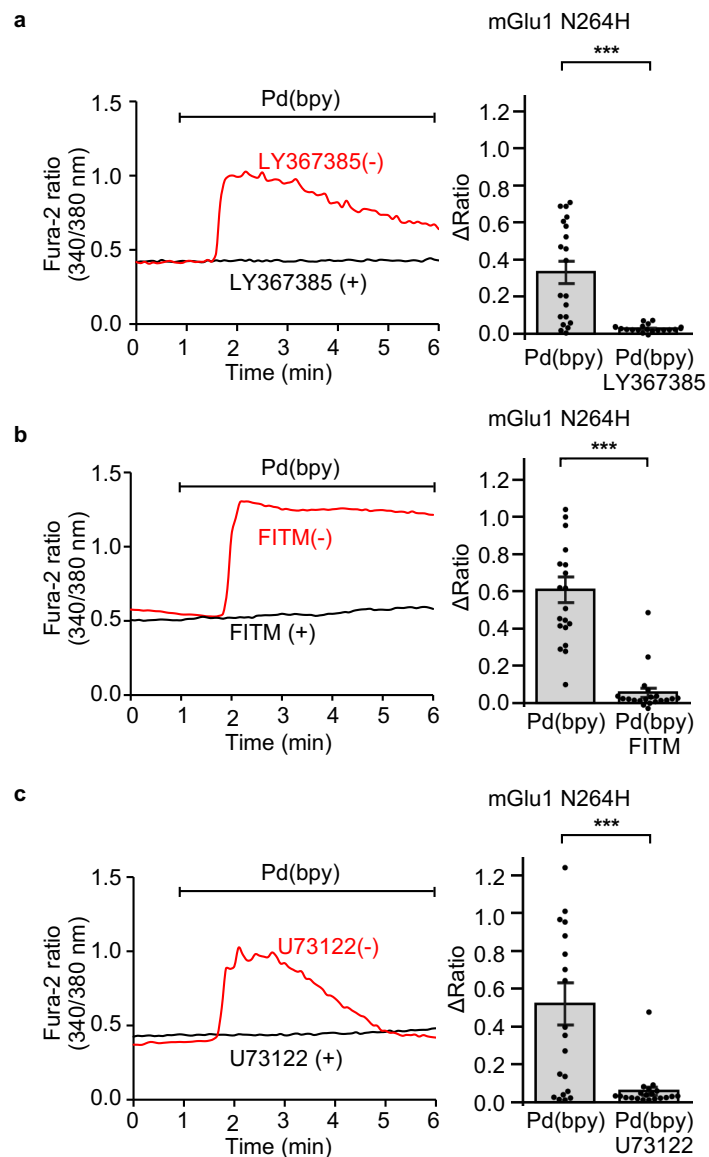


**Fig. 9 | Inhibition of Pd(bpy) induced- $\text{Ca}^{2+}$  responses using LY367385, FITM, or U73122.** Left: Representative trace of 10  $\mu\text{M}$  Pd(bpy)-induced responses pre-treated with 10  $\mu\text{M}$  LY367385 (in **a**), 1  $\mu\text{M}$  FITM (in **b**), or 10  $\mu\text{M}$  U73122 (in **c**) in HEK293 cells expressing mGlu1 N264H. Right: averaged  $\Delta$ ratio. (n = 20). \*\*\*Significant difference ( $P < 0.001$ , two-tailed Welch's  $t$ -test). Data are presented as mean  $\pm$  s.e.m.

### 3-2-4, Design of low cytotoxic Pd(bpy) derivatives for neurons.

Palladium complexes have attracted much attention as anti-cancer drugs because their geometry and complex forming processes are similar to those of platinum-based drugs such as cisplatin<sup>17,18</sup>. The putative molecular mechanism of the anti-tumor activity underlies DNA binding of these metal complexes. However, neurotoxicity has been reported for the clinical use of platinum drugs<sup>19</sup>. Although previous reports show palladium complexes having favorable neurotoxicity when compared with that of platinum drugs, the neurotoxicity of palladium complexes needs to be examined when used in neurons or brain tissues.

Pd(bpy) toxicity was examined in PC12 cells, a neuron-like cell-line, or in primary cortical neurons (Fig. 10). The effect of Pd(bpy) on neuronal outgrowth, a characteristic feature of neurons, was evaluated in PC12 cells after differentiation of the cells by nerve growth factor (NGF). As shown in Fig. 10b, neurite outgrowth was not affected even at a high concentration of Pd(bpy) ([Pd(bpy)] = 100  $\mu$ M). However, 30  $\mu$ M Pd(bpy) clearly suppressed cell growth in undifferentiated PC12 cells (Fig. 10c). In primary cortical neurons, gradual  $[Ca^{2+}]_i$  elevation was observed by treatment with 10  $\mu$ M Pd(bpy), which became more prominent by 30  $\mu$ M Pd(bpy) (Fig. 10d). Importantly, this  $[Ca^{2+}]_i$  elevation was suppressed by neither the mGlu1 inhibitors (LY367385 and FITM) nor the PLC inhibitor (U73122) (Fig. 11), which indicated a side effect of Pd(bpy) at the concentration used with the neurons. Considering the action of palladium complexes as anti-cancer drugs in the intracellular area, these unfavorable effects of Pd(bpy) are likely caused by cell permeability of the complex.

I then newly designed palladium complexes bearing hydrophilic or anionic ligands to suppress permeation of these compounds into cells (Fig. 10a). As shown in Fig. 10e, 3  $\mu$ M Pd(OH-bpy) and Pd(sulfo-bpy) successfully activated mGlu1(N264H). However, Pd(EG-bpy) showed weakened responses, and Pd(di-sulfo-bpy) failed to activate mGlu1(N264H) at the same concentration (Fig. 10e). The EC<sub>50</sub> values of Pd(OH-bpy)



and Pd(sulfo-bpy) for mGlu1(N264H) activation were 1.1 and 0.62  $\mu\text{M}$ , respectively (Fig. 10f). I next examined the effect of Pd(OH-bpy) or Pd(sulfo-bpy) on cell growth of PC12 cells. As with the case of Pd(bpy), cell growth was suppressed by 30  $\mu\text{M}$  Pd(OH-bpy). In contrast, for Pd(sulfo-bpy), cell growth was unaffected even at the high concentration ( $[\text{Pd(sulfo-bpy)}] = 100 \mu\text{M}$ ) (Fig. 10c). More critically, in cortical neurons, the influence on  $[\text{Ca}^{2+}]_i$  elevation was not observed following treatment with 30  $\mu\text{M}$  Pd(sulfo-bpy) (Fig. 10d), suggesting that the side effects were successfully suppressed using Pd(sulfo-bpy) bearing the anionic ligand. Consistently, the solubility of Pd(sulfo-bpy) was clearly improved when compared with that of Pd(bpy) (Fig. 10g). In the case of Pd(bpy), a linear increase of the absorbance at 312 nm was lost over 300  $\mu\text{M}$  Pd(bpy) in artificial cerebrospinal fluid (ACSF), a buffer solution used for brain tissue experiments in the next section. In contrast, linearity of the absorbance was observed over 1 mM for Pd(sulfo-bpy), indicating that Pd(sulfo-bpy) stock solutions can be prepared in ACSF, which is another improvement when applying the palladium complex to brain slices.

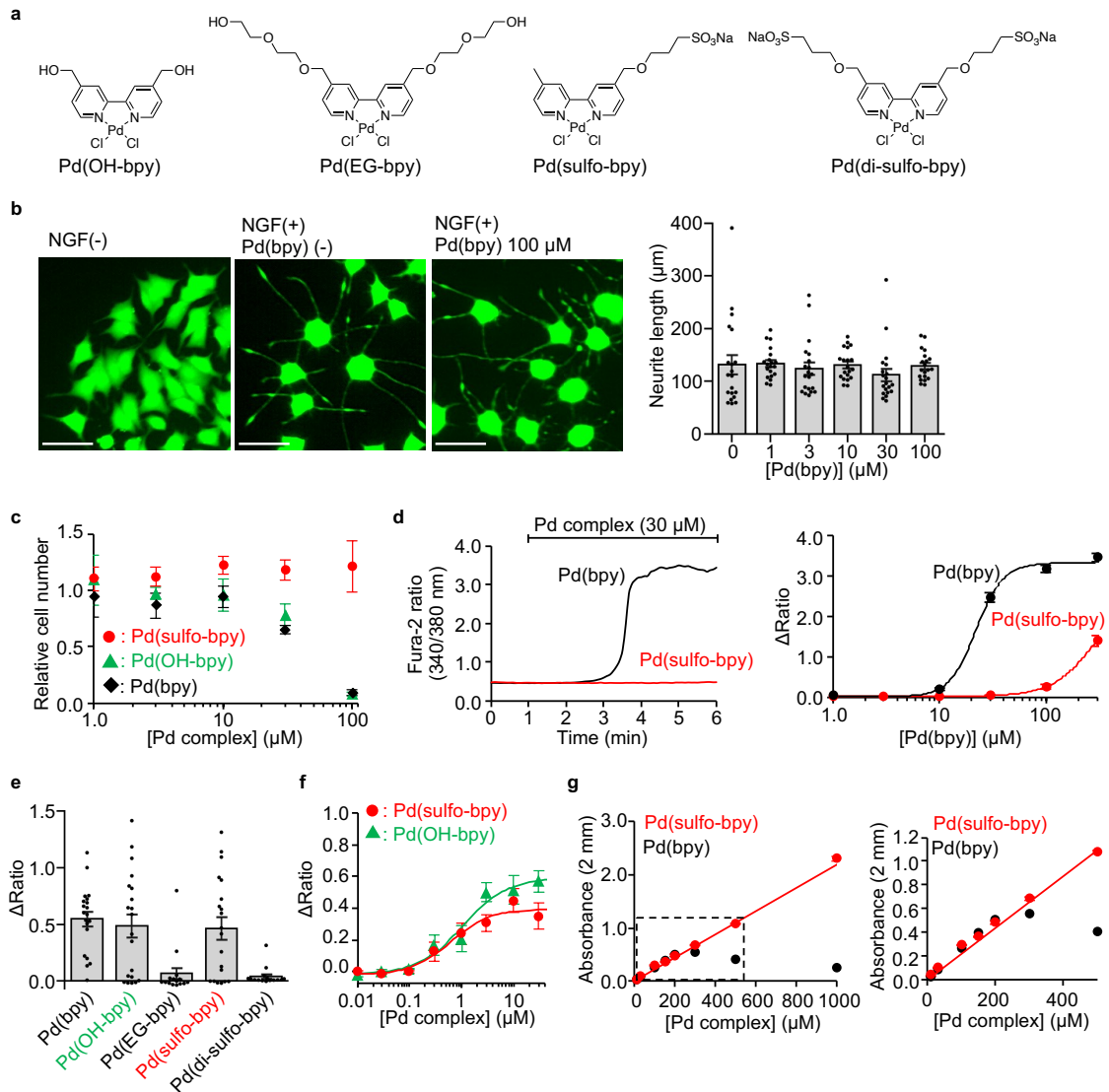


**Fig. 10 | Low toxic Pd(bpy) derivatives for neuronal studies. (a)** Chemical structures of the Pd(bpy) derivatives. **(b)** Evaluation of the effect of Pd(bpy) for NGF-induced neurite outgrowth of PC12 cells. Left: representative fluorescent images of PC12 cells treated with or without Pd(bpy). PC12 cells were visualized using Calcein-AM. Right: concentration-dependency of Pd(bpy) for neurite outgrowth in the PC12 cells after treatment of 1 ng/mL NGF. (n = 20). Scale bars, 50  $\mu\text{m}$ . **(c)** Concentration-dependency of Pd(bpy) derivatives on the cell growth in undifferentiated PC12 cells. (n = 3). **(d)** The abnormal  $\text{Ca}^{2+}$  response by Pd(bpy) (black) or Pd(sulfo-bpy) (red) in the cultured cortical neurons. Left: representative trace of the  $\text{Ca}^{2+}$  response induced by 30  $\mu\text{M}$  Pd(bpy) (black) or Pd(sulfo-bpy) (red). Right: concentration-dependence curves for Pd(bpy) (black) or Pd(sulfo-bpy) (red). (n = 30). **(e)**  $\text{Ca}^{2+}$  responses of Pd(bpy) derivatives for mGlu1 N264H mutant in HEK293 cells. Left: averaged  $\Delta\text{Ratio}$  induced by 3  $\mu\text{M}$  Pd(bpy) derivatives. (n = 15-20). Data are presented as mean  $\pm$  s.e.m. **(f)** Concentration-dependent curves for Pd(sulfo-bpy) (red) and Pd(OH-bpy) (green) in HEK293 cells expressing mGlu1 N264H mutant (n = 20). **(g)** Solubility assay of the

Pd(bpy) (black) and Pd(sulfo-bpy) (red) in ACSF using UV-vis spectroscopy. Linear increment of absorbance at 312 nm corresponding to the palladium complexes indicates the solubility of the complexes. The concentration dependency of the absorbance of Pd complexes in the high (left) and low (right) concentration range ( $n = 3$ ). Data are presented as mean  $\pm$  s.e.m.

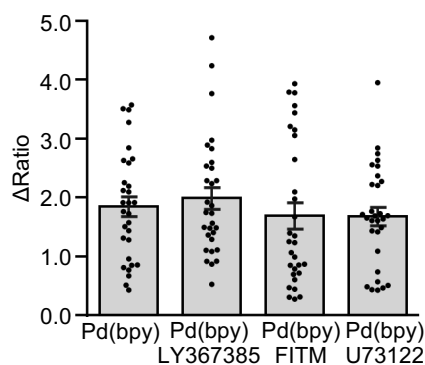


**Fig. 11 | The abnormal  $\text{Ca}^{2+}$  response of Pd(bpy) was inhibited by neither mGlu1 inhibitors nor a PLC inhibitor in the cultured cortical neurons.** Averaged  $\Delta$ ratio of 30  $\mu\text{M}$  Pd(bpy)-induced responses in cultured cortical neuron co-treated with 30  $\mu\text{M}$  LY367385, 1  $\mu\text{M}$  FITM, or 10  $\mu\text{M}$  U73122. ( $n = 30$ ). Data are presented as mean  $\pm$  s.e.m.

### 3-2-5, Knock-in of the N264H mutation does not alter mGlu1 function in mice.

With Pd(sulfo-bpy) showing low cytotoxicity in hand, I aimed to evaluate chemogenetic activation of endogenous mGlu1 to understand the physiological roles in the mouse brain. The mGlu family is composed of eight subtypes (mGlu1–8) divided into three groups (group I–III) according to their pharmacological properties<sup>11</sup>. mGlu1 belongs to the group I family with the cognate mGlu5 and is highly expressed in the dendritic regions of Purkinje cells in the cerebellum (Fig. 12a)<sup>20</sup>. The mGlu1 agonist 3,5-dihydroxyphenylglycine (DHPG) is typically used to examine the physiological role of mGlu1; however, DHPG cannot discriminate between mGlu1 and mGlu5. Moreover, mGlu5 is expressed in neurons and non-neuronal (glial) cells such as astrocytes<sup>21</sup>. Thus, the contribution of DHPG in brain tissues is complicated. Alternatively, mGlu1 selective PAM reagents would be useful; however, the effect of PAM reflects the difference in the extracellular glutamate concentration, as described in the “Introduction”. Therefore, a direct activation method of mGlu1, such as dA-CBC strategy, should be ideal to understand the physiological roles of mGlu1 in brain tissues.

I generated knock-in (KI) mice harboring the point mutation (N264H) in the mouse gene were generated using the CRISPR/Cas9 system<sup>22</sup> to chemogenetically control endogenous mGlu1 function (Fig. 12b and Fig. 13a). The KI mouse was termed the coordination-based chemogenetics (CBC) ready mouse (*mGlu1*<sup>CBC/CBC</sup> and *mGlu1*<sup>CBC/+</sup> for homozygous and heterozygous, respectively). Bodyweight and gross anatomy of the cerebellum were unaffected in *mGlu1*<sup>CBC/CBC</sup> mice (Fig. 13b, c). However, given the severe ataxic phenotypes in mGlu1 knock-out (*mGlu1*<sup>-/-</sup>) mice<sup>23,24</sup> and autosomal-recessive congenital cerebellar ataxia by familial mutations in the *mGlu1* gene in humans<sup>25-27</sup>, I analyzed *mGlu1*<sup>CBC/CBC</sup> mice in detail.

Western blotting of mGlu1 indicated that the expression level of mGlu1 was unchanged in the cerebellum of *mGlu1*<sup>CBC/CBC</sup> mice (Fig. 12c). In addition, the expression of excitatory postsynaptic glutamate receptors [AMPA and  $\delta$ 2-type

glutamate receptor (GluD2)] were also unaffected in the mutant mice. The cell-surface expression level of mGlu1 in the acutely prepared cerebellar slices was examined using FITM-Cy3. Prominent fluorescence was observed from the molecular layer of the cerebellum, where mGlu1 is highly expressed (Fig. 12a, d). Given the membrane impermeability of FITM-Cy3 and disappearance of fluorescence in the co-presence of excess FITM, the fluorescent signals correspond to cell-surface mGlu1 and surface mGlu1 levels were the same between WT and *mGlu1<sup>CBC/CBC</sup>* mice (Fig. 12d).

Next, I evaluated the distribution of the mGlu1(N264H) mutant in the cerebellum. Immunohistochemistry using an anti-mGlu1 antibody clearly indicated that mGlu1 localized in the dendritic spines of Purkinje cells (Fig. 14a, b). Notably, super-resolution microscopy showed that immune-positive signals for mGlu1 were predominantly localized at the edges of synaptic contacts, which were represented by signals for a parallel fiber (PF)–Purkinje cell synapse specific-postsynaptic protein (GluD2) and a presynaptic protein (bassoon), indicating perisynaptic localization of mGlu1 in both WT and mutant *mGlu1<sup>CBC/CBC</sup>* mice (Fig. 14c). This result is consistent with the similar subcellular localization of mGlu1 revealed by immunoelectron microscopy<sup>27,28</sup>.

Subsequently, the function of the mGlu1(N264H) mutant was evaluated by whole-cell patch-clamp recordings of Purkinje cells in the cerebellar slices. I first confirmed that excitatory postsynaptic currents (EPSCs) evoked by PF and climbing fiber (CF) stimuli (PF-EPSCs and CF-EPSCs, respectively) were normal in amplitude and the paired-pulse ratio, reflecting presynaptic functions<sup>29</sup>, of *mGlu1<sup>CBC/CBC</sup>* mice (Fig. 15a and Fig. 16). mGlu1 is required for synapse elimination of surplus CF inputs to Purkinje cells during development to make a one-to-one relationship in adults, and the relationship is impaired in *mGlu1*-deficient mice. In this context, 90% of Purkinje cells had a single step of CF-EPSC amplitude by increasing CF stimuli in adult *mGlu1<sup>CBC/CBC</sup>* mice, as with the case of WT (91%,  $P > 0.05$  by two-way repeated ANOVA; Fig. 15b), suggesting that mGlu1(N264H) is functioning normally for CF synapse elimination

during development. Furthermore, burst PF stimulation (2–10 times of PF stimuli at 100 Hz) induced robust TRPC-mediated slow currents (designated as slowEPSCs) by activation of the perisynaptic mGlu1 in *mGlu1<sup>CBC/CBC</sup>* Purkinje cells and WT cells (Fig. 15c). Because these slowEPSCs are often used to evaluate the degree of mGlu1 activation<sup>30</sup>, these results indicate that the mGlu1(N264H) mutant functions in a neuronal activity-dependent manner.

Consistent with the intact subcellular localization and function of the mGlu1(N264H) mutant endogenously expressed in mice, the ataxic phenotype observed in *mGlu1<sup>-/-</sup>* mice was never observed in the *mGlu1<sup>CBC/CBC</sup>* mice. In addition, *mGlu1<sup>CBC/CBC</sup>* mice showed high performance in the rota-rod test (Fig. 17), which contrasts to *mGlu1<sup>-/-</sup>* mice whose behaviors were severely impaired in motor coordination, as reported previously<sup>23,24</sup>. Taken together, the introduction of the N264H mutation in mGlu1 does not affect original receptor activity *in vivo*.

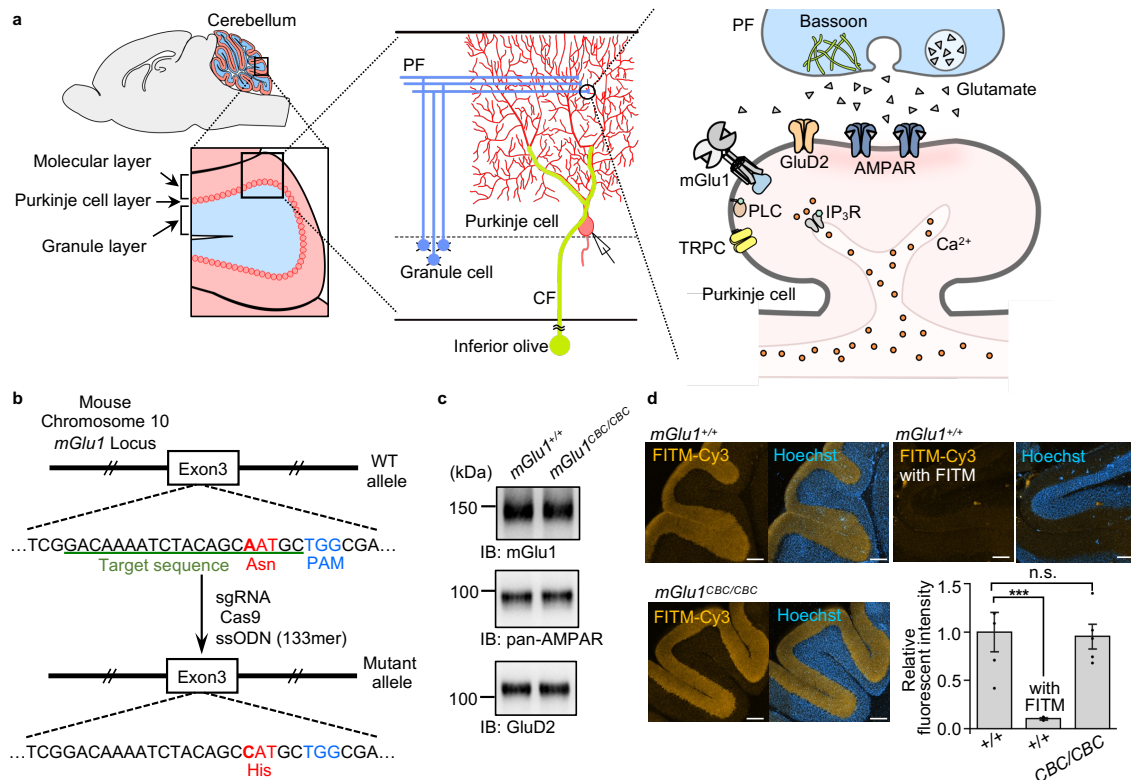


**Fig. 12 | Chemogenetic regulation of endogenous mGlu1 in brain tissue. (a)** The architecture of the cerebellum in a mouse. Left: schematic illustration of a sagittal section of the mouse brain and enlarged image of the cerebellum. Middle: schematic illustration of major components of the cerebellar cortical neuronal circuits. Right: PF-Purkinje cell synapses. PF, parallel fiber; CF, climbing fiber; AMPAR, AMPA receptor; IP<sub>3</sub>R, inositol triphosphate receptor; PLC, phospholipase C; TRPC, transient receptor potential channel canonical. **(b)** Illustration for preparing *mGlu1*(N264H) KI mice (*mGlu1*<sup>CBC/CBC</sup>) using CRISPR-Cas9 system. **(c)** Evaluation of the protein expression level of mGlu1, AMPAR and GluD2 between *mGlu1*<sup>+/+</sup> and *mGlu1*<sup>CBC/CBC</sup> in the cerebellum by western blotting. **(d)** Quantification of the surface expression level of mGlu1 between *mGlu1*<sup>+/+</sup> and *mGlu1*<sup>CBC/CBC</sup> in acute cerebellar slices using FITM-Cy3. Scale bars, 200  $\mu$ m. (n = 2–5, biologically independent experiments). \*\*\*Significant difference ( $P < 0.001$ , One-way ANOVA with Dunnet's test). n.s., not significant ( $P > 0.05$ ).

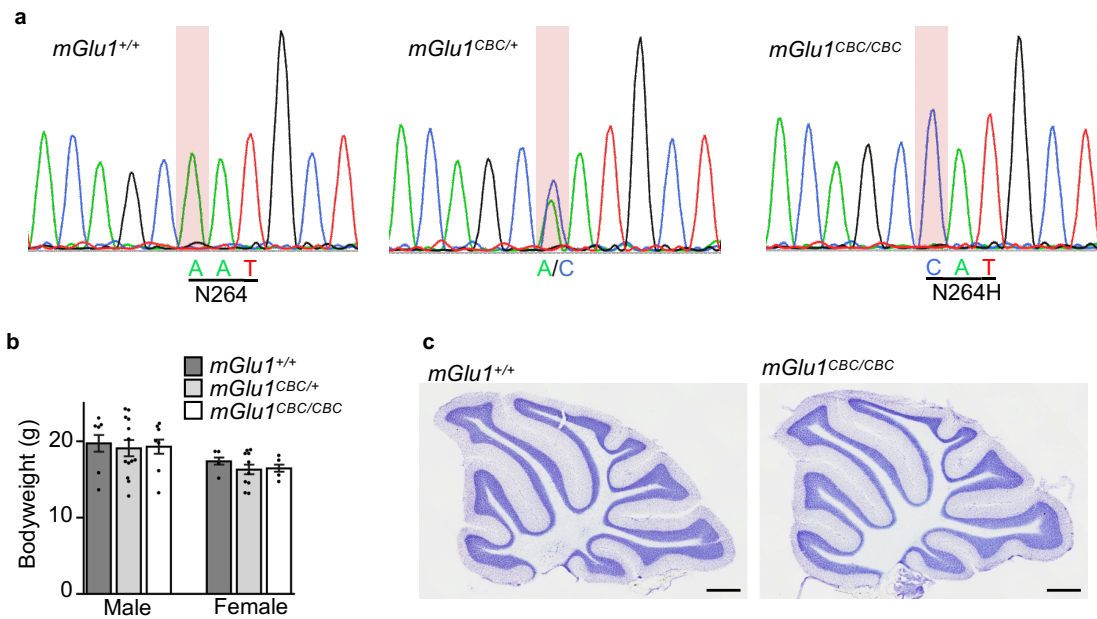


**Fig. 13 | Evaluation of functionality of the mGlu1 knock-in mouse. (a)** Sequence analyses of exon 3 of mGlu1 using *mGlu1*<sup>+/+</sup>, *mGlu1*<sup>CBC/+</sup>, or *mGlu1*<sup>CBC/CBC</sup> genome. **(b)** Bodyweight of the *mGlu1*<sup>+/+</sup>, *mGlu1*<sup>CBC/+</sup> and *mGlu1*<sup>CBC/CBC</sup> mice (6 weeks old). (n= 4–13) **(c)** Cresyl violet-stained sagittal sections of adult *mGlu1*<sup>+/+</sup> and *mGlu1*<sup>CBC/CBC</sup> mouse cerebella. Scale bar, 500  $\mu$ m. Data are presented as mean  $\pm$  s.e.m.



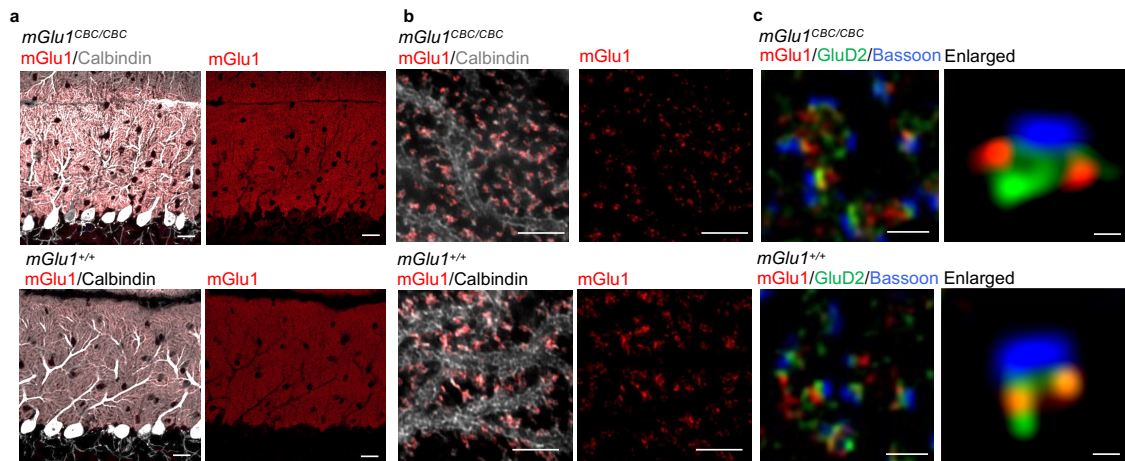


**Fig. 14** | Immunohistochemistry using anti-mGlu1 antibody in *mGlu1*<sup>CBC/CBC</sup> and *mGlu1*<sup>+/+</sup> cerebellar slice. (a, b) Conventional confocal (in a) and super-resolution (in b) microscopy images of immune-positive signals for mGlu1 (red) and calbindin (white) in the molecular layer of a *mGlu1*<sup>CBC/CBC</sup> (upper) and *mGlu1*<sup>+/+</sup> (lower) cerebellar slice. Scale bars, 20  $\mu\text{m}$  (in a) and 2  $\mu\text{m}$  (in b). (c) Super-resolution microscopic images of immune-positive signals for mGlu1 (red), GluD2 (green) and Bassoon (blue). Scale bars, 1  $\mu\text{m}$ . An enlarged view is shown in a right panel. Scale bars, 200 nm.

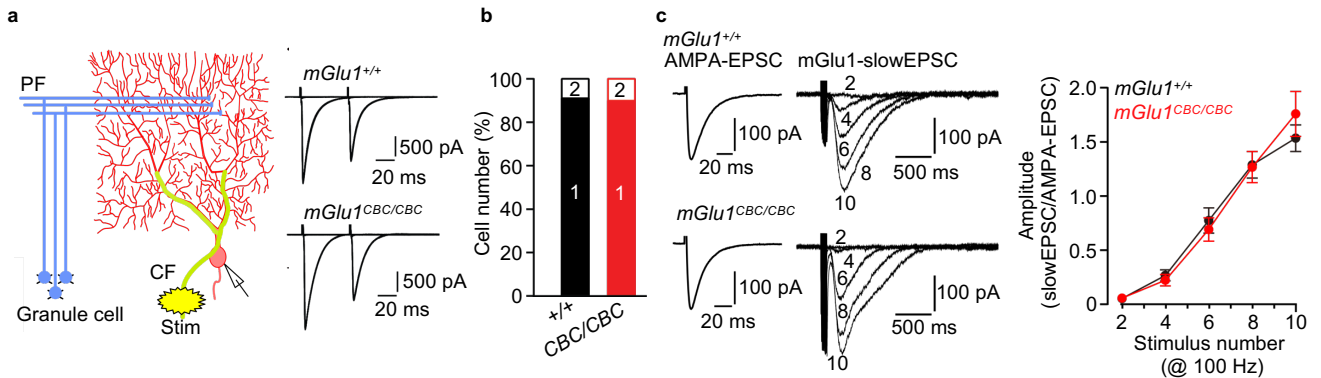


**Fig. 15 | Characterization of synaptic transmission in *mGlu1*<sup>CBC/CBC</sup> mice. (a)** Representative CF-EPSC traces from *mGlu1*<sup>+/+</sup> (top) and *mGlu1*<sup>CBC/CBC</sup> (bottom). **(b)** A histogram showing the percentage of the number of CFs innervating single Purkinje cells. [n = 32 cells (*mGlu1*<sup>+/+</sup>) or 30 cells (*mGlu1*<sup>CBC/CBC</sup>)]. **(c)** mGlu1-mediated slowEPSC data. By adjusting PF stimulus intensities, similar sizes of PF-evoked AMPA-EPSC (left traces) were obtained. Then, slowEPSC (right traces) were recorded by application of 2-10 times of PF stimuli at 100 Hz in the presence of AMPAR blockers. Amplitudes of slowEPSC were normalized by amplitudes of AMPA-EPSCs and plotted against the number of stimulations (right graph). [n = 9 cells (*mGlu1*<sup>+/+</sup>) or 13 cells (*mGlu1*<sup>CBC/CBC</sup>)]. Data are presented as mean ± s.e.m.

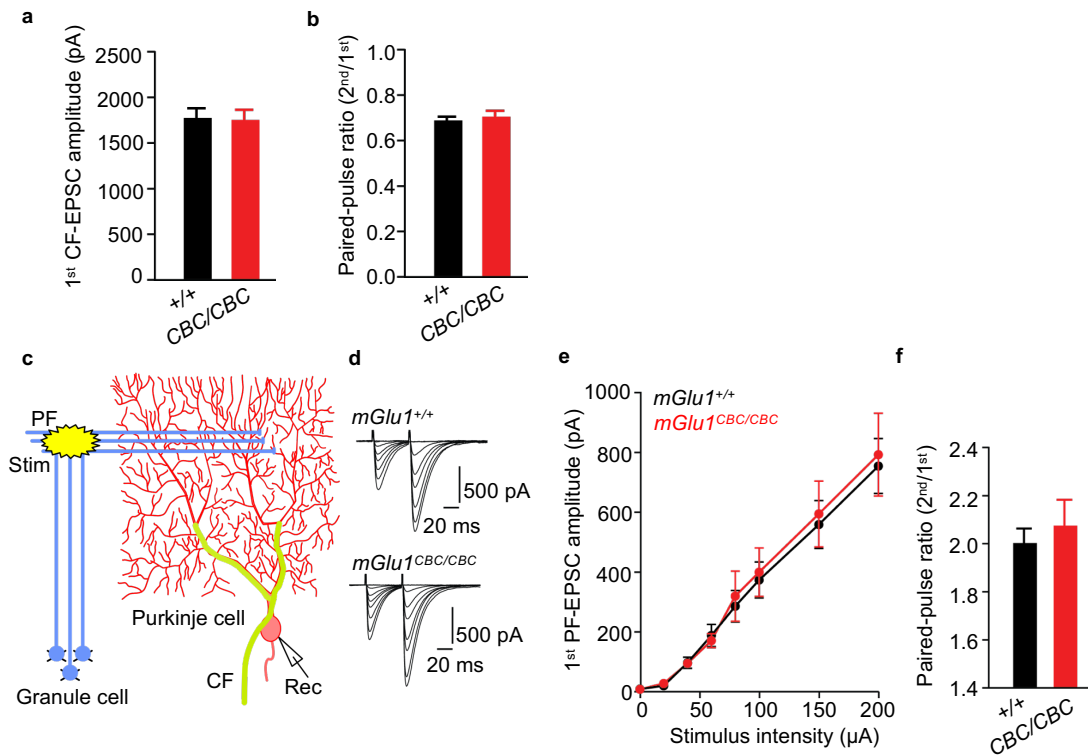


**Fig. 16 | Basic synaptic transmission is normal at CF and PF-Purkinje cells in *mGlu1*<sup>CBC/CBC</sup> mice. (a, b)** Histograms showing CF-EPSC amplitude (a) and a paired-pulse ratio of CF-EPSC amplitudes (The amplitude of 2nd EPSC is normalized by that of 1st EPSC) in *mGlu1*<sup>+/+</sup> (black columns, n = 32 cells) and *mGlu1*<sup>CBC/CBC</sup> (red columns, n = 30 cells,  $P > 0.05$  by Mann-Whitney U test) mice. (c, d) An orientation of stimulus and recording electrodes and stimulus condition (in c) to evoke PF-EPSCs (in d). In these experiments, EPSCs were evoked by the paired-pulse stimulation with various stimulus intensities (0, 20, 40, 60, 80, 100, 150, 200  $\mu$ A; 50-ms inter-stimulus interval). (e, f) Input-Output relationship (in e) and paired-pulse ratio (in f) of the PF-EPSCs from *mGlu1*<sup>+/+</sup> (black, n = 13 cells) or *mGlu1*<sup>CBC/CBC</sup> (red, n = 13 cells,  $P > 0.05$  by two-way repeated ANOVA in (e) and Mann-Whitney U test in (f)) mice. Data are represented as mean  $\pm$  s.e.m.

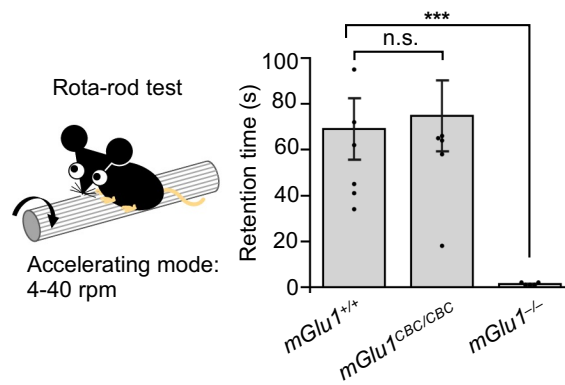


**Fig 17 | Motor coordination is normal in *mGlu1*<sup>CBC/CBC</sup> mice.** To evaluate motor coordination of the mouse, accelerating rotor-rod test (4-40 rpm for 5 min) was performed. Histogram shows averaged retention time on rota-rod in each mouse groups. High performance was observed in *mGlu1*<sup>+/+</sup> and *mGlu1*<sup>CBC/CBC</sup> mice but not *mGlu1*<sup>-/-</sup> mice. (n = 5–7). \*\*\*,  $P < 0.001$  and ns,  $P > 0.05$  by Kruskal-Wallis test followed by the Scheffe *post hoc* test. Data are presented as mean ± s.e.m.

### 3-2-6, Induction of synaptic plasticity by mGlu1 dA-CBC in the cerebellum.

In brains, synaptic plasticity such as long-term potentiation (LTP) and LTD of excitatory transmission has been proposed as a cellular substrate for learning and memory<sup>31,32</sup>. In particular, cerebellar LTD, which occurs at PF–Purkinje cell synapses by the simultaneous activation of PF and CF inputs, generally underlies a certain form of motor-related learning. mGlu1 is highly expressed at PF–Purkinje cell synapses as described (Fig. 12a, d) and absolutely required for the induction of cerebellar LTD. I first examined whether cerebellar LTD occurs in acute cerebellar slices from *mGlu1<sup>CBC/CBC</sup>* mice following electric stimulation (Fig. 18a). When PF stimuli were applied repetitively and simultaneously with Purkinje cell depolarization, mimicking a CF input, at 1 Hz (LTD-stim), a robust LTD occurred in *mGlu1<sup>CBC/CBC</sup>* mice ( $68 \pm 4\%$  at  $t = 26 \pm 30$  min) and WT mice ( $72 \pm 5\%$  at  $t = 26 \pm 30$  min,  $P > 0.05$  by Mann-Whitney U test; Fig. 18b). Furthermore, application of the mGlu1/mGlu5 activator, DHPG (50  $\mu$ M for 10 min under a current-clamp mode) also caused a chemical-induced LTD (chemLTD) in cerebellar slices from WT ( $55 \pm 7\%$  at  $t = 31 \pm 35$  min) and *mGlu1<sup>CBC/CBC</sup>* ( $56 \pm 6\%$  at  $t = 31 \pm 35$  min,  $P > 0.05$  by Mann-Whitney U test; Fig. 18c) mice. These results also emphasize that the mGlu1(N264H) mutant works functionally.

I then examined the direct activation of mGlu1 using dA-CBC in brain slices to clarify the contribution of mGlu1 activation in LTD. For this purpose, 1  $\mu$ M Pd(sulfo-bpy) was used as the treatment instead of 50  $\mu$ M DHPG. As shown in Fig. 18d, after washing out Pd(sulfo-bpy), sustained decreases of the PF-EPSC were observed in *mGlu1<sup>CBC/CBC</sup>* mice ( $71 \pm 5\%$  at  $t = 31 \pm 35$  min; Fig. 18d). In contrast, the decrease was not observed by treating WT mice with Pd(sulfo-bpy) ( $99 \pm 4\%$  at  $t = 31 \pm 35$  min,  $P < 0.01$  vs *mGlu1<sup>CBC/CBC</sup>* by Kruskal-Wallis test followed by the Scheffe *post hoc* test), indicating successful activation of endogenous mGlu1 and induction of synaptic plasticity using Pd(sulfo-bpy). Interestingly, Pd(sulfo-bpy)-induced chemLTD was also observed in heterozygous *mGlu1<sup>CBC/+</sup>* mice ( $68 \pm 5\%$  at  $t = 31 \pm 35$  min; Fig. 18d) and

similar to homozygous *mGlu1<sup>CBC/+</sup>* mice ( $P > 0.05$  vs *mGlu1<sup>CBC/CBC</sup>* by Kruskal-Wallis test followed by the Scheffe *post hoc* test; Fig. 18d), suggesting that a half amount of mGlu1 in WT mice is sufficient to induce chemLTD. In summary, dA-CBC was successfully applied for chemogenetic activation of mGlu1 in mice, which clarified the essential roles of mGlu1 activation for LTD, the putative mechanism of motor learning in the cerebellum.

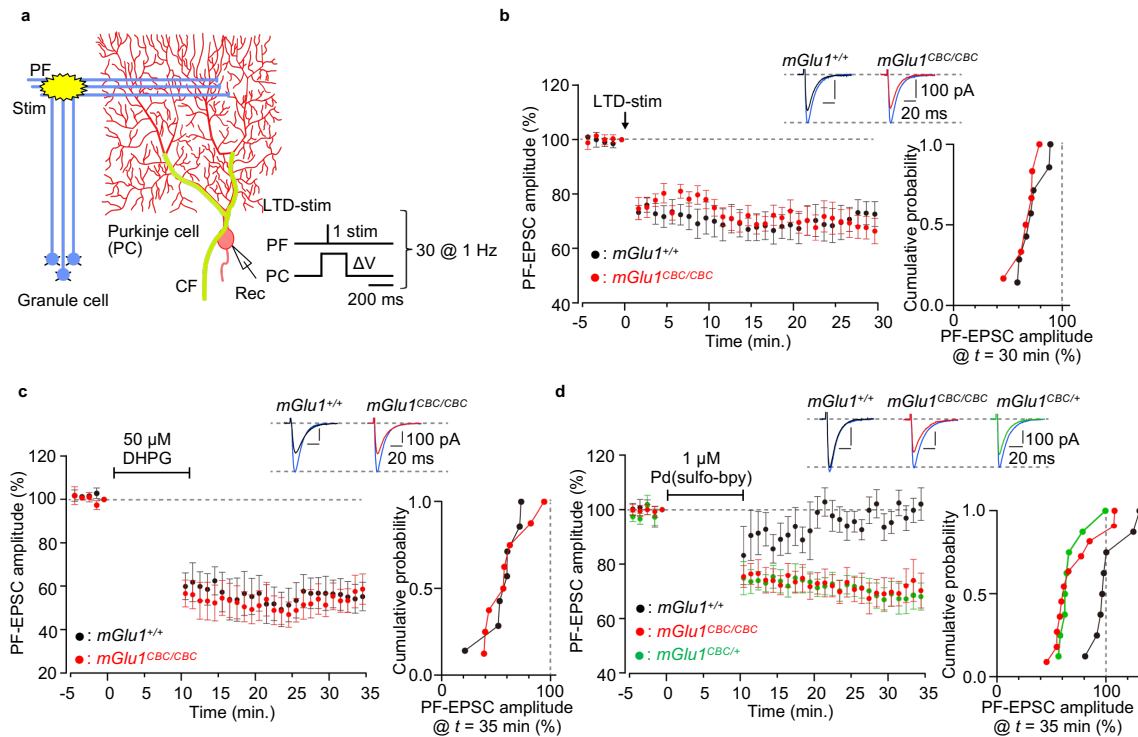


**Fig. 18 | Cerebellar LTD is induced by direct activation of the mGlu1 mutant by dA-CBC. (a)** A schematic diagram illustrating the experimental set-up. Conjunctive stimulus [PF/DV-stim, 30 × (PF stimuli plus PC depolarization) at 1 Hz] was applied to induce LTD at PF–Purkinje cell synapses (LTD-stim). **(b)** Averaged data of LTD recordings from *mGlu1*<sup>+/+</sup> (black circles) and *mGlu1*<sup>CBC/CBC</sup> (red circles) mice. Insets, representative PF-EPSC traces just before (blue; *t* = -1 min) and 30 min after (black and red) LTD-stim in *mGlu1*<sup>+/+</sup> and *mGlu1*<sup>CBC/CBC</sup> mice, respectively. Right graph shows a cumulative probability of the degree of LTD at *t* = 30 min. [n = 7 cells (*mGlu1*<sup>+/+</sup>) or 6 cells (*mGlu1*<sup>CBC/CBC</sup>)]. **(c, d)** Averaged data of DHPG-induced (in **c**) or Pd(sulfo-bpy)-induced (in **d**) chemLTD recordings from *mGlu1*<sup>+/+</sup> (black circles), *mGlu1*<sup>CBC/CBC</sup> (red circles) and *mGlu1*<sup>CBC/+</sup> (green circles in **d**) mice. Insets, representative PF-EPSC traces just before (blue; *t* = -1 min) and 25 min after (black, red, or green) drug washout in each mouse group. Right graph shows a cumulative probability of the degree of LTD at *t* = 35 min. [n = 7 cells (*mGlu1*<sup>+/+</sup>) or 8 cells (*mGlu1*<sup>CBC/CBC</sup>)]. Data are presented as mean ± s.e.m.

### 3-3, Conclusion

I developed a direct-activation method of mGlu1 without affecting glutamate affinity using dA-CBC, in which a single point mutation (N264H) was sufficient for chemogenetics activation by Pd(bpy). To demonstrate the chemogenetic activation of mGlu1 endogenously expressed in neurons, I generated mGlu1(N264H)-KI (*mGlu1<sup>CBC/CBC</sup>*) mice using the CRISPR-Cas9 system and obtained *mGlu1<sup>CBC/CBC</sup>* mice that exhibited no obvious abnormal phenotypes. Pd(sulfo-bpy), which showed low toxicity to neurons, successfully activated the mGlu1 mutant in the cerebellar slice prepared from *mGlu1<sup>CBC/CBC</sup>* mice. Notably, Pd(sulfo-bpy) induced chemLTD in cerebellar slices, which indicated that activation of endogenous mGlu1 is sufficient to evoke the cellular basis of motor learning.

Thus, the dA-CBC method is a notable chemogenetic strategy for controlling endogenous receptor function, which can be potentially used to understand the physiological roles of other class C GPCR subtypes.

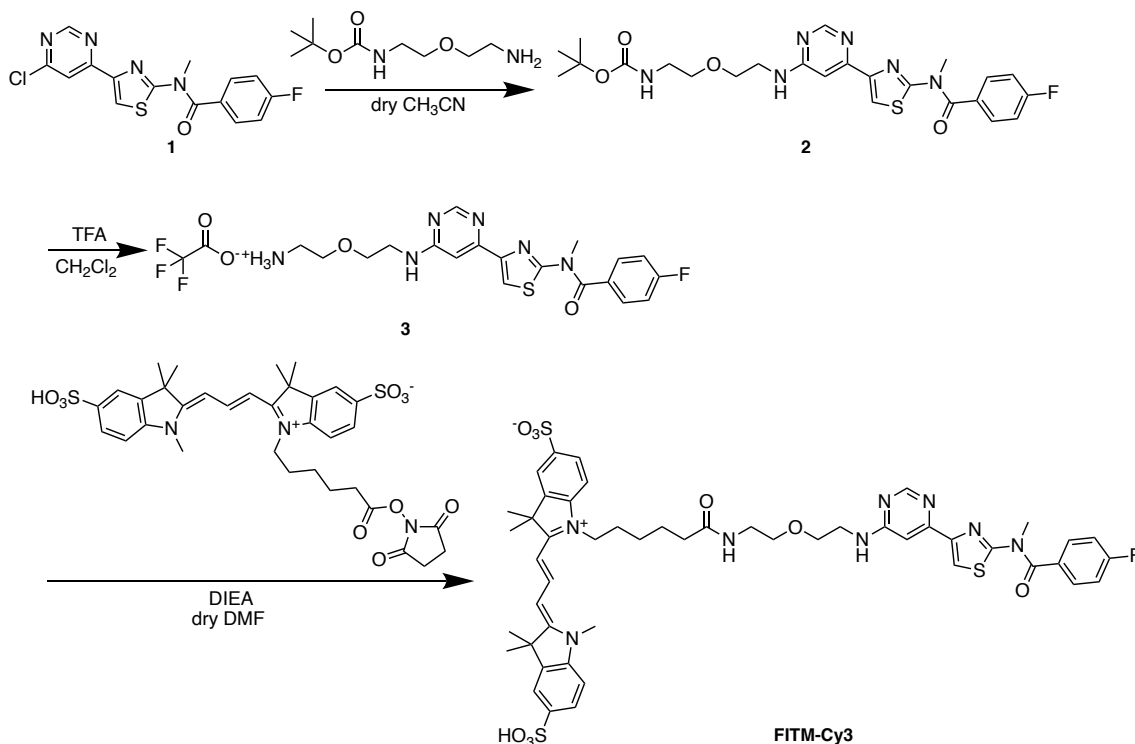


### **3-4, Experimental Section**

#### **Synthesis and Characterization**

##### **General materials and methods for organic synthesis.**

All chemical reagents and solvents were purchased from commercial sources (FUJIFILM Wako pure chemical, TCI chemical, Sigma-Aldrich) and were used without further purification. Thin layer chromatography (TLC) was performed on silica gel 60 F254 precoated aluminum sheets (Merck). Chromatographic purification was performed using flash column chromatography on silica gel 60 N (neutral, 40–50  $\mu\text{m}$ , Kanto Chemical).  $^1\text{H}$ -NMR or  $^{13}\text{C}$ -NMR spectra were recorded in deuterated solvents on an Advance III HD 500 MHz or Advance III HD 300 MHz (Bruker). Chemical shifts were referenced to residual solvent peaks or tetramethylsilane ( $\delta = 0$  ppm). Multiplicities are abbreviated as follows: s = singlet, d = doublet, t = triplet, m = multiplet, brs = broad singlet. High resolution mass spectra were measured on a compact (Bruker) equipped with electron spray ionization (ESI). Reversed-phase HPLC (RP-HPLC) was carried out on a Hitachi Chromaster system equipped with a UV detector, and an YMC-Pack ODS-A column.

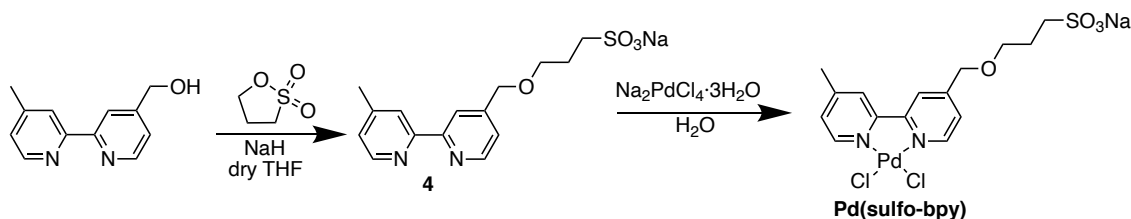
**Synthesis of Compound FITM-Cy3****Synthesis of Compound 2**

*N*-(*tert*-Butoxycarbonyl)-2-(2-aminoethoxy) ethylamine (ref. 33) (50 mg, 0.25 mmol) was added to a solution of **1** (ref. 34) (30 mg, 86  $\mu$ mol) in dry CH<sub>3</sub>CN (5 mL). The reaction mixture was stirred for 61 h in a N<sub>2</sub> atmosphere at 80 °C. The reaction mixture was evaporated to distil away CH<sub>3</sub>CN, and CHCl<sub>3</sub> was added to the residue. The mixture was washed with saturated NH<sub>4</sub>Cl aqueous solution and brine. The organic layer was dried with Na<sub>2</sub>SO<sub>4</sub> and concentrated *in vacuo*. The residue was purified by column chromatography (silica gel, EtOAc/*n*-hexane = 2/1) to afford compound **2** (33 mg, 0.064 mmol, 74% yield) as a colorless amorphous substance. <sup>1</sup>H-NMR (500 MHz, CDCl<sub>3</sub>)  $\delta$  8.59 (s, 1H), 7.93 (s, 1H), 7.61 (dd, *J* = 5.3, 8.8 Hz, 2H), 7.20 (t, *J* = 8.8 Hz, 2H), 7.13 (d, *J* = 1.0 Hz, 1H), 5.54 (brs, 1H, NH), 4.97 (brs, 1H, NH), 3.74 (s, 3H), 3.68 (brt, *J* = 4.2 Hz, 2H), 3.66-3.60 (m, 2H), 3.55 (brt, *J* = 5.1 Hz, 2H), 3.36-3.30 (m, 2H), 1.44 (s, 9H); <sup>13</sup>C-NMR (126 MHz, CDCl<sub>3</sub>)  $\delta$  169.6, 165.3, 163.3, 160.5, 158.6, 156.2, 132.6, 131.0, 130.6, 130.3, 128.9, 116.1, 79.6, 70.4, 69.7, 68.3, 41.1, 40.5, 38.6, 28.5;

HRMS (ESI<sup>+</sup>): calcd for [M + Na]<sup>+</sup> (C<sub>24</sub>H<sub>29</sub>FN<sub>6</sub>NaO<sub>4</sub>S) 539.1847, found 539.1851.

### Synthesis of FITM-Cy3

Trifluoroacetic acid (200  $\mu$ L, 298 mg, 2.6 mmol) was added to a solution of **2** (28 mg, 54  $\mu$ mol) in CH<sub>2</sub>Cl<sub>2</sub> (1 mL). The reaction solution was stirred for 1 h at room temperature. After confirming the consumption of **2**, the reaction solution was concentrated *in vacuo* to obtain **3**. Sulfo-Cy3 NHS ester (1 mg, 1.3  $\mu$ mol) and *N,N*-diisopropylethylamine (5  $\mu$ L, 3.7 mg, 28.7  $\mu$ mol) were added to a solution of **3** (5.0 mg, 9.4  $\mu$ mol) in dry DMF (500  $\mu$ L). The reaction solution was stirred overnight in a N<sub>2</sub> atmosphere at room temperature. The residue was purified by RP-HPLC (ODS-A, 250 x 10 mm, mobile phase; CH<sub>3</sub>CN: 10 mM AcONH<sub>4</sub> aq. = 5:95 (0 min), 65:35 (60 min), flow rate; 3.0 mL/min, detection; UV (220 nm)) to afford FITM-Cy3 (0.58  $\mu$ mol determined using the molecular extinction coefficient of Sulfo-Cy3 NHS ester (162,000 M<sup>-1</sup>cm<sup>-1</sup>), 45% yield) as a magenta powder. <sup>1</sup>H NMR (500 MHz, CD<sub>3</sub>OD)  $\delta$  8.52 (t, *J* = 13.5 Hz, 1H), 8.38 (s, 1H), 7.95 (d, *J* = 1.6 Hz, 1H), 7.94 (d, *J* = 1.6 Hz, 1H), 7.91 (dd, *J* = 1.6, 8.3 Hz, 1H), 7.91 (dd, *J* = 1.6, 8.3 Hz, 1H), 7.89 (s, 1H), 7.68 (dd, *J* = 5.3, 8.8 Hz, 2H), 7.38 (d, *J* = 8.3 Hz, 1H), 7.34 (d, *J* = 8.3 Hz, 1H), 7.29 (t, *J* = 8.8 Hz, 2H), 7.28 (d, *J* = 0.9 Hz, 1H), 6.45 (d, *J* = 13.5 Hz, 1H), 6.40 (d, *J* = 13.4 Hz, 1H), 4.09 (brt, *J* = 7.5 Hz, 2H), 3.72 (s, 3H), 3.69 (s, 3H), 3.64 (brt, *J* = 4.5 Hz, 2H), 3.62-3.56 (m, 2H), 3.52 (t, *J* = 5.5 Hz, 2H), 3.34 (t, *J* = 5.5 Hz, 2H), 2.18 (brt, *J* = 6.4 Hz, 2H), 1.83-1.76 (m, 2H), 1.71-1.63 (m, 2H), 1.45-1.38 (m, 2H); HRMS (ESI<sup>-</sup>): calcd for [M - H]<sup>-</sup> (C<sub>49</sub>H<sub>54</sub>FN<sub>8</sub>O<sub>9</sub>S<sub>3</sub>) 1013.3165, found 1013.3163.

**Synthesis of Pd(sulfo-bpy)****Synthesis of compound 4**

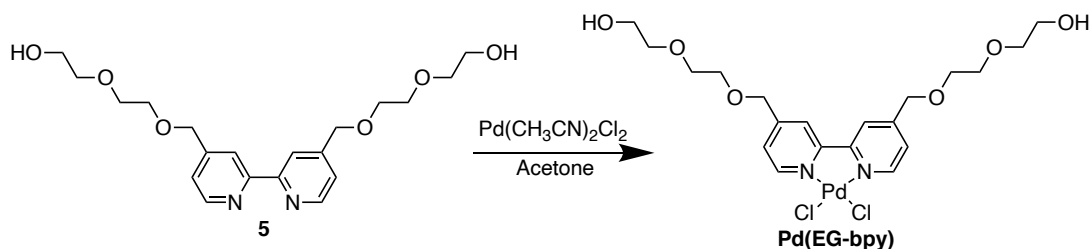
A solution of 4-hydroxymethyl-4'-methyl-2,2'-bipyridine (100 mg, 0.5 mmol) and sodium hydride (24 mg, 1.0 mmol) in dry THF (5 mL) was stirred on ice for 30 min under N<sub>2</sub> atmosphere. 1,3-propane sultone 73 mg (0.6 mmol) was added to the solution and stirred for 14 h at room temperature. After removal of the solvent by evaporation, the crude was purified by RP-HPLC (ODS-A, 250 x 10 mm, mobile phase; CH<sub>3</sub>CN: 10 mM AcONH<sub>4</sub> aq. = 5:95 (0 min), 5:95 (10 min), 40:60 (60 min), flow rate; 3.0 mL/min, detection; UV (220 nm)) and neutralized with 1M NaOH, giving compound 4 (60 mg, 0.17 mmol, 34%) as a colorless oil. <sup>1</sup>H-NMR (500 MHz, CD<sub>3</sub>OD) δ 8.61 (d, *J* = 5.0 Hz, 1H), 8.51 (d, *J* = 5.0 Hz, 1H), 8.23 (s, 1H), 8.15 (s, 1H), 7.46 (d, *J* = 5.0 Hz, 1H), 7.34 (d, *J* = 5.0 Hz, 1H), 4.66 (s, 2H), 3.71 (t, *J* = 6.3 Hz, 2H), 3.00-2.96 (m, 2H), 2.48 (s, 3H), 2.18-2.13 (m, 2H). <sup>13</sup>C-NMR (126 MHz, D<sub>2</sub>O) δ 155.8, 150.9, 150.4, 150.0, 148.7, 144.8, 126.6, 123.9, 120.6, 120.5, 70.3, 69.2, 47.8, 24.4, 21.0.

**Synthesis of Pd(sulfo-bpy)**

A solution of compound 4 (55 mg, 160 μmol) in H<sub>2</sub>O (3.0 mL) was added to a solution of sodium tetrachloropalladate trihydrate (II) (56 mg, 160 μmol) in H<sub>2</sub>O (2.0 mL). The solution was stirred at room temperature for 12 h. After concentration of the solution to 0.5 ml by evaporation, crystals were obtained from vapor diffusion of acetone into a H<sub>2</sub>O at room temperature, giving Pd(sulfo-bpy) (49 mg, 94 μmol, 59%) as an orange solid. <sup>1</sup>H-NMR (500 MHz, CD<sub>3</sub>OD) δ 9.10 (s, 1H), 9.00 (s, 1H), 8.39 (s, 1H), 8.36 (s, 1H), 7.63 (d, *J* = 6.0 Hz, 1H), 7.52 (d, *J* = 6.0 Hz, 1H), 4.76 (s, 2H), 3.78 (t, *J* = 6.0 Hz,

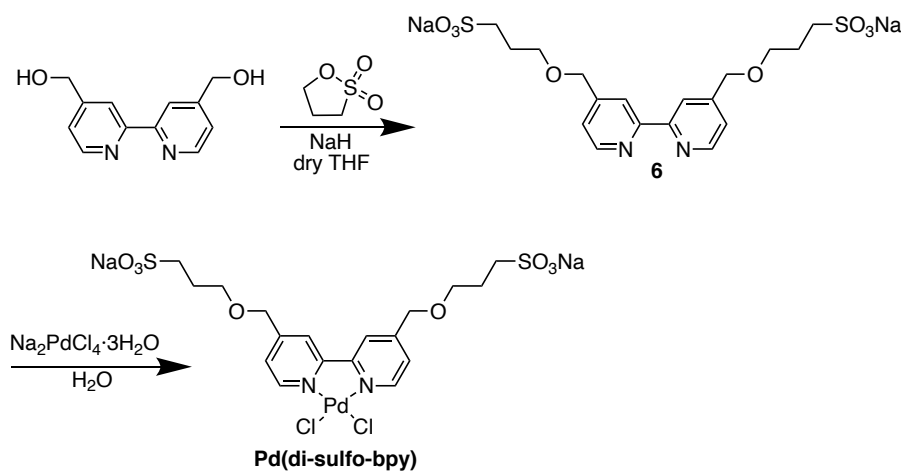
2H), 2.99 (t,  $J = 7.5$  Hz, 2H), 2.20-2.14 (m, 2H).  $^{13}\text{C-NMR}$  (126 MHz,  $\text{D}_2\text{O}$ ):  $\delta$  155.1, 154.9, 154.4, 154.2, 149.2, 148.5, 128.1, 125.2, 124.6, 121.6, 69.8, 69.6, 48.0, 24.5, 21.1.

### Synthesis of Pd(EG-bpy)



A solution of compound **5** (ref. 35) (10 mg, 26  $\mu\text{mol}$ ) in acetone (0.4 mL) was added to a solution of Bis(acetonitrile) dichloro palladium (II) (6 mg, 23  $\mu\text{mol}$ ) in acetone. The solution was stood still at room temperature for 3 days, and filtered to obtain Pd(EG-bpy) (5.7 mg, 26  $\mu\text{mol}$ , 59%) as an orange needle crystal.  $^1\text{H-NMR}$  (500 MHz,  $\text{CD}_3\text{OD}$ )  $\delta$  8.64 (d,  $J = 5.0$  Hz, 2H), 8.40 (s, 2H), 7.32 (m, 2H), 4.68 (s, 2H), 3.74 (t,  $J = 6.5$  Hz, 4H), 2.98 (m, 4H), 2.17 (m, 4H);  $^{13}\text{C-NMR}$  (126 MHz,  $\text{CDCl}_3$ )  $\delta$  155.8, 153.8, 149.9, 124.1, 121.6, 72.7, 70.7, 70.5, 70.2, 61.6.

### Synthesis of Pd(di-sulfo-bpy)



### Chapter 3

#### Synthesis of compound **6**

A solution of 4,4'-hydroxymethyl-2,2'-bipyridine (200 mg, 0.92 mmol) and sodium hydride (48 mg, 2.0 mmol) in dry THF (5 mL) was stirred on ice for 15 min under N<sub>2</sub> atmosphere. 1,3-propane sultone 244 mg (2.0 mmol) was added to the solution and stirred for 3 days at room temperature. The precipitation was collected and purified by RP-HPLC (ODS-A, 250 x 10 mm, mobile phase; CH<sub>3</sub>CN: 10 mM AcONH<sub>4</sub> aq. = 0:100 (0 min), 0:100 (10 min), 40:60 (60 min), flow rate; 3.0 mL/min, detection; UV (220 nm)), and neutralized with 1M NaOH, giving compound **6** (60 mg, 0.17 mmol, 34%) as a colorless oil. <sup>1</sup>H-NMR (500 MHz, CD<sub>3</sub>OD)  $\delta$  8.63 (d,  $J$  = 5.0 Hz, 2H), 8.29 (s, 2H), 7.48 (d,  $J$  = 5.0 Hz, 2H), 4.69 (s, 2H), 3.74 (t,  $J$  = 6.5 Hz, 4H), 2.98-2.96 (m, 4H), 2.20-2.14 (m, 4H); <sup>13</sup>C-NMR (126 MHz, D<sub>2</sub>O)  $\delta$  154.9, 149.3, 149.0, 122.8, 120.4, 70.6, 69.1, 47.9, 24.4.

#### Synthesis of **Pd(di-sulfo-bpy)**

A solution of compound **6** (45 mg, 89  $\mu$ mol) in MeOH (2.2 mL) was added to a solution of sodium tetrachloropalladate trihydrate (II) (23 mg, 89  $\mu$ mol) in MeOH (12 mL). The solution was stirred at room temperature for 1 h. After removal of the solvent by evaporation, the solid was dissolved in MeOH, and reprecipitated with diethylether, giving Pd(di-sulfo-bpy) (18 mg, 26  $\mu$ mol, 30%) as an orange solid. <sup>1</sup>H-NMR (300 MHz, CD<sub>3</sub>OD)  $\delta$  9.14 (d,  $J$  = 6.0 Hz, 2H), 8.40 (s, 2H), 7.70 (d,  $J$  = 6.6 Hz, 2H), 4.77 (s, 2H), 3.77 (t,  $J$  = 6.6 Hz, 4H), 3.00-2.95 (m, 4H), 2.20-2.11 (m, 4H); <sup>13</sup>C-NMR (126 MHz, D<sub>2</sub>O):  $\delta$  155.6, 154.2, 149.5, 124.8, 121.9, 69.9, 69.6, 48.0, 24.5.

### **Construction of expression vector of mGlu1 mutants**

Site-directed mutagenesis was performed using the QuikChange II XL site-directed mutagenesis kits (Stratagene) or the Q5® Site-Directed Mutagenesis kit (NEB) with pBluescript II SK(+) encoding rat mGlu1<sup>9</sup>, according to the manufacturer's instruction. After sequencing the cDNA region of mGlu1 mutants, the cDNA was subcloned into pCAGGS vector to obtain the expression vectors as previously reported<sup>9</sup>.

### **Cell culture and transfection**

HEK293 cells were maintained in Dulbecco's modified Eagle's medium (DMEM) supplemented with 100 unit/mL penicillin and 100 µg/mL streptomycin and 10% FBS (Sigma) at 37 °C in a humidified atmosphere of 95% air and 5% CO<sub>2</sub>. HEK293 cells were transfected with plasmids (WT mGlu1, the mGlu1 mutants, or the control vector) using SuperFect transfection reagent (Qiagen) or Viafect (promega) according to the manufacturer's instruction. The cells were co-transfected with pEGFP-F (Clontech), pDsRed monomer-F (Clontech), or iRFP670 (kindly gifted from Prof. Verkhusa) as the transfection marker. After transfection, the cells were cultured in DMEM supplemented with 10% dialyzed FBS (Gibco) instead of 10% FBS to decrease cytotoxicity. After 36–48 h incubation, the transfected HEK293 cells were utilized for experiments.

PC12 cells were maintained in DMEM supplemented with 100 unit/mL penicillin and 100 µg/mL streptomycin and 10% horse serum (Gibco) at 37 °C in a humidified atmosphere of 95% air and 5% CO<sub>2</sub>.

### **Fluorescent Ca<sup>2+</sup> imaging**

The transfected HEK293 cells were seeded on glass coverslips (Matsunami) coated with poly-L-lysine solution (Sigma-Aldrich) then incubated for 4–10 hours. HEK293 cells or cultured neurons were loaded with 5 µM Fura-2 AM (Dojindo) for 15–20 minutes in the growth medium. Fura-2 fluorescence was measured in HBS (107 mM NaCl, 6 mM KCl,

### Chapter 3

1.2 mM MgSO<sub>4</sub>, 2 mM CaCl<sub>2</sub>, 11.5 mM glucose and 20 mM HEPES, pH 7.4). Fluorescence images were obtained using a fluorescence microscope (IX71, Olympus) equipped with a complementary metal-oxide semiconductor (CMOS) camera (ORCA-flash 4.0, Hamamatsu Photonics) under xenon-lamp illumination, and analyzed with a video imaging system (AQUACOSMOS, Hamamatsu Photonics) according to the manufacturer's protocol. The ratio of 340:380 nm fluorescence was determined from the images, on a pixel-by-pixel basis. To facilitate the screening assay in HEK293 cells, three different cell lines that expressed one of the constructs were co-cultured on a glass coverslip. Each mutant can be distinguished by co-transfected fluorescent proteins that have distinct colors as a marker, and the glutamate responses of three different mutants were assayed simultaneously. The  $\Delta$ ratio was defined as the difference between the maximum and the initial ratio values. The  $\Delta$ ratio was fitted with KaleidaGraph using following equation (1):  $a + (b-a)/(1+(x/c)^d)$ , and the EC<sub>50</sub> value was calculated.

#### **Western blotting analyses of HEK293 cells expressing mGlu1**

The transfected HEK293 cells were washed with PBS, and then lysed with RIPA buffer (25 mM Tris-HCl, 150 mM NaCl, pH 7.4 supplemented with 1% NP-40, 0.25% sodium deoxycholate, and 0.1% SDS) containing 1% Protease Inhibitor Cocktail (Nacalaitesque) at 4 °C for 30 min. The lysate was mixed with 5× Laemmli buffer (325 mM Tris-HCl, 15% SDS, 20% sucrose, 0.06% bromophenol blue, and 250 mM DTT, pH 6.8) and incubated at room temperature for 1 h. The sample was subject to SDS-polyacrylamide gel electrophoresis (SDS-PAGE) (7.5%) and then transferred to a polyvinylidene fluoride membrane (Bio-rad). After blocking in TBS-T (TBS with 0.05% Tween-20) supplemented with 5% skim milk powder (Wako) at room temperature for 1 h, the membranes were incubated overnight with primary antibodies in TBS-T supplemented with 1% skim milk powder at 4 °C. The membranes were washed three times with TBS-T, incubated with secondary antibodies in TBS-T with 1%



skim milk powder at room temperature for 1 h, and washed three times with TBS-T. Used primary antibodies were as follows: anti-mGluR1 antibody (BD biosciences, 610964, 1:2000) and anti- $\beta$  actin antibody (MBL, M177-3, 1:3000). Used secondary antibodies were as follows: anti-mouse-IgG-HRP antibody (MBL, 330, 1:3000). The signal was developed by ECL prime (cytiva) and detected with a Fusion Solo S imaging system (Vilber Lourmat). The target bands were manually selected, and the intensity was calculated with subtraction of background.

### **Confocal live cell imaging of cell-surface mGlu1 in HEK293 cells**

HEK293 cells were co-transfected with mGlu1 plasmid (WT mGlu1, the mGlu1 mutant, or the control vector) and iRFP-670 as a transfection marker. The cells were added with 1  $\mu$ M FITM-Cy3, and incubated for 30 min at 16 °C to suppress endocytosis. Confocal live imaging was performed with a confocal microscope (LSM900, Carl Zeiss) equipped with a 63 $\times$ , numerical aperture (NA)=1.4 oil-immersion objective. Fluorescence images were acquired by excitation at 561 or 640 nm derived from diode lasers. To quantify the fluorescence intensity of Cy3 at the cell-surface, iRFP 670 positive cells were selected and the maximum signal intensity of the cell-surface was calculated by ZEN blue software (Carl Zeiss). The membrane intensity was fitted with KaleidaGraph (Synergy Software), and the  $K_d$  value of FITM-Cy3 was calculated.

### **Evaluation of Neurite outgrowth in differentiated PC12 cells**

PC12 cells were seeded on the 24-well plate at  $1.0 \times 10^4$  cells. Twelve h after seeding, the PC12 cells were differentiated by treating with 100 ng/mL NGF- $\beta$  (Sigma-Aldrich), and each concentration of Pd(bpy) was added simultaneously in DMEM supplemented with 100 unit/mL penicillin and 100  $\mu$ g ml<sup>-1</sup> streptomycin and 2% FBS. After incubation for 3 days, PC12 cells bearing neurites were randomly selected, and the length of the longest neurite in each cell was measured using ImageJ package Fiji.

### **Cell proliferation assay of PC12 cells**

PC12 cells were seeded on the 24-well plate at  $1 \times 10^4$  cells. One to two days after seeding, the cells were treated with Pd(bpy) or Pd(sulfo-bpy) for 3-4 days. To visualize the live cells, the cells were loaded with 2  $\mu$ M calcein-AM (dojindo) for 15 min in HBS, and then washed with HBS. The fluorescent images of the cells were obtained with fluorescent microscopy (Axio Observer7, Carl Zeiss) equipped with CMOS camera (Axiocam712mono, Carl Zeiss), and the cell numbers were automatically counted with ZEN blue software (Carl Zeiss).

### **Animal experiments**

Pregnant ICR mice maintained under specific pathogen-free conditions and C57BL6/J mice were purchased from Japan SLC, Inc (Shizuoka, Japan). The animals were housed in a controlled environment (25 °C, 12 h light/dark cycle) and had free access to food and water, according to the regulations of the Guidance for Proper Conduct of Animal Experiments by the Ministry of Education, Culture, Sports, Science, and Technology of Japan. All experimental procedures were performed in accordance with the National Institute of Health Guide for the Care and Use of Laboratory Animals, and were approved by the Institutional Animal Use Committees of Nagoya University, Kyoto University, and Keio University.

### **Preparation of primary cortical neuronal culture**

Glass coverslips (Matsunami) in 24-well plates (BD Falcon) were coated with poly-D-lysine (Sigma-Aldrich) and washed with sterile water three times. Cerebral cortices from 16-day-old ICR mouse embryos were aseptically dissected and digested with 0.25 w/v% trypsin (Nacalai tesque) for 20 min at 37 °C. The cells were re-suspended in Neurobasal Plus medium (Invitrogen) supplemented with 10% FBS,

penicillin (100 units/mL), and streptomycin (100 µg/mL) and filtered by Cell Strainer (100 µm, Falcon) and centrifuged at 1,000 rpm for 5 min. The cells were resuspended in Neurobasal Plus medium supplemented with 2% of B-27 Plus Supplement (Invitrogen), 1.25 mM GlutaMAX I (Invitrogen), penicillin (100 units/mL), and streptomycin (100 µg/mL) and plated at a density of  $2 \times 10^5$  cells on the 24-well plate. The cultures were maintained at 37 °C in a 95% air and 5% CO<sub>2</sub> humidified incubator. The neurons were used for fluorescent Ca<sup>2+</sup> imaging experiment at 3 DIV (day in vitro).

#### **Evaluation of the solubility of Pd complexes in ACSF**

Pd complexes were dissolved in ACSF (125 mM NaCl, 2.5 mM KCl, 2 mM Ca<sub>2</sub>Cl, 1 mM MgCl<sub>2</sub>, 1.25 mM NaH<sub>2</sub>PO<sub>4</sub>, 26 mM NaHCO<sub>3</sub>, 10 mM Glucose) gassed with 5% CO<sub>2</sub> and 95% O<sub>2</sub>, and incubated for 1 h at 4 °C. The solution was centrifuged for 15 min at 15,000 rpm, and the supernatant was collected. The UV-vis absorption spectra of the samples were measured in the range of 250–450 nm with 1 nm resolution using a UV-vis spectrophotometer UV-2600 (SHIMADZU) at room temperature. Maximal absorption in aqueous solution at 312 nm was used to quantification.

#### **Generation of *mGlu1<sup>CBC/CBC</sup>* and *mGlu1<sup>-/-</sup>* by CRISPR/Cas9 system**

Mutant mice carrying mGlu1 N264H mutation were generated using the CRISPR-Cas9 system according to our previously report<sup>2</sup> with some modification. For generation of the mutant mice, *pX330* plasmid DNA vector<sup>37</sup>, donor single-stranded oligodeoxynucleotide (ssODN), and fertilized eggs of C57BL/6J mice were used. The sequence (5'-GACAAAATCTACAGCAATGC-3') in exon 3 was selected as the gRNA target, and it was inserted into entry site of the *pX330*. The donor ssODN was designed to induce a point mutation of N264H (c.790A>C) as shown in Fig. 12b, and the 113 mer ssDNA was synthesized (Integrated DNA Technologies). Female C57BL/6J mice were injected with pregnant mare serum gonadotropin and human chorionic gonadotropin

### Chapter 3

with a 48-h interval, and mated with male C57BL/6J mice. We then collected zygotes from oviducts in mated female and mixture of the *pX330* (circular, 5 ng/ $\mu$ L, each) and the ssODN (10 ng/ $\mu$ L) was microinjected into zygotes. Subsequently, survived injected zygotes were transferred into oviducts in pseudopregnant ICR female and newborns were obtained. Genotypes of the F0 mice were determined by PCR with the following primer sets; *forward* for WT and N264H (5'-GCAATACCACCCTCCTCTGA-3'), *reverse* for WT (5'-CGCATGGCACTCAGTAACC-3'), *reverse* for N264H (5'-AGCTCTTCTCGCCAGCATG-3') to give 321 bp or 218 bp product for WT or N264H, respectively. The candidate F0 mice were mated with the C57BL/6J mice to obtain F1 offspring. Genotypes of F1 mice were determined by PCR with the following primer sets; *forward* (5'-GCAATACCACCCTCCTCTGA-3') and *reverse* (5'-CGCATGGCACTCAGTAACC-3'), and the PCR products were sequenced by Sanger sequencing. The F1 mice having mGlu1 N264H mutation were crossed with the C57BL/6J mice to obtain *mGlu1<sup>CBC/+</sup>* mice. The *mGlu1<sup>CBC/+</sup>* mice were mated to obtain *mGlu1<sup>CBC/CBC</sup>* mice.

The genotype analysis of the F1 mice also gave a mouse showing 5 bp deletion (c.790\_794del) in the same exon. This deletion caused frameshift mutation and introduction of a stop codon in the same exon. Thus, the indel mice were crossed with the C57BL/6J mice to obtain *mGlu1<sup>-/+</sup>* mice. The *mGlu1<sup>-/+</sup>* mice were mated to obtain *mGlu1<sup>-/-</sup>* mice.

#### **Preparation of acute cerebellar slices**

C57BL/6J mice (aged 3 weeks) were anesthetized with isoflurane, and their brains were transferred to ice-cold cutting solution buffer (120 mM Choline Chloride, 3 mM KCl, 8 mM MgCl<sub>2</sub>, 1.25 mM NaH<sub>2</sub>PO<sub>4</sub>, 28 mM NaHCO<sub>3</sub>, 22 mM Glucose, 0.5 mM Na ascorbate) gassed with 5% CO<sub>2</sub> and 95% O<sub>2</sub> and incubated for 5 min. Sagittal cerebellar slices were cut with a microslicer (Linear slicer Pro7; DOSAKA EM) in cutting solution

buffer and then incubated in ACSF gassed with 5% CO<sub>2</sub> and 95% O<sub>2</sub> at room temperature.

#### **Western blotting analysis of the cerebellar slices**

The cerebellar slices prepared from *mGlu1*<sup>+/+</sup> mice or *mGlu1*<sup>CBC/CBC</sup> mice, were homogenized in homogenization buffer (20 mM Tris-HCl, 150 mM NaCl, 5 mM EDTA, pH 8.0) and sonicated. Samples were solubilized by 1.0 % SDS and denatured at 70 °C in Laemmli sample buffer. Proteins were then resolved on SDS-PAGE and analyzed using western blotting with primary antibodies (polyclonal antibodies obtained from Frontier institute; anti-mGluR1a [Frontier Institute, rabbit, 1:5,000], anti-GluD2 [Frontier Institute, guinea pig, 1:1,000] and anti-pan AMPAR [Frontier Institute, guinea pig, 1:1,000] and secondary antibodies (horseradish peroxidase-conjugated anti-rabbit antibody [Cytiva, 1:2,500] or anti-guinea pig antibody [Millipore, 1:5000]). Chemiluminescent or fluorescent signals were detected with iBright FL1000 (ThermoFisher) and quantified using ImageJ (NIH).

#### **Confocal live cell imaging of cell-surface mGlu1 in the cerebellar slices**

The cerebellar slices prepared from *mGlu1*<sup>+/+</sup> mice or *mGlu1*<sup>CBC/CBC</sup> mice, were incubated with 10 nM FITM-Cy3 and 10 µg/mL Hoechst33342 for 30 min at room temperature in a humidified atmosphere of 5% CO<sub>2</sub> and 95% O<sub>2</sub>. As a negative control, cerebellar slices prepared from *mGlu1*<sup>+/+</sup> mice were incubated with 10 nM FITM-Cy3, 10 µg/mL Hoechst33342, and 500 nM FITM. Then, the slices were subjected to confocal live imaging using a confocal microscope (LSM900, Carl Zeiss). The fluorescence intensity of Cy3 at the molecular layer were quantified by ZEN blue software (Carl Zeiss).

#### **Gross cerebellar anatomy**

To observe gross structure in adult mouse cerebella, cresyl violet-staining was performed, as previously described<sup>38</sup>. Bright-field images were captured using a CCD camera (DP70, Olympus) attached to a stereomicroscope (SMZ1000, Nikon).

### **Immunohistochemistry of the cerebellar slices**

Under deep anesthesia with a pentobarbital, mice were fixed by cardiac perfusion with 0.1 M sodium phosphate buffer (PB, pH7.4) containing 4% paraformaldehyde (4% PFA/PB); the brain was then removed and soaked in 4% PFA/PB for 2h. After rinsing the specimens with PB, parasagittal slices (50- $\mu$ m thickness) were prepared using a microslicer (DTK-2000; D.S.K.). Microslicer sections were permeabilized with 0.1% Triton X-100 (Sigma) in PB with 10% normal donkey serum or 2% normal goat serum/2% bovine serum albumin (BSA) for 20 min. Sections of freshly frozen brains were also prepared by cryostat (Leica) at 20  $\mu$ m thickness, mounted on glass slides and fixed with 3% glyoxal for 15 min, followed by blocking with 10% donkey serum for 30 min at RT and permeabilization with PBS containing 0.1% Triton X-100 (wash buffer). Immunohistochemical staining was performed using selective primary antibodies (anti-mGlu1 $\alpha$  (1:1,000; Frontier Institute), anti-calbindin (1:10,000; Swant), anti-GluD2 (1:500; Frontier Institute) and anti-Bassoon (1:500, Synaptic Systems) antibodies) overnight at room temperature, followed by incubation with the proper fluorescent dye-conjugate secondary antibodies (1: 1,000, Invitrogen) for 1 h. Finally, the sections were mounted with Fluoromount-G (SouthernBiotech). Photographs were taken with a confocal laser-scanning microscope (FLUOVIEW, FV1000; Olympus) and a super-resolution microscopy (OSR; Olympus).

### **Electrophysiology of the cerebellar slices**

Whole-cell recordings were made from visually identified Purkinje cells using a 60 $\times$  water-immersion objective attached to an upright microscope (BX51WI, Olympus) at

room temperature, as described previously<sup>39</sup>. The resistance of patch pipettes was 1.5–3 M $\Omega$  when filled with an intracellular solution of the following composition: 65 mM Cs-methanesulfonate, 65 mM K-gluconate, 20 mM HEPES, 10 mM KCl, 1 mM MgCl<sub>2</sub>, 4 mM Na<sub>2</sub>ATP, 1 mM Na<sub>2</sub>GTP, 5 mM sucrose, and 0.4 mM EGTA, pH 7.25 (295 mOsm/kg). The solution used for slice storage and recording consisted of the following: 125 mM NaCl, 2.5 mM KCl, 2 mM CaCl<sub>2</sub>, 1 mM MgCl<sub>2</sub>, 1.25 mM NaH<sub>2</sub>PO<sub>4</sub>, 26 mM NaHCO<sub>3</sub>, and 10 mM D-glucose, bubbled continuously with a mixture of 95% O<sub>2</sub> and 5% CO<sub>2</sub>. Picrotoxin (100  $\mu$ M; Sigma) was always added to the saline to block inhibitory synaptic transmission. To evoke EPSCs derived from CF (CF-EPSCs) and PF (PF-EPSCs) inputs onto Purkinje cells, square pulses were applied through a stimulating electrode placed on the granular layer and the molecular layer (50  $\mu$ m away from the pial surface), respectively. The selective stimulation of CFs and PFs was confirmed by the paired-pulse depression (PPD) and paired-pulse facilitation (PPF) of EPSC amplitudes at a 50-ms interstimulus interval (ISI), respectively. To search for multiple CFs innervating the recorded Purkinje cell, the stimulating electrode was moved systematically in the granular layer, and the stimulus intensity was gradually increased at each stimulation site (pulse width, 50  $\mu$ s; strength, 0–200  $\mu$ A). For the LTD sessions, PF-EPSCs were recorded successively at a frequency of 0.1 Hz from Purkinje cells clamped at –80 mV. After a stable PF-EPSC amplitude had been observed for at least 5 min, a conjunctive stimulation that consisted of 30 single PF stimuli together with a 200 ms depolarizing pulse from a holding potential of –60 to +20 mV was applied for LTD induction. To chemically induce LTD, 50  $\mu$ M (S)-3,5-dihydroxyphenylglycine (DHPG) or 1  $\mu$ M Pd(sulfo-bpy) was applied for 10 min in a current-clamp mode. Access resistances were monitored every 10 s by measuring the peak currents in response to 2 mV, 50-ms hyperpolarizing steps throughout the experiments; the measurements were discarded if the resistance changed by >20% of its original value. The normalized EPSC amplitude on the ordinate represents the EPSC amplitude for the average of six traces

for 1 min divided by that of the average of six traces for 1 min immediately before the conjunctive stimulation. The EPSCs were recorded using an Axopatch 200B amplifier (Molecular Devices), and the pClamp system (version 9.2; Molecular Devices) was used for data acquisition and analysis. The signals were filtered at 1 kHz and digitized at 4 kHz.

### **Rota-rod test**

To evaluate motor coordination of *mGlu1*<sup>+/+</sup>, *mGlu1*<sup>CBC/CBC</sup> or *mGlu1*<sup>-/-</sup> mice, accelerating rota-rod test was performed at 4–40 rpm using a single lane rota-rod treadmill (MK-630B, Muromachi Kikai Co., Ltd.), and the time that each mouse stayed on the rod was measured.

### **Statistical analysis**

All data are expressed as mean  $\pm$  s.e.m. We accumulated the data for each condition from at least three independent experiments. We evaluated statistical significance with the two-tailed Welch's *t*-test, Mann-Whitney U test, one-way ANOVA with Dunnett's test, or Kruskal-Wallis test followed by the Scheffe *post hoc* test. A value of  $P < 0.05$  was considered significant.



**3-5, Reference**

1. Jeffrey Conn, P., Christopoulos, A. & Lindsley, C. W. Allosteric modulators of GPCRs: A novel approach for the treatment of CNS disorders. *Nat. Rev. Drug Discov.* **8**, 41–54 (2009).
2. Foster, D. J. & Conn, P. J. Allosteric Modulation of GPCRs: New Insights and Potential Utility for Treatment of Schizophrenia and Other CNS Disorders. *Neuron* **94**, 431–446 (2017).
3. May, L. T., Leach, K., Sexton, P. M. & Christopoulos, A. Allosteric modulation of G protein-coupled receptors. *Annu. Rev. Pharmacol. Toxicol.* **47**, 1–51 (2007).
4. Moussawi, K., Riegel, A., Nair, S. & Kalivas, P. W. Extracellular glutamate: Functional compartments operate in different concentration ranges. *Front. Syst. Neurosci.* **5**, 1–9 (2011).
5. Sternson, S. M. & Roth, B. L. Chemogenetic tools to interrogate brain functions. *Annu. Rev. Neurosci.* **37**, 387–407 (2014).
6. Armbruster, B. N., Li, X., Pausch, M. H., Herlitze, S. & Roth, B. L. Evolving the lock to fit the key to create a family of G protein-coupled receptors potently activated by an inert ligand. *Proc. Natl. Acad. Sci. U. S. A.* **104**, 5163–5168 (2007).
7. Vardy, E. *et al.* A New DREADD Facilitates the Multiplexed Chemogenetic Interrogation of Behavior. *Neuron* **86**, 936–946 (2015).
8. Nagai, Y. *et al.* Deschloroclozapine, a potent and selective chemogenetic actuator enables rapid neuronal and behavioral modulations in mice and monkeys. *Nat. Neurosci.* **23**, 1157–1167 (2020).
9. Kiyonaka, S. *et al.* Allosteric activation of membrane-bound glutamate receptors using coordination chemistry within living cells. *Nat. Chem.* **8**, 958–967 (2016).
10. Kubota, R., Kiyonaka, S., & Hamachi, I. On-cell coordination chemistry: Chemogenetic activation of membrane-bound glutamate receptors in living cells. *Meth. enzymol.* **622**, 411-430 (2019).

11. Niswender, C. M. & Conn, P. J. Metabotropic glutamate receptors: Physiology, pharmacology, and disease. *Annu. Rev. Pharmacol. Toxicol.* **50**, 295–322 (2010).
12. Kunishima, N. *et al.* Structural basis of glutamate recognition by a dimeric metabotropic glutamate receptor. *Nature* **407**, 971–977 (2000).
13. Tsuchiya, D., Kunishima, N., Kamiya, N., Jingami, H. & Morikawa, K. Structural views of the ligand-binding cores of a metabotropic glutamate receptor complexed with an antagonist and both glutamate and  $Gd^{3+}$ . *Proc. Natl. Acad. Sci. U. S. A.* **99**, 2660–2665 (2002).
14. Clark, B. P., Baker, S. R., Goldsworthy, J., Harris, J. R. & Kingston, A. E. (+)-2-Methyl-4-carboxyphenylglycine (LY367385) selectively antagonises metabotropic glutamate mGluR1 receptors. *Bioorganic Med. Chem. Lett.* **7**, 2777–2780 (1997).
15. Satoh, A. *et al.* Discovery and in vitro and in vivo profiles of 4-fluoro-*N*-[4-[6-(isopropylamino)pyrimidin-4-yl]-1,3-thiazol-2-yl]-*N*-methylbenzamide as novel class of an orally active metabotropic glutamate receptor 1 (mGluR1) antagonist. *Bioorganic Med. Chem. Lett.* **19**, 5464–5468 (2009)
16. Wu, H. *et al.* Structure of a Class C GPCR Metabotropic Glutamate Receptor 1 Bound to an Allosteric Modulator. *Science* **344**, 58–64 (2014).
17. Kapdi, A. R. & Fairlamb, I. J. S. Anti-cancer palladium complexes: A focus on  $PdX_2L_2$ , palladacycles and related complexes. *Chem. Soc. Rev.* **43**, 4751–4777 (2014).
18. Puthraya, K. H., Srivastava, T. S., Amonkar, A. J., Adwankar, M. K. & Chitnis, M. P. Some mixed-ligand palladium(II) complexes of 2,2'-bipyridine and amino acids as potential anticancer agents. *J. Inorg. Biochem.* **25**, 207–215 (1985).
19. McWhinney, S. R., Goldberg, R. M. & McLeod, H. L. Platinum neurotoxicity pharmacogenetics. *Mol. Cancer Ther.* **8**, 10–16 (2009).
20. Martin, L. J., Blackstone, C. D., Haganir, R. L. & Price, D. L. Cellular localization

- of a metabotropic glutamate receptor in rat brain. *Neuron* **9**, 259–270 (1992).
21. Panatier, A. & Robitaille, R. Astrocytic mGluR5 and the tripartite synapse. *Neuroscience* **323**, 29–34 (2016).
  22. Cong, L. *et al.* Multiplex genome engineering using CRISPR/Cas systems. *Science* **339**, 819–823 (2013).
  23. Aiba, A. *et al.* Deficient cerebellar long-term depression and impaired motor learning in mGluR1 mutant mice. *Cell* **79**, 377–388 (1994).
  24. Conquet, F. *et al.* Motor deficit and impairment of synaptic plasticity in mice lacking mGluR1. *Nature* **372**, 237–243 (1994).
  25. Guergueltcheva, V. *et al.* Autosomal-recessive congenital cerebellar ataxia is caused by mutations in metabotropic glutamate receptor 1. *Am. J. Hum. Genet.* **91**, 553–564 (2012).
  26. Watson, L. M. *et al.* Dominant Mutations in GRM1 Cause Spinocerebellar Ataxia Type 44. *Am. J. Hum. Genet.* **101**, 451–458 (2017).
  27. Yamasaki, M., Aiba, A., Kano, M. & Watanabe, M. mGluR1 signaling in cerebellar Purkinje cells: Subcellular organization and involvement in cerebellar function and disease. *Neuropharmacology* **194**, 108629 (2021).
  28. Luján, R., Roberts, J. D. B., Shigemoto, R., Ohishi, H. & Somogyi, P. Differential plasma membrane distribution of metabotropic glutamate receptors mGluR1 $\alpha$ , mGluR2 and mGluR5, relative to neurotransmitter release sites. *J. Chem. Neuroanat.* **13**, 219–241 (1997).
  29. Zucker, R. S. & Regehr, W. G. Short-term synaptic plasticity. *Annu. Rev. Physiol.* **64**, 355–405 (2002).
  30. Kohda, K. *et al.* The  $\delta 2$  glutamate receptor gates long-term depression by coordinating interactions between two AMPA receptor phosphorylation sites. *Proc. Natl. Acad. Sci. U. S. A.* **110**, (2013).
  31. Herring, B. E. & Nicoll, R. A. Long-Term Potentiation: From CaMKII to AMPA

- Receptor Trafficking. *Annu. Rev. Physiol.* **78**, 351–365 (2016).
32. Collingridge, G. L., Peineau, S., Howland, J. G. & Wang, Y. T. Long-term depression in the CNS. *Nat. Rev. Neurosci.* **11**, 459–473 (2010).
  33. Traquete, R. *et al.* Evaluation of linker length effects on a BET bromodomain probe. *Chem. Commun.* **55**, 10128-10131 (2019).
  34. Satoh, A. *et al.* Discovery and in vitro and in vivo profiles of 4-fluoro-*N*-[4-[6-(isopropylamino)pyrimidin-4-yl]-1,3-thiazol-2-yl]-*N*-methylbenzamide as novel class of an orally active metabotropic glutamate receptor 1 (mGluR1) antagonist. *Bioorg. Med. Chem. Lett.* **19**, 5464-5468 (2009).
  35. Miyoshi, D. *et al.* Artificial G-Wire Switch with 2,2'-Bipyridine Units Responsive to Divalent Metal Ions. *J. Am. Chem. Soc.* **129**, 5919–5925 (2007).
  36. Niwa, H., Yamamura, K. & Miyazaki, J. Efficient selection for high-expression transfectants with a novel eukaryotic vector. *Gene* **108**, 193–199 (1991).
  37. Mizuno, S. *et al.* Simple generation of albino C57BL/6J mice with G291T mutation in the tyrosinase gene by the CRISPR/Cas9 system. *Mamm. Genome* **25**, 327–334 (2014).
  38. Kakegawa, W. *et al.* Anterograde C1ql1 signaling is required in order to determine and maintain a single-winner climbing fiber in the mouse cerebellum. *Neuron* **85**, 316–329 (2015).
  39. Kakegawa, W. *et al.* Optogenetic Control of Synaptic AMPA Receptor Endocytosis Reveals Roles of LTD in Motor Learning. *Neuron* **99**, 985-998.e6 (2018).

**List of publication**

**Chapter 1 and 2**

Ligand-directed two-step labeling to quantify neuronal glutamate receptor trafficking

Kento Ojima, Kazuki Shiraiwa, Kyohei Soga, Tomohiro Doura, Mikiko Takato, Kazuhiro Komatsu, Michisuke Yuzaki, Itaru Hamachi, Shigeki Kiyonaka

*Nat. Commun.*, **12**, 831 (2021)

**Chapter 3**

Coordination chemogenetics for activation of GPCR-type glutamate receptors in brain tissue

Kento Ojima, Wataru Kakegawa, Masayuki Ito, Yuta Miura, Yukiko Michibata, Ryou Kubota, Tomohiro Doura, Tokiwa Yamasaki, Eriko Miura, Hiroshi Nonaka, Seiya Mizuno, Satoru Takahashi, Michisuke Yuzaki, Itaru Hamachi, Shigeki Kiyonaka

*bioRxiv*, doi: <https://doi.org/10.1101/2021.10.01.462737> (2021)

**Other Publications**

Chemogenetic Approach Using Ni(II) Complex–Agonist Conjugates Allows Selective Activation of Class A G-Protein-Coupled Receptors

Ryou Kubota, Wataru Nomura, Takuma Iwasaka, Kento Ojima, Shigeki Kiyonaka, Itaru Hamachi.

*ACS Cent. Sci.*, **4**, 9, 1211–1221 (2018)

Orthogonal activation of metabotropic glutamate receptor using coordination chemogenetics

Akinobu Senoo, Yutaro Yamada, Kento Ojima, Tomohiro Doura, Itaru Hamachi, Shigeki Kiyonaka.

*Front. Chem.*, **9**, 1–10 (2022).

*List of Publications and Presentations*

**Reviews and Books**

分子から迫る神経薬理学 ケモジェネティクス-遺伝子工学と化学的なアプローチを組み合わせた受容体の人為的な活性制御

清中 茂樹, 小島 憲人、浜地 格

*CLINICAL NEUROSCIENCE*, **35**, 260-261 (2017)

ケモジェネティクスによる神経伝達物質受容体の人為的な活性制御

小島 憲人, 清中 茂樹、浜地 格

医学のあゆみ, **262**, 11, 1036-1037 (2017)

**List of Presentations**

1) Membrane Receptor Engineering by On-Cell Coordination Chemistry (2): Direct Activation of Metabotropic Glutamate Receptors by Pd Complex.

Kento Ojima, Yukiko Michibata, Ryou Kubota, Shigeki Kiyonaka, Itaru Hamachi  
96<sup>th</sup> Annual Meeting of Chemistry Society of Japan, Kyoto, March **2016**.

2) Metal complex-selectivity for artificial activation of glutamate receptors.

Kento Ojima, Yukiko Michibata, Ryou Kubota, Shigeki Kiyonaka, Itaru Hamachi  
10<sup>th</sup> Joint Symposium on Biofunctional Chemistry, Ishikawa, September **2016**.

3) Metallo-chemical genetics (1): Orthogonal Activation of Glutamate Receptor Subtypes.

Kento Ojima, Yukiko Michibata, Ryou Kubota, Shigeki Kiyonaka, Itaru Hamachi  
97<sup>th</sup> Annual Meeting of Chemistry Society of Japan, Kanagawa, March **2017**.

4) 配位ケモジェネティクスによるグルタミン酸受容体の直交的な活性化

Kento Ojima, Yukiko Michibata, Ryou Kubota, Shigeki Kiyonaka, Itaru Hamachi  
Summer School in 29<sup>th</sup> Symposium on Biofunctional Chemistry, Shimane, July **2017**.

5) Allosteric Activation or Inhibition of Glutamate Receptors by Metallo-Chemogenetics.

Kento Ojima, Yukiko Michibata, Ryou Kubota, Shigeki Kiyonaka, Itaru Hamachi  
11<sup>th</sup> Joint Symposium on Biofunctional Chemistry, Tokyo, September **2017**.

6) Allosteric activation of metabotropic glutamate receptors by coordination-chemogenetics.

Kento Ojima, Yukiko Michibata, Ryou Kubota, Shigeki Kiyonaka, Itaru Hamachi

*List of Publications and Presentations*

The Second International Symposium on Biofunctional Chemistry, Kyoto, December **2017**.

7) Brain cell-type specific activation of metabotropic glutamate receptors by coordination-chemogenetics.

Kento Ojima, Yukiko Michibata, Ryou Kubota, Shigeki Kiyonaka, Itaru Hamachi

98<sup>th</sup> Annual Meeting of Chemistry Society of Japan, Chiba, March **2018**.

8) 配位ケモジェネティクスによる代謝型グルタミン酸受容体の脳細胞種選択的な活性化

Kento Ojima, Yukiko Michibata, Ryou Kubota, Shigeki Kiyonaka, Itaru Hamachi

Summer School in 30<sup>th</sup> Symposium on Biofunctional Chemistry, Miyazaki, July **2018**.

9) Combination of LDAI chemistry and IEDDA click reaction for dynamics study of AMPA-type glutamate receptors.

Kento Ojima, Mikiko Takato, Shigeki Kiyonaka, Itaru Hamachi

12<sup>th</sup> Joint Symposium on Biofunctional Chemistry, Osaka, September **2018**.

10) Two-step labeling allows analysis of AMPA-type glutamate receptor dynamics “beyond optical resolution limit”.

Kento Ojima, Mikiko Takato, Shigeki Kiyonaka, Itaru Hamachi

99<sup>th</sup> Annual Meeting of Chemistry Society of Japan, Hyogo, March **2019**.

11) Development of the novel chemogenetic method for artificial activation of glutamate receptors.

Kento Ojima, Wataru Kakegawa, Yukiko Michibata, Ryou Kubota, Michisuke Yuzaki, Itaru Hamachi, Shigeki Kiyonaka



The 92nd Annual Meeting of the Japanese Biochemical Society, Kanagawa, September **2019**.

12) Quantification of neuronal AMPA-type glutamate receptor dynamics by combining ligand-directed chemistry and IEDDA click reaction.

Kento Ojima, Kazuki Shiraiwa, Shigeki Kiyonaka, Itaru Hamachi

100<sup>th</sup> Annual Meeting of Chemistry Society of Japan, Chiba, March **2020**.

13) リガンド指向性化学を用いた 2 段階ラベル化戦略による AMPA 受容体の動態解析

Kento Ojima, Itaru Hamachi Shigeki Kiyonaka

生理研シナプス研究会, On-line, December **2020**.

14) Ligand-directed two-step labeling to quantify AMPA-type glutamate receptor trafficking.

Kento Ojima, Kyohei Soga, Itaru Hamachi, Shigeki Kiyonaka

101<sup>th</sup> Annual Meeting of Chemistry Society of Japan, On-line, March **2021**.

15) Coordination chemogenetics for direct activation of GPCR-type glutamate receptors in brain tissue.

Kento Ojima, Wataru Kakegawa, Masayuki Ito, Michisuke Yuzaki, Itaru Hamachi, Shigeki Kiyonaka

15<sup>th</sup> Joint Symposium on Biofunctional Chemistry, On-line, September **2021**.

16) 記憶メカニズムの解明に向けた配位ケモジェネティクスによる代謝型グルタミン酸受容体の直接活性化

Kento Ojima, Wataru Kakegawa, Masayuki Ito, Michisuke Yuzaki, Itaru Hamachi,

*List of Publications and Presentations*

Shigeki Kiyonaka

52nd Annual Meeting of Union of Chemistry-Related Societies in Chubu Area, On-line,  
October **2021**.

**List of Honors**

1) Japan Society for the Promotion of Science (JSPS) research fellowships for young  
scientist (DC1, 2018-2021)

2) Best Poster Award, Summer School in 29<sup>th</sup> Symposium on Biofunctional Chemistry,  
Shimane, July **2017**.